



CAGE - Centre for Arctic Gas Hydrate Environment and Climate Report Series, Volume 2 (2014)

To be cited as: To be cited as: Bünz, S., & Panieri, G. (2023). CAGE14-1 Cruise Report: CAGE research school in Arctic Marine Geology and Geophysics. *CAGE - Centre for Arctic Gas Hydrate Environment and Climate Report Series, Volume 2*. <https://doi.org/10.7557/cage.6898>

Additional info at: <https://septentrio.uit.no/index.php/cage/database>

© The authors. This report is licensed under the Creative Commons Attribution 4.0 International License (<https://creativecommons.org/licenses/by/4.0/>)

ISSN: 2703-9625

Publisher: Septentrio Academic Publishing Tromsø Norway

## **UNIVERSITY OF TROMSØ cruise report**

Tromsø – Longyearbyen 19-06-14 to 30-06-14

**R/V Helmer Hanssen**

### **CAGE research school in Arctic Marine Geology and Geophysics**



**Centre for Arctic Gas Hydrate,  
Environment and Climate (CAGE))**

*Institutt for Geologi, Dramsveien 201  
Universitetet i Tromsø*

**Stefan Bünz & Giuliana Panieri (co-chief scientists)**

## Table of Contents

PARTICIPANT LIST .....	4
INTRODUCTION AND OBJECTIVES .....	6
1. Study area and geological background.....	8
2. Multibeam and chirp sonar survey .....	12
2.1. Data acquisition and methods.....	12
2.2. Data processing.....	13
2.3. Bathymetry and acoustic stratigraphy .....	14
3. 2D Seismic study of the Svyatogor Ridge .....	24
3.1. Acquisition.....	24
3.2. Processing.....	26
3.3. Interpretation .....	31
3.4. Evidence for gas hydrate and free gas reservoirs on Svyatogor Ridge .....	32
3.5. Faults and their origins .....	34
3.6. Paleo-depression features along the Svyatogor Ridge .....	37
4. Hydrographic survey .....	38
4.1. Instrumentation and procedures for data collection .....	38
4.2. Conductivity, temperature, depth (CTD survey).....	38
4.3. Sampling of dissolved methane gas in the water column.....	39
4.4. Nutrient sampling .....	40
4.5. ADCP.....	41
4.6. Split beam echosounder.....	41
4.7. USGS-GAS (US Geological Survey – Gas Analysis System).....	42
4.8. Preliminary results.....	44
5. Micropaleontology and pore water sampling.....	51
5.1. Study sites.....	51
5.2. Methods .....	54
5.3. Subsampling the core material .....	55
5.4. Sampling for methane in sediments.....	57
5.5. Porewater sampling .....	59

5.6.	Onboard analyses and preliminary results.....	59
5.7.	Methane and porewater .....	68
5.8.	Agglutinated foraminifera and authigenic carbonates in active vent sites .....	73
5.9.	Authigenic carbonates .....	74
6.	Benthic macro fauna analysis.....	76
6.1.	<i>Benthic community structure</i> .....	76
6.2.	<i>Stable isotopes</i> .....	77
6.3.	<i>Sclerochronology</i> .....	78
6.4.	Materials and methods.....	78
6.5.	<i>Sampling</i> .....	79
6.6.	Results .....	82
6.7.	Discussion.....	86
7.	Sedimentology.....	89
7.1.	Methods .....	89
7.2	Core description .....	94
7.3.	Synthesis.....	99
8.	References .....	100
9.	Appendix .....	105
9.1.	Appendix 1 .....	105
9.2.	Appendix 2 .....	109
	NARRATIVE OF THE CRUISE.....	119
	ACKNOWLEDGEMENT .....	120

## PARTICIPANT LIST

Stefan Bünz (chief scientist)	University of Tromsø, Norway
Giuliana Paneri (co-chief scientist)	University of Tromsø, Norway
Michael Carroll	Akvaplan Niva, Norway
Joel Johnson	University of Tromsø, Norway
Anna Silyakova	University of Tromsø, Norway
Bjørn Runar Olsen	University of Tromsø, Norway
Jens Greinert	Geomar, Germany
John Pohlman	USGS, USA
Michael Casso	USGS, USA
Giacomo Osti	University of Tromsø, Norway
Alexey Portnov	University of Tromsø, Norway
Kate Waghorn	University of Tromsø, Norway
Andrea Schneider	University of Tromsø, Norway
Sandra Hurter	University of Tromsø, Norway
Emmelie Åström	University of Tromsø, Norway
Sunny Singhroha Alias Sunny Kumar	University of Tromsø, Norway
Emilia Daria Piasecka	University of Tromsø, Norway
Pär Jansson	University of Tromsø, Norway
Dimitrios Ktenas	University of Tromsø
Simone Sauer	Norwegian Geological Survey
Benjamin Bellwald	University of Bergen, Norway
Julia Hofmann	GEUS Danmark
Oscar Fransner	UNIS &UiT



## INTRODUCTION AND OBJECTIVES

Cruise CAGE14-1 is one of several cruises in 2014 that will be carried out to collect cross-disciplinary data for addressing the objectives of the Norwegian Centre for Arctic Gas Hydrate, Environment and Climate, CAGE. CAGE is funded by the Norwegian Research Council for a period of 10 years to address main scientific questions about gas hydrate environments in Arctic regions.

Cruise CAGE14-1 was also hosting this year's AMGG research school cruise with 14 PhD students participating, most of them from CAGE. The cruise focussed on acquisition of seismic, oceanographic, atmospheric, geochemical and sediment and benthic fauna sampling data from three target areas: the shallow shelf and shelf edge methane seepage sites at Prins Karls Foreland, a sediment drift on the western flank of the Knipovich Ridge and the Vestnesa Ridge. Research objectives were planned along the goals of CAGE and its individual work packages, and the teaching would be organized along these goals.

Scientific problems that are to be addressed in these two key target areas include the periodicity of seepage (i.e. time scales of active, inactive and reactivated systems), quantification of methane concentrations in surface sediments, water column and above the sea surface, gas and hydrates, the nature of gas sources, and the benthic communities occurring at the seep sites.

Specific objectives of cruise CAGE14-1 were as follow:

- Hydro-acoustic mapping of methane bubble plumes above shallow and deep-water vent fields.
- Seismic surveying and multibeam mapping across the contourites on the Svyatogor Rise.
- Sediment sampling using gravity, box and multi-corer for sediment and pore-water geochemical analyses
- Sampling of benthic fauna at several seep sites and reference stations in all three target areas.
- Acquisition of oceanographic data for measuring oceanographic conditions and methane concentrations in the water column, particularly at the shallow shelf sites.



Figure 1: Location of the study area.

## 1. Study area and geological background

The study area includes a large region of the western Svalbard continental shelf west of Prins Karls Forland (Hornsund Fracture Zone), as well as part of Knipovich Ridge south of the Molloy Fracture Zone and part of Vestnesa Ridge (Fig. 1.1). The western Svalbard margin is located in the proximity of the active ocean ridge and covered by several hundreds of meters of sediments which are dated to approximately 20 Ma (Buenz et al., 2012). Knipovich Ridge as northernmost part of the Mid-Atlantic Ridge is an area of ultra-slow spreading. It extends in S-N orientation at water depths of approx. 2300 m, from Mohns Ridge in the south 500 km northwards where it reaches the Molloy Fracture Zone (Kandilarov et al., 2010; Buenz et al., 2012). Knipovich Ridge lies in an area of spreading oblique to the plate boundary and was created due to the northward propagation of the Mid-Atlantic Ridge (Kandilarov et al., 2010). Vestnesa is an elongated ~100 km long, SE-NW oriented sediment drift, located at about 79°N at water depths of ~1200 m, north of the Molloy Transform Fault. The whole study area is characterized by intensive faulting and rifting, associated with high heat flow values (up to three times higher than in the Barents Sea and the rest of Norway). The processes of sedimentation and fluid/gas release as well as the distribution of heat flow are mostly controlled by the warm West Spitsbergen Current (Vanneste et al., 2005a; Buenz et al., 2012).

The opening of the Norwegian-Greenland Sea occurred at multiple times throughout the Cenozoic era, but seafloor spreading started during Early Eocene and Oligocene (Lundin et al., 2002). The Fram Strait formed between 15 and 7 Ma, opening a deep water passage for the Atlantic-Arctic Ocean. The Fram Strait is a key area for the northern oceanic circulation (Thiede and Myhre, 1996) and plays an important role in the distribution of hydrocarbon gases in sediments and the water column in the western Svalbard continental shelf area. The warm Atlantic surface current constitutes a main heat source for the western Svalbard shelf, where the Atlantic water descends at water depths of 100-500 m at the Arctic Front north of 78°N, affecting the regional circulation and redistributing methane and associated gases towards the north-west (Rasmussen et al., 2007). Since the 1980's, a warming of the West Spitsbergen Current by 1°C has been documented. It is likely that this warming caused a significant reduction in the extent of the GHSZ, increasing the rate of methane release from the sea subsurface (Westbrook et al., 2009).

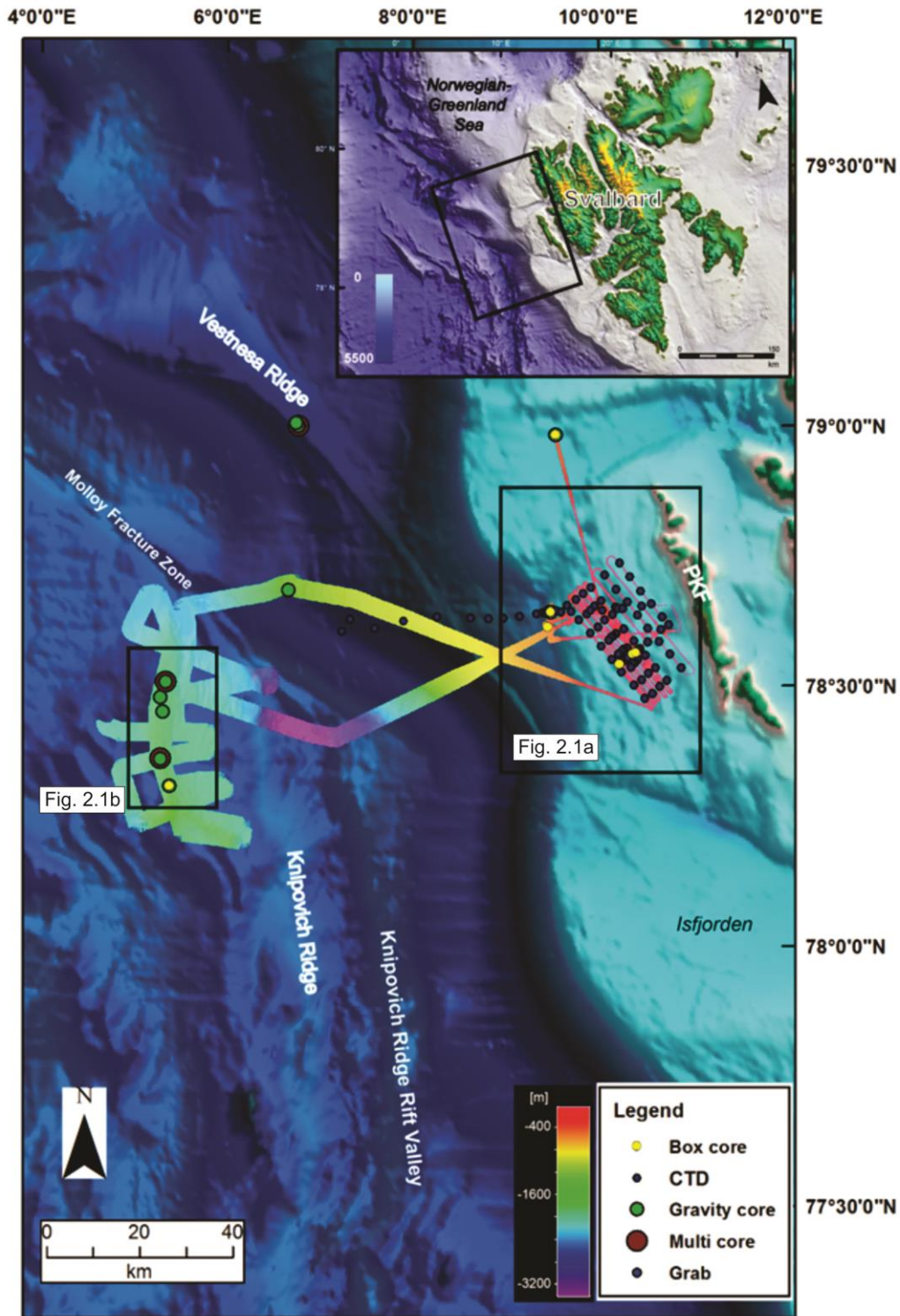


Fig. 1.1 Map of the study area – western Svalbard margin, Knipovich Ridge and Vestnesa. Multibeam survey performed during the cruise is plotted on the map. Sampling sites marked with coloured dots.

Gas hydrate systems are widely distributed within the study area between the West Svalbard margin and the Molloy Transform Fault. The occurrence of methane plumes has been

detected from many sources along the West Svalbard margin (e.g. Westbrook et al., 2009; Hustoft et al., 2009; Buenz et al., 2012; Chand et al., 2012). Due to large variations in temperature and water depth over the last 15 kyr, the gas hydrate stability zone in this region formed at relatively shallow water depths and can be found at a maximum depth of 400 m at a temperature of 3°C. Over 250 active fluid vents have been discovered in areas shallower than 400 m, reaching water depths of up to 350 m (Westbrook et al., 2009). On seismic profiles from the West Svalbard margin and Vestnesa, many pipe- and chimney-like features associated with gas release are documented, but the distribution of gas in sediments is much wider and can be identified based on a strong negative-seismic reflection (Eiken and Hinz, 1993; Vanneste et al., 2005a; Buenz et al., 2012). Therefore, this region is considered as the largest gas hydrate province along the Arctic continental margin (Hustoft et al., 2009) and constitutes a representative study area of gas migration and release (Fig. 1.2A).

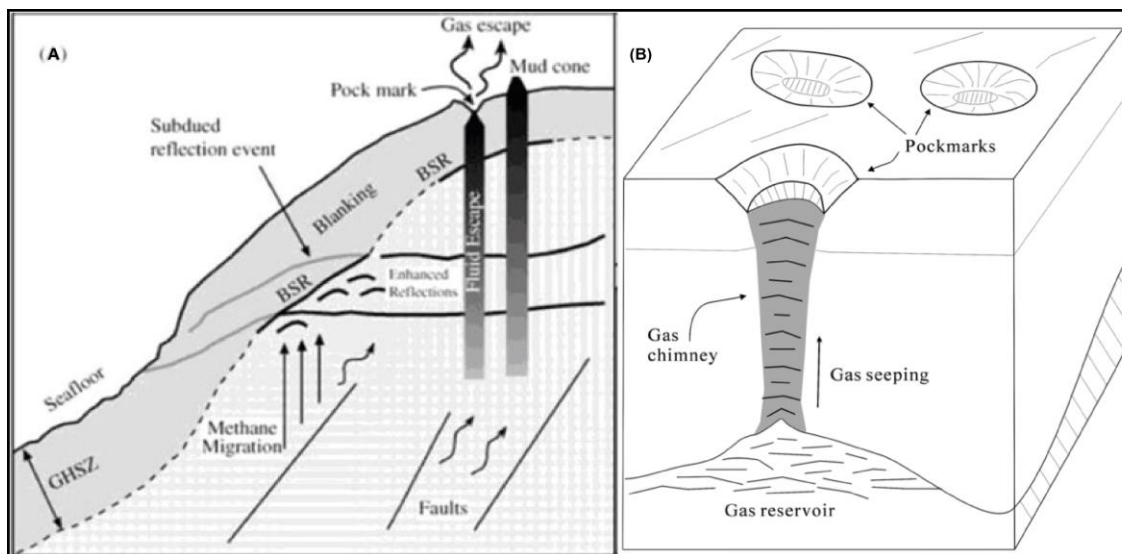


Fig. 1.2 (A) Sketch showing gas hydrate release and related features along a passive continental margin. BSR (bottom-simulating reflection) indicates the base of the GHSZ (gas hydrate stability zone) (adapted from Kvenvolden, 1998). (B) Gas saturated fluids escape through vents and migrate within soft marine sediments. Sediment collapse results in the creation of pockmarks (Cathles et al., 2010).

The highest concentration of flares is located west of Svalbard, in areas with shallow water depth (sometimes less than 200 m), at the edge of the GHSZ and at the shelf, approximately 15 km away from this zone. Since the gas hydrate stability zone cannot develop at temperatures higher than 0°C and at water depths less than 300 m, the gas plumes in the study area are probably fed by

a primary geological methane source created after the glacial retreat at about 13 ka (Landvik et al., 2005). According to the bathymetry, there is numerous evidence of fluid flow on Vestnesa Ridge and in the shallow shelf area west of Svalbard, where the pockmarks are most prominent. Their size varies from several to hundreds of meters in diameter and to tens of meters in depth (Vogt et al., 1994). Seismic data displays a strong negative-polarity seismic reflection beneath Vestnesa Ridge and the western Svalbard margin. For Vestnesa Ridge, a spatial distribution of gas hydrates of approximately 3000 km<sup>2</sup> has been calculated (Vanneste et al., 2005; Buenz et al., 2008). Although no gas hydrates have been sampled from the shelf area so far, seismic data revealed a strong negative-amplitude reflection representing the bottom-simulating reflector (BSR) (Eiken and Hinz, 1993; Vanneste et al., 2005a). It is suggested that the pockmark features are directly linked to the seismically transparent zones (e.g. gas chimneys) (Buenz et al., 2012; Smith et al., 2013). Pockmarks occur where fluids escape through the soft, permeable, surficial sediments leaving a prominent trace in form of a depression, which afterwards may be subject to winnowing and erosion. Pockmarks are also closely linked to faults and often directly connected to hydrocarbon saturated sedimentary rocks (Hovland et al., 2002). Most of the pockmarks seem to be inactive as fluids tend to migrate along sediment layers and escape wherever there is a crack in the surface (Fig. 1.2B). Pockmarks are therefore collapsed remnants of former gas seepage. However, many of them seem to be periodically active, mostly during extreme events, such as tides, storms etc. (Hovland et al., 2002).

A set of research methods incorporated under the framework of CAGE 14-1 cruise on RV Helmer Hansen included multibeam and chirp data acquisition, 2D seismic survey, hydrographic survey, micropaleontology and pore water sampling, benthic macro fauna analysis.

## 2. Multibeam and chirp sonar survey

### 2.1. Data acquisition and methods

The geophysical datasets used here were acquired during the CAGE-14-1 cruise onboard the research vessel R/V Helmer Hanssen in June 2014. The vessel has a hull mounted Kongsberg EM300 multibeam sonar system used for swath-bathymetrical surveys. In this survey, the multibeam sonar was operating in a frequency of 30 kHz.

The multibeam bathymetry data are derived from the two-way travel time for simultaneously emitted sound pulses that travel through the water column and eventually are reflected on the seafloor (Masetti and Calder, 2012). The spread of the pulses is given by the opening angle of the transducer, which therefore affects the swath width – the part of the seabed hit by the pulses (Hamilton and Parnum, 2011). In order to register the reflected sound pulses, the swath width is divided into foot prints, from where the echo is ensonified (Hell, 2011). The relation in between the foot print, depth and opening angle is explained by the following equation (Jakobsson, 2012a);

$$F = 2d \tan\left(\frac{a}{2}\right)$$

Where  $F$  is the footprint,  $d$  is the water depth and  $a$  is the opening angle of the multibeam sonar.

To detect gas seepage in the water column, a Simrad ER60 single beam system was used (for details see chapter 4.6). The acoustic subbottom data was acquired using a towed Edgetech Discover sb 3200-xs chirp sonar, which operates in between 1.5 kHz and 9 kHz. The acquired subbottom data is derived from the acoustic impedance of the penetrated sediment units. The acoustic impedance is in turn dependent on the density of the sediments and the velocity of the incoming sound waves. When the sound wave penetrates a medium of different acoustic impedance, one part of the energy from the sound wave is reflected and eventually registered by the chirp sonar system. The other part of the sound wave energy continues further down until another acoustic impedance is penetrated, where the signal splits again. This procedure reoccurs until the signal weakens and is lost. The higher the contrast in between two acoustic impedances, the stronger the reflector will be. Since physical properties of sediments often vary, their acoustic impedance can be used to map and interpret different sedimentary units (Penrose et al., 2005).

For chirp sonars, the difference in between the minimum and maximum frequencies of the emitted sound pulses defines the bandwidth of the sonar, which in turn affects the resolution of the data according to the following formula (Jakobsson, 2012b):

$$R = V/(B * 2)$$

where R is the resolution, V the sound velocity and B the frequency bandwidth.

## **2.2. Data processing**

All raw data for this cruise report was processed and interpreted onboard R/V Helmer Hanssen during the cruise. In order to finalize figures and maps before leaving the vessel, no data collected after Friday, the 26<sup>th</sup> of June, at 19:00 pm (GMT+2) has been included in this report.

The raw multibeam data was processed in Dmagic and visualized in Fledermaus – both softwares belonging to the Fledermaus Suite. To achieve bathymetry maps with highest resolution possible, the raw data was subdivided into several areas depending on depth. This led to cell sizes varying from 3 to 25 meters. During the gridding in Dmagic, the default gridding algorithm “weighted moving average” was used. After gridding the bathymetry, a slope map was produced, also in Dmagic. Instead of showing the depth, the slope maps are displaying slope angles derived from the bathymetry. These maps were valuable for the identification of pockmarks in the study area – a major goal of the cruise.

The acoustic water column raw data was processed and interpreted in FM Midwater – another software in the Fledermaus Suite. FM Midwater was used to digitize gas flares in the water column. After the digitization, the results were exported as text files to Fledermaus where the gas flares were merged with the gridded bathymetry (see chapter 4.6 for details).

The chirp sonar profiles were interpreted in the Edgetech software “Discover”. Key profiles were exported to Fledermaus where they were merged with the bathymetry data. The focus here was to connect bathymetrical pockmarks with chimneys in the acoustic stratigraphy and also to describe the general sedimentary sequence in the study area.

Arc Map was used to make the final map of the cruise, combining the gridded bathymetry surface with all the sediment core and CTD locations. The final map was produced with the coordinate system WGS 1984, UTM zone 32N. IBCAO 3.0 was used as the basemap for the final cruise map.

### 2.3. Bathymetry and acoustic stratigraphy

Fig. 1.1 shows the regional swath bathymetry, gridded with a cell size of 25 m. The study area extends ~125 km in east-west and ~60 km in north-south direction. The depth varies from 80 - 220 m on the shelf of W-Svalbard (Fig. 2.1a) and from 1500 m on the NW-flank of Knipovich Ridge, just south of the Molloy Fracture Zone, to 3200 m in the Knipovich Ridge Rift Valley. The survey along the West Svalbard margin includes the 14 km wide and 30 km long relatively shallow shelf area close to Prins Karls Forland. Here, the depth is ~100 m on average. In this region, the seabed morphology is diverse with ridges and depressions distributed all over the shelf. The depressions, probably of glacial origin, are 20 - 50 m deep and 400 - 1000 m wide. As suggested by Landvik et al. (2005) as well as Ingólfsson and Landvik (2013), during the LGM, this area was located between two active ice-streams, while the shelf area and strandflats were covered by less dynamic ice. Processes of squeezing and shearing caused the formation of transverse ridges, while the depressions were probably formed as a consequence of glacial melting. However, the exact genesis and timing of their formation is unknown and requires further study.

Pockmarks of various shapes and dimensions are abundantly distributed across the shelf. They are most abundant close to Kongsfjordrenna, near the lateral moraine of a former ice-stream. During earlier glaciations, this area was affected by intense shearing. Those pockmarks are also associated with fluid escape from the seafloor and will be described in more detail further in the text. From the continental shelf towards the deep sea, the seafloor dips gently in SW direction with a mean slope angle of  $0.5^\circ$  until it reaches the shelf break. It then dips rapidly with an inclination of  $\sim 16^\circ$  and continues further towards the rift valley, where the inclination decreases gradually to an angle of  $1-3^\circ$ . Within the rift valley further to the west, the morphology is rather homogenous and flat, occasionally crosscut by small ridges and transverse grooves. Some indication of slumping on the western slope of the valley can be observed. The slope angle is up to  $0.5^\circ$  in the flat area, while it reaches up to  $14^\circ$  on the flanks. It can be inferred that the valley extends at a depth of 3100-3200 m from the south to the north, bending distinctly towards NW as it reaches the Molloy Transform Fault.

The westernmost part of the survey covers the NW-flank of Knipovich Ridge and comprises a small, arcuate sedimented morphological feature, which extends over 60 km close to Knipovich Ridge (Fig. 2.1b). In the SE, this associated ridge joins Knipovich Ridge and bends in

northward direction, following the main drift in a mirror-like manner. The detailed morphology of this feature is described later in the text.

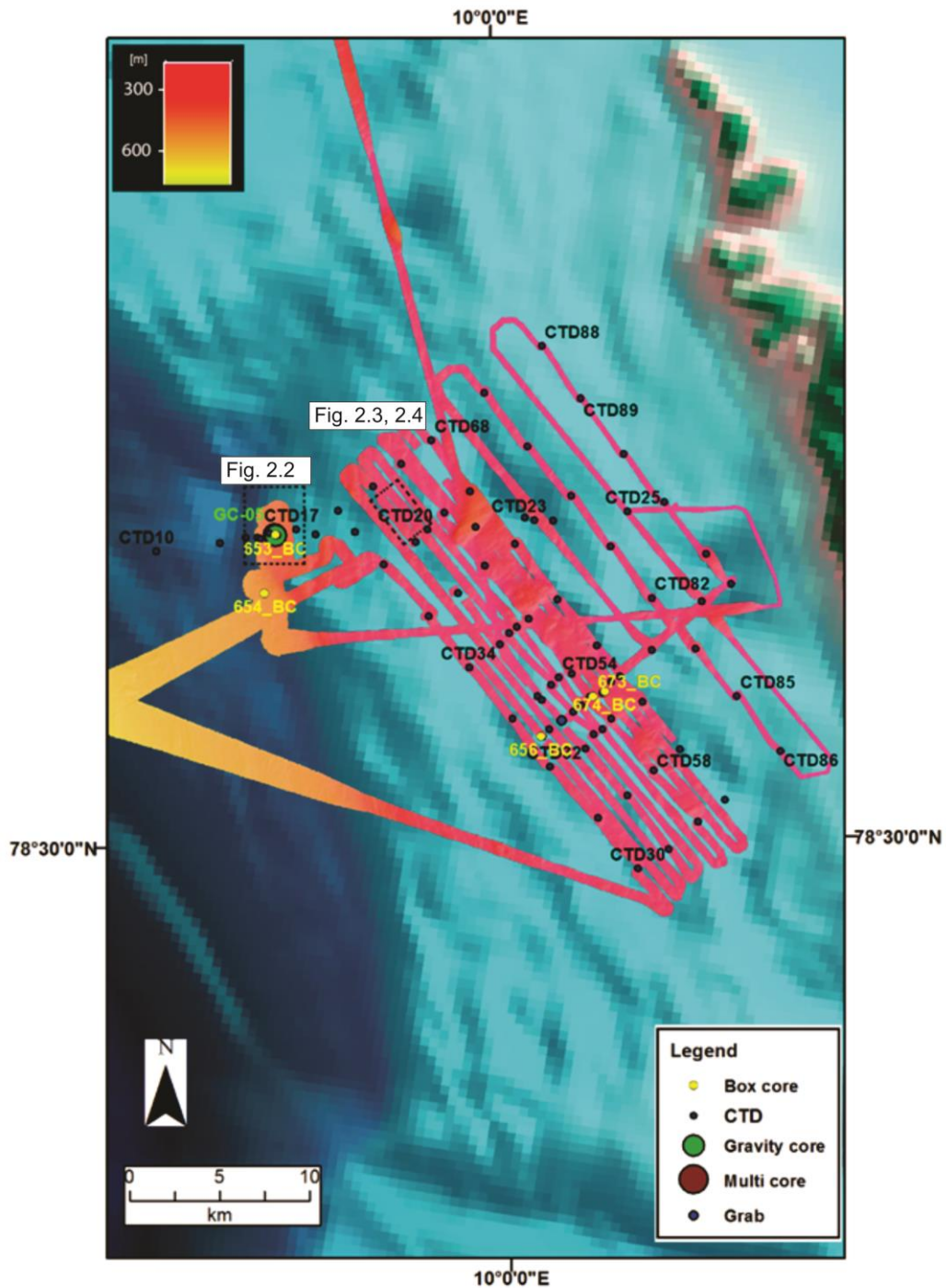


Fig. 2.1a Close-up of the multibeam survey along the continental shelf offshore western Svalbard, west of Prins Karls Forland. Coring and water sampling sites displayed with coloured dots.

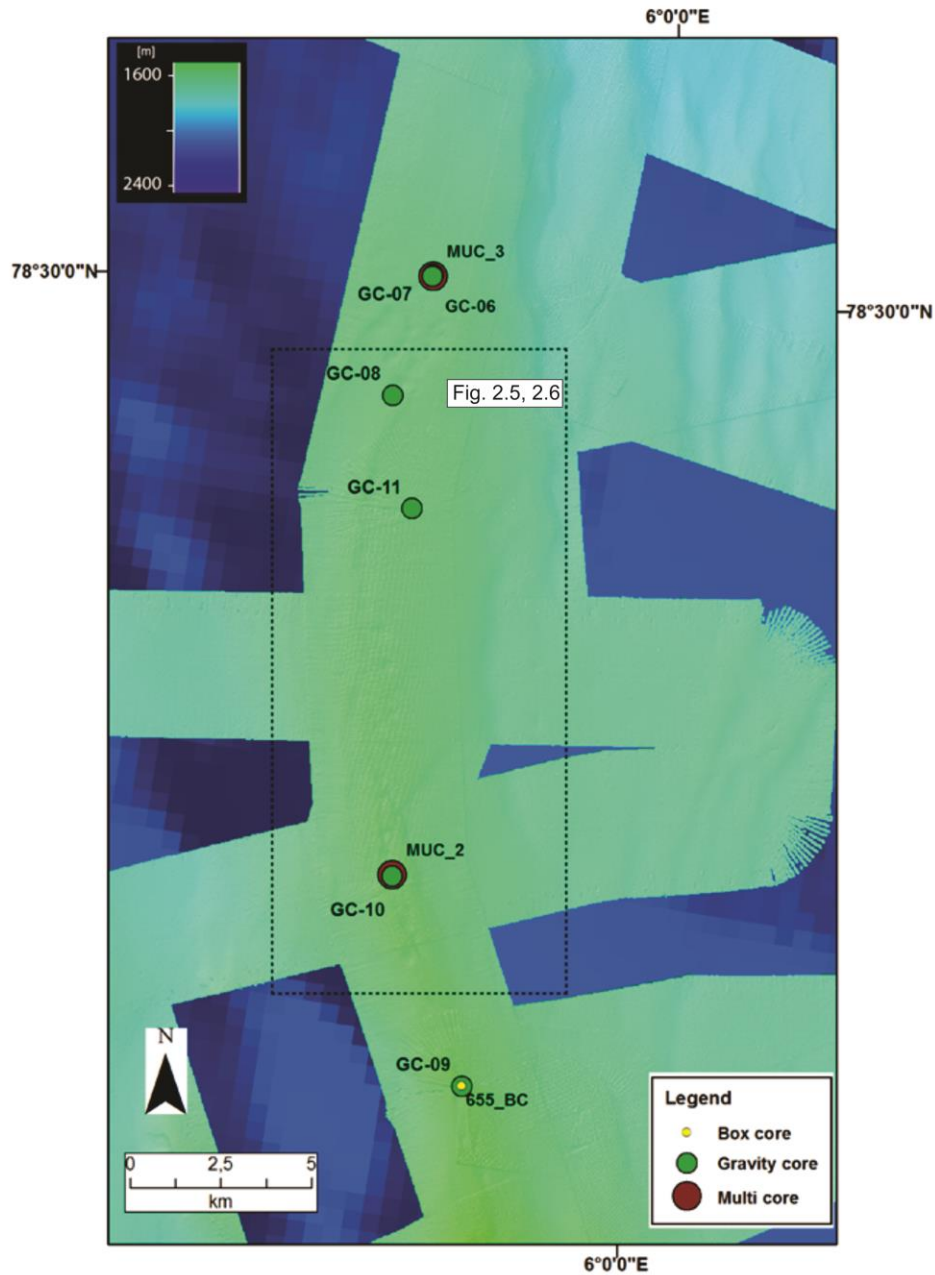


Fig. 2.1b Close-up of the multibeam survey west of Knipovich Ridge. Dashed rectangle indicates the pockmark area (Fig. 2.5 and 2.6). Coring sites indicated by coloured dots.

The most prominent geomorphological features can be found in the shelf area (Fig. 2.1a), south of Kongsfjordrenna, such as oblique and transverse ridges, densely distributed, circular and elongated, small depressions interpreted as pockmarks as well as irregular, large depressions probably created by glacial meltwater. The topography on the shelf is generally rough and

irregular indicating an intense deformation of the soft sediments. Due to the main goal of this cruise, we focus here on indications of gas accumulation and seepage.

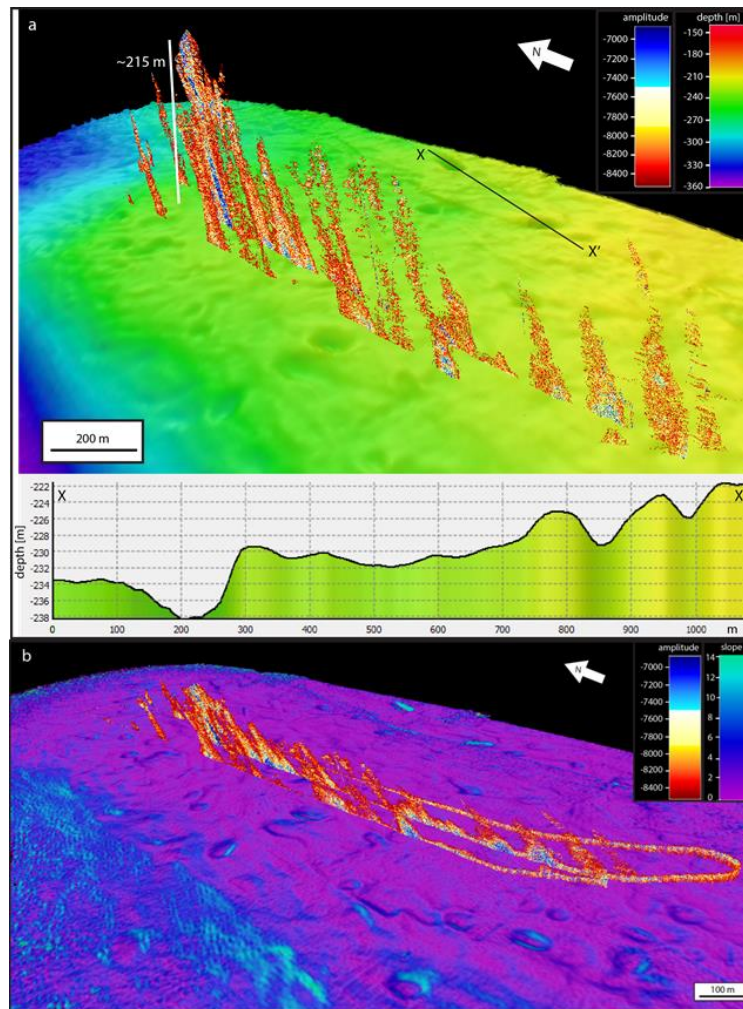


Fig. 2.2 (a) Perspective view of the rough seabed topography in the pockmark area at the shelf break close to Prins Karls Forland (vertical exaggeration: x6, for location see Fig. 1.1 and 2.1a). Pockmarks are associated with events of intense gas or fluid seepage shown by the high-amplitude echo sounder reflections. Profile X-X' displays the cross-section through two deep pockmarks. (b) Perspective view of the same area as in Fig. 2a, with a slope-angle filter applied in order to highlight the pockmark features.

The pockmarks are most abundant in the northern part of the shelf area (Fig. 2.2a and 2.2b) and at the shelf break, where the pockmarks are associated with gas/fluid seepage (flares), identified by echo sounding. Over 50 irregularly distributed, circular or elongated pockmarks of different size have been discovered at the shelf break. Their size varies from 30 to 100 m in diameter and from 1 to 5 m in depth. Some of the pockmarks have a more elongated shape and a greater depth than the circular ones. The pockmarks are mostly located in short distance from each

other and at least 10 of them are connected through irregular depressions comprising 2-3 pockmarks each. The echo sounder record of flares plotted together with the bathymetry displays a very good - although not direct - correlation between pockmark occurrence and gas/fluid seepage. The flares are present in areas of highest seabed roughness and, in several cases, flares with highest amplitudes coincide with multiple pockmarks. Flares have also been detected on the continental slope, although there are only few pockmark-resembling features located in this area.

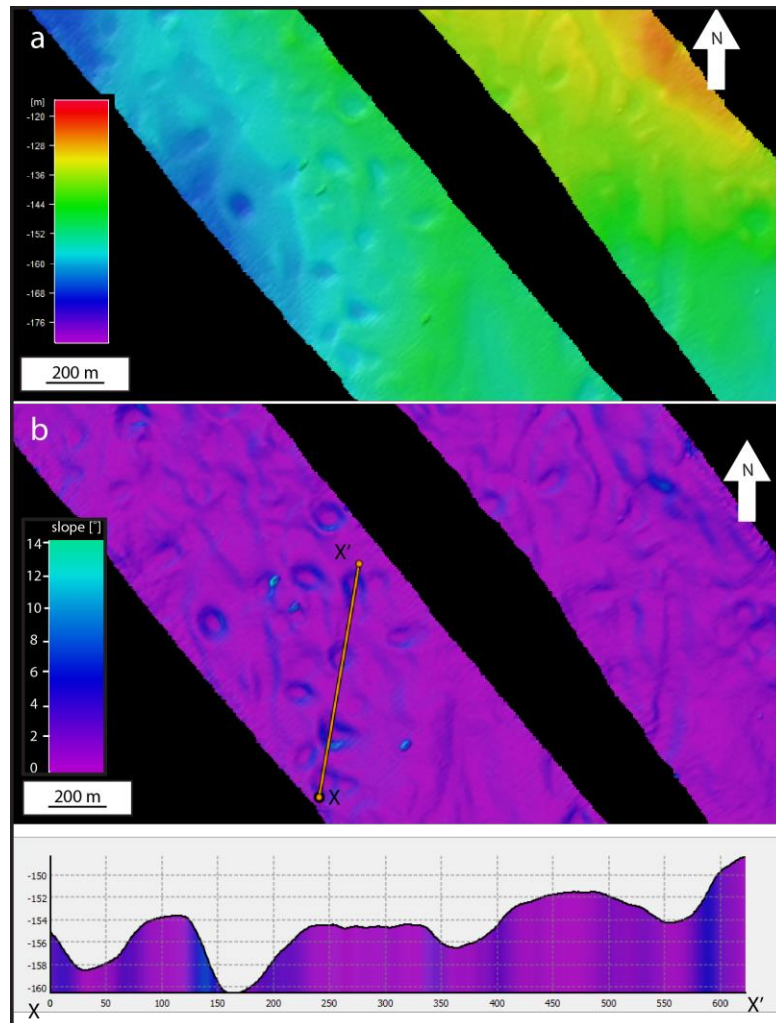


Fig. 2.3 (a) Rough and deformed seafloor morphology in the shelf area east of the continental slope (see Fig. 1.1 and 2.1a for location). (b) Perspective view of the same area as in Fig. 2.3a, with applied slope angle filter. Profile X-X' shows the cross-section through four aligned pockmarks.

High concentrations of pockmarks occur also further east on the shelf, where the area is characterized by a very rough topography due to former and/or present glacial and meltwater

activity. The area shown in Figures 2.3 and 2.4 is located just south of Kongsfjordrenna at its flank and probably influenced by processes related to this trough. The seabed here dips slightly westward with an average slope angle of  $1.5^\circ$ . The pockmarks are densely distributed, sometimes overprinting the 3-7 m high ridges oriented perpendicular to the continental slope. At least 30 pockmarks, both irregular and oval, have been identified on the seafloor in this area. Those pockmarks are shallower and wider than the pockmarks at the shelf break, with a more uniform and a flatter internal morphology. Their size varies from 50 to 110 m in width and from 2 to 4 m in depth.

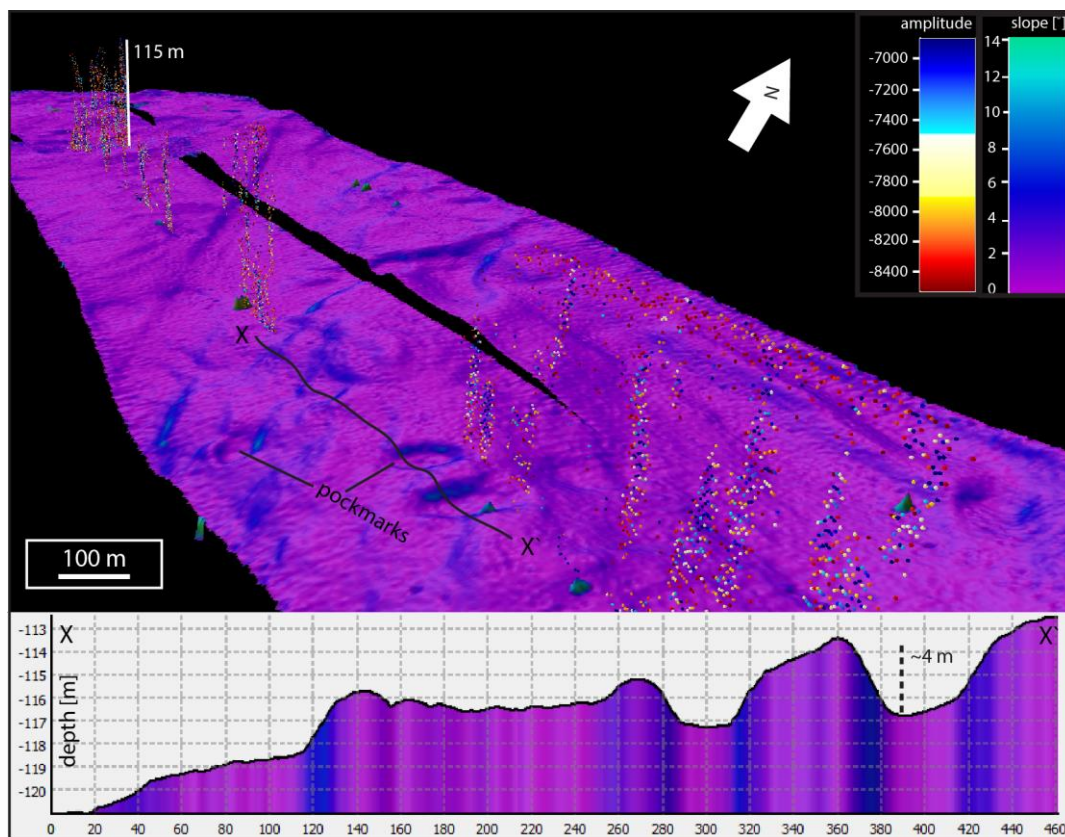


Fig. 2.4 Perspective view of the shelf area east of the shelf break, with the slope angle attribute applied. Visible evidence of flares associated with seabed deformation. Profile X-X' cross-cuts several large pockmarks aligned transversely to the ridge.

Fig. 2.3b reveals the highest pockmark concentration irregularly distributed along the transversely oriented ridge, probably of glacial or glactectonic origin. The detailed morphology of this feature cannot be described due to a lack of data. Further to the east on the shelf, some 200-300 m long, shallow and branching features are interpreted as meltwater channels. Another

prominent, elongated feature can be observed in Fig. 2.4 just NW of the ridge following the ridge towards the shelf break. It is 1.7 km long, up to 5 m deep and has a relatively uniform surface. This feature is also interpreted as a meltwater channel. However, its nearly linear orientation does not exclude processes of ploughing.

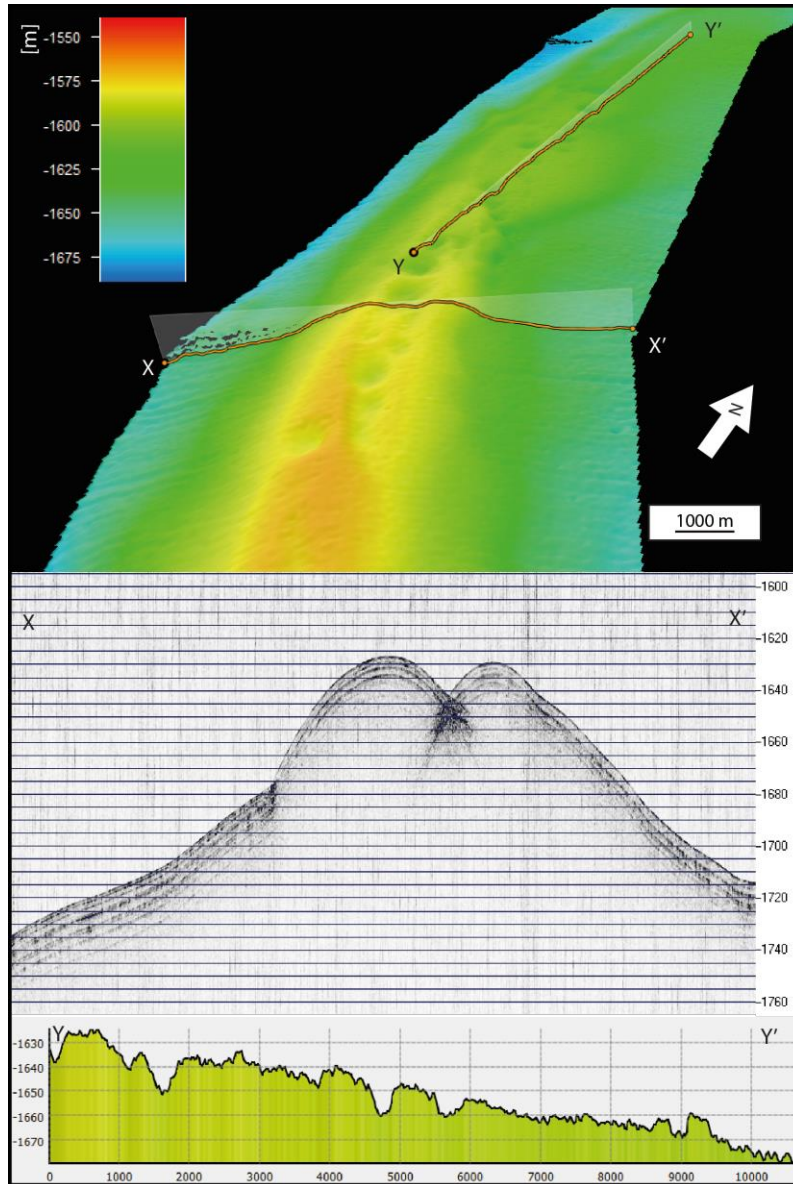


Fig. 2.5 Perspective view of the pockmark area on the north-western flank of Knipovich Ridge (vertical exaggeration: x6). Pockmarks are concentrated along the crest of the ridge which indicates a vertical migration of gas through the sediments. Profile X-X' shows a chirp cross-section across the ridge. The Y-Y' profile shows a cross-section along the pockmark field on the crest of the ridge.

The multibeam survey performed at the north-western part of Knipovich Ridge, south of the Molloy Fracture Zone, reveals an arcuate S-N oriented ridge bending from SE and then following the main drift towards north (Fig. 1.1 and 2.1b). It is located at depths of 1600 m on average and has a narrow elongated crest along the whole ridge (Fig. 2.5). The average slope angle on the western flank of the ridge is 3-4°, whereas on the eastern flank it is 2°.

Chirp profile X-X' displays a pockmark located on the crest of Knipovich Ridge (Fig. 2.5). The pockmark is imaged as v-shaped seabed depression. The chirp profile indicates that the bottom of the pockmark has a relatively high acoustic impedance, suggesting no - or little sediment infill in the crater. The pockmark is located at a water depth of c. 1630 m. It is about 660 m wide and 15 m deep. Beneath the seabed depression, vertically stacked concave reflections can be observed. They show the same width as the pockmark and dip into the center of a bowtie artefact. This artefact is typically associated with the geometry of pockmarks imaged by the profiler and the presence of gas within the sediments (Judd and Hovland, 2007). However, within this profile, it was not possible to determine gassy sediments and gas chimneys which can be distinguished by very bright reflections from their upper boundary. The ridge is covered by a sedimentary package comprising at least three parallel to sub-parallel, well-stratified reflectors of medium intensity. The sediment thickness of this acoustically stratified unit varies, i.e. thinner at the crest and the eastern flank (~7 m) and thicker at the base of the western flank (up to 14 m), where Eiken and Hinz (1993) suggested a possible current controlled origin for the sediments.

At the northern part of Knipovich Ridge, the eastern slope angle is up to 12° (Fig. 2.6). The slope dips gradually towards a rift valley, where the average inclination is 0.5°. There is also some indication of slumping, which appears as gradual, irregular corrugations oriented transversely to the slope. Over 50 oval depressions have been identified in this area. Their dimension varies from 2 to 16 m in diameter and 40 to 500 m in depth.

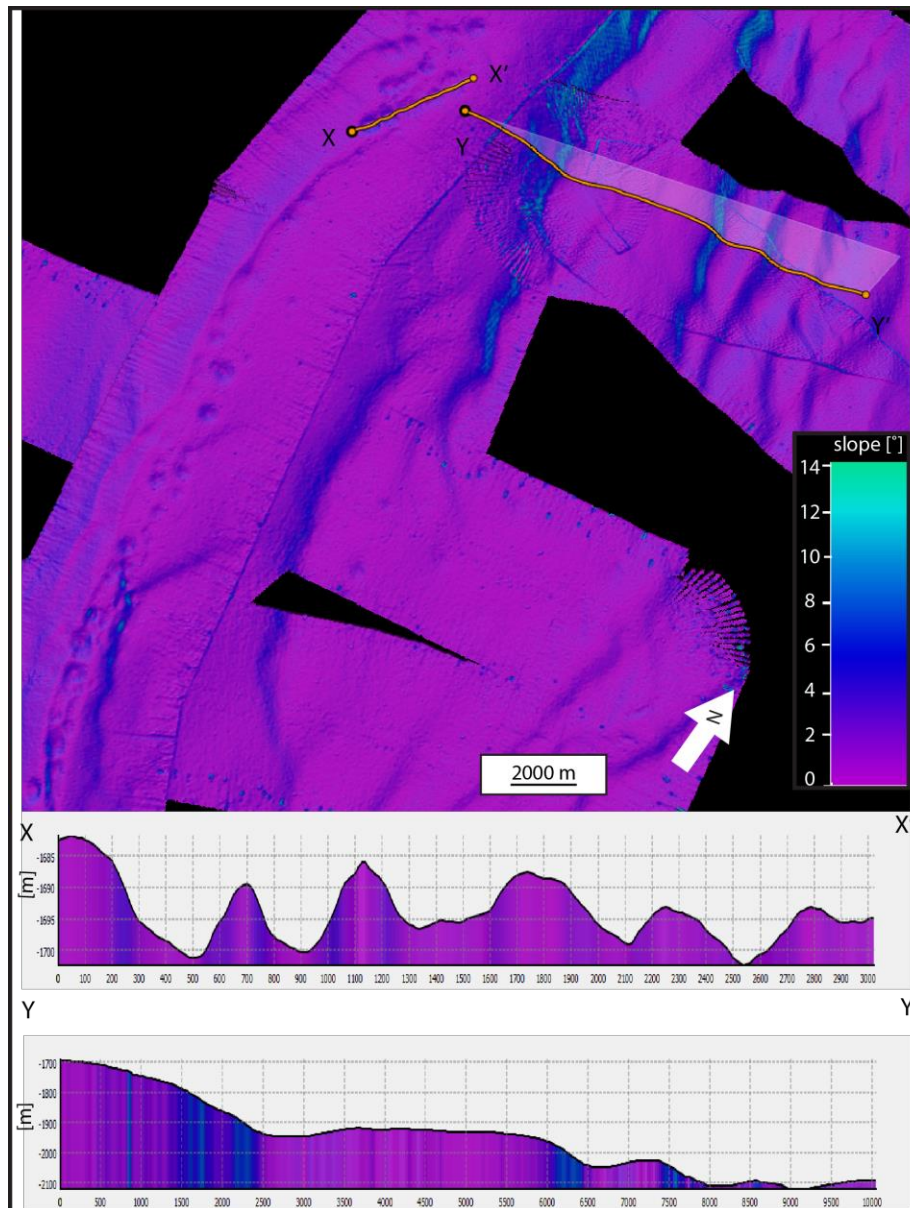


Fig. 2.6 Vertical projection of the pockmark field on the crest of Knipovich Ridge, with emphasized slope angle. Profile X-X' shows a cross-section along five closely spaced pockmarks at the northern part of the ridge, whereas profile Y-Y' cross-cuts the transversely oriented corrugations on the slope.

Pockmarks occur throughout the whole sediment drift, but are mostly concentrated along the center of the ridge, following the crest. The pockmark field on the ridge has a length of 2.8 km. It can be divided into 3 areas, where the depressions occur in 'clusters' in relatively short distance from each other. The southernmost field covers an area of 1.5 km<sup>2</sup> and consists of at least 16 very closely spaced, small pockmarks, with a size ranging from 1-2 m in depth and from 40-100 m in diameter. The middle pockmark field extends along the crest over 14 km and consists of 27

pockmarks with varied shapes and sizes ranging from 2 to 11 m in depth and 100 to 300 m in diameter (Fig. 2.5 and profile Y-Y' in the same figure). The northernmost pockmark field is 3 km long and 2.2 km wide. It comprises 13 large pockmarks, linearly distributed next to each other and closely spaced, so that each pockmark chain is parallel to the other (Fig. 2.6 and profile X-X' in the same figure). The pockmarks in this field have a regular shape and similar size varying from 7 to 11 m in depth and 200 to 400 m in width. The internal morphology of the pockmarks on the ridge is irregular. The surface is hummocky and all the features are closely spaced, in several cases overlapping each other. This indicates focused and local events of fluid or gas seepage. However, no flares associated with the pockmark fields have been identified in this area. Compared to the shelf area, the general morphology of the ridge is more uniform and not as intensely deformed. The pockmarks on the ridge are significantly deeper and wider than those on the shelf. They are also more regularly distributed and not connected, except for a few cases where they overlap.

### 3. 2D Seismic study of the Svyatogor Ridge

#### 3.1. Acquisition

A 2D seismic dataset was acquired using the P-Cable system (e.g. Petersen et al., 2010; VBPR patent 2003). The P-Cable system is designed for high-resolution imaging of shallow subsurface horizons (penetration depth is usually less than the seafloor multiple). The P-Cable system can be deployed as a 2D streamer or 3D array. The streamers used during CAGE 14-1 are solid-state streamers, designed to reduce both noise from the shallow sub-surface and along-streamer noise. In this case streamers were arranged in a single line for 2D acquisition (Table 3.1). The streamer is towed behind the ship with an offset of 100m, where channel 1 is the closest to the airgun (Fig. 3.1). Acquisition of the 2D seismic data began on 22/06/2014 (day 4 of CAGE 14-1 cruise).

Table 3.1: Acquisition parameters of 2D seismic data aboard H/V Helmer Hanssen (CAGE 14/1)

Shot rate	5-6s
Max. ship speed	5 knots
Number of channels	32
Channel Spacing	3.125m
Streamer length	25m per section
Near offset (gun offset)	65m (15m)
Air gun	2x mini-GI (15/15 in <sup>3</sup> and 40/40 in <sup>3</sup> )
Gun position behind ship	33m
Shooting pressure	160-170 bar
Signal frequency	10-400Hz
Record length	1.5-2s
Sampling rate	0.25-0.5ms
Delay	0-3.5s

Some acquisition parameters like sampling rate, recording time delay and record length need to be adjusted as per depth of sea floor and our area of interest. All the changes in the recording parameters are saved in the log file (Appendix 1). Seismic data was collected over two days, with 10 lines acquired (Fig. 3.2; Fig. 3.3) across the Knipovich spreading ridge and the southern extension of the Vestnesa Ridge.

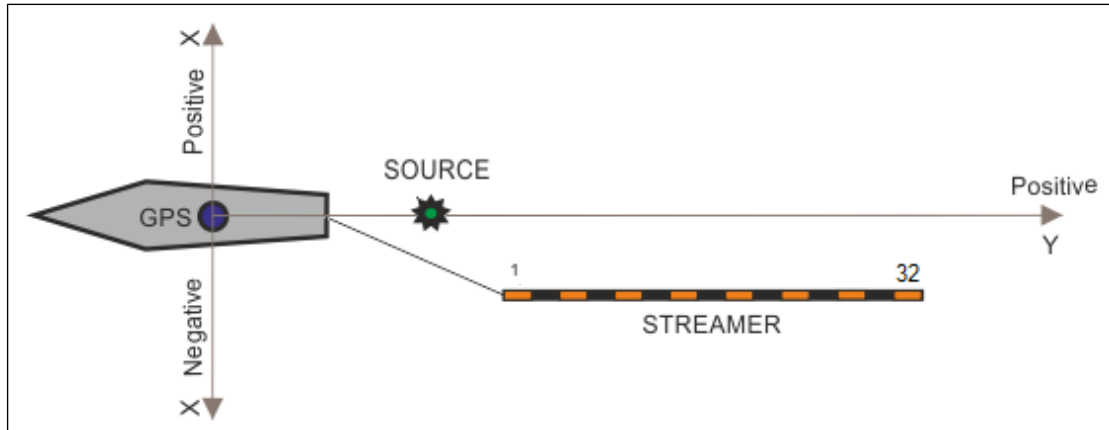


Fig. 3.1 Survey configuration

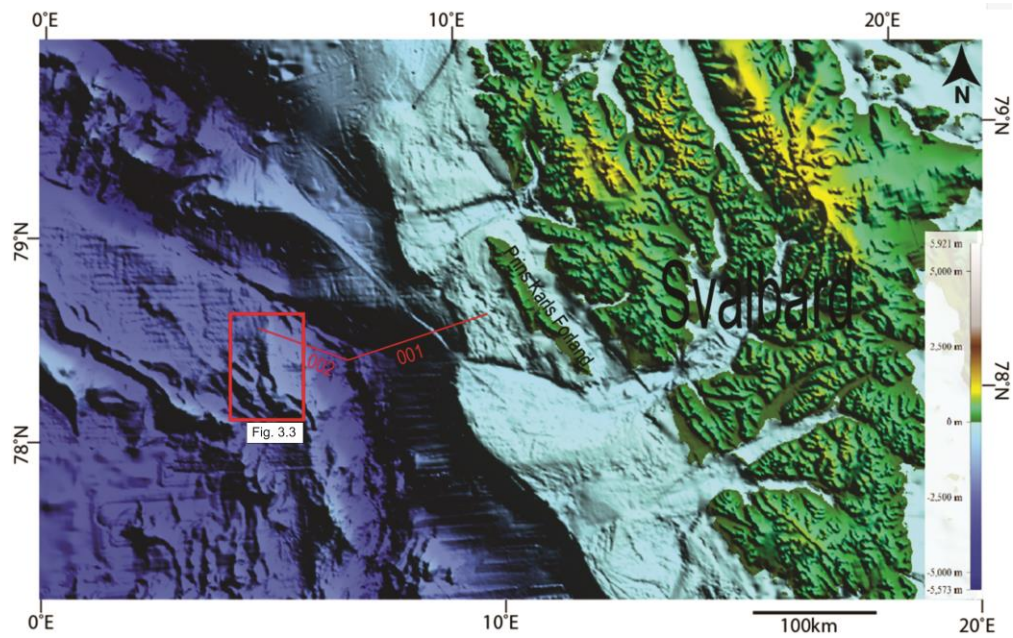


Fig. 3.2 Orientation and position of 2D seismic lines 001 and 002 regionally. Fig. 3.3 box shows the area that is the focus of this survey.

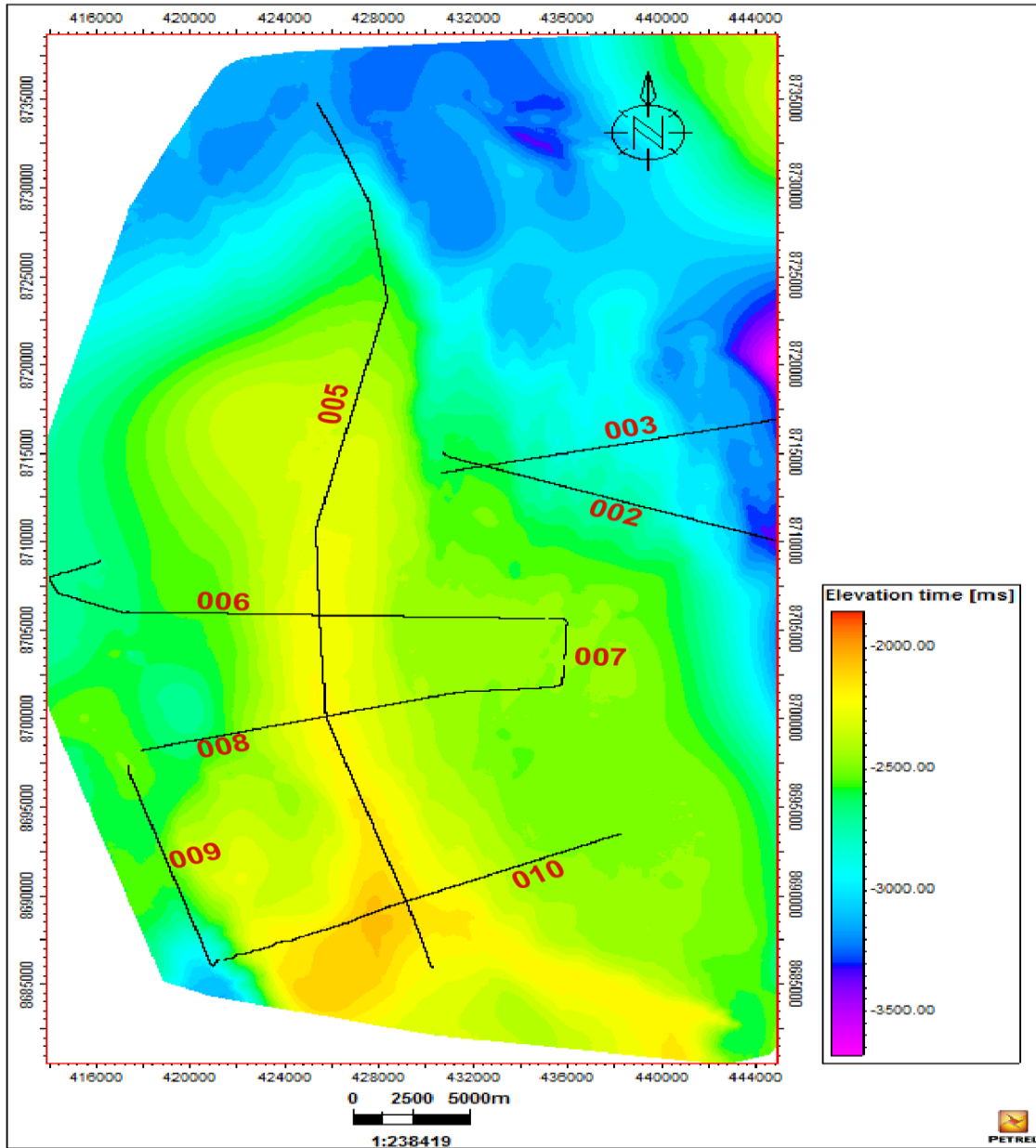


Fig. 3.3 Bathymetry data taken over the study area (Svyatogor Ridge) and the corresponding seismic lines. Line 004 is missing in the final data set. Line 005-010 are the focus of interest, line 002 extended a line from a previous survey and line 003 is a transit line.

### 3.2. Processing

On-board processing of the 2D seismic data was carried out in RadExPro®, software designed by DECO Geophysical. The data processing flow is shown in Fig. 3.4.

Seismic data is recorded in SEG-D format and imported into RadExPro for processing. This data contains shot gathers i.e. every file contains traces from all the channels. Some channels may be discarded during acquisition if quality of signal recorded by that channel is poor. In this case channel number 29 and 32 were discarded due to high noise level.

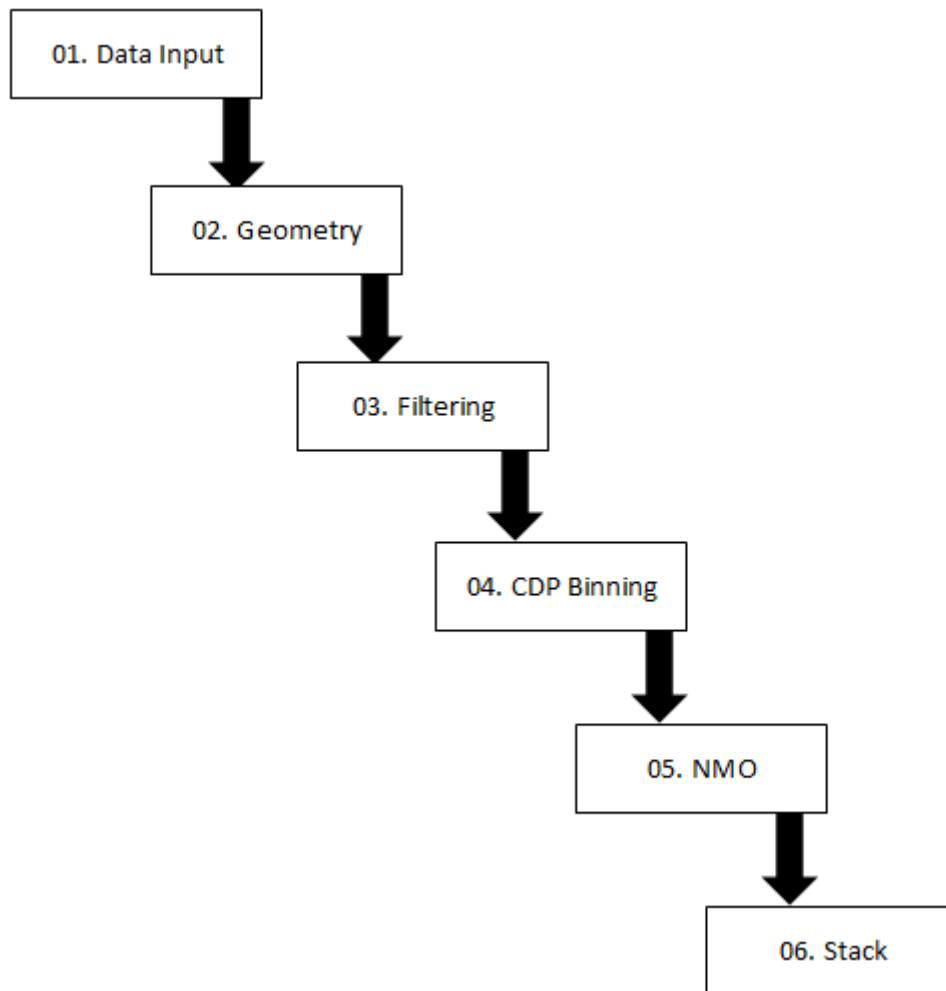


Fig. 3.4 Workflow of basic on-board processing of seismic data during CAGE 14-1

After SEG-D files have been imported in the RadExPro software, geometry needs to be assigned for further processing of seismic data. In order to completely define geometry, coordinates of every shot point and receiver group have to be imported. A GPS is attached below the air gun, which continuously records location of the source. The time at which a shot has been

fired is also recorded with an accuracy of  $1\mu\text{s}$ . There can be a difference between the trigger time and firing time of a shot, called the gun delay (usually around 14ms). This delay is accounted for while recording shot time. Location of receiver groups when the shot is fired can be estimated by taking into account the distance between source and receiver groups. All these parameters are imported in software using the “Marine Geometry Input” module in RadExPro. The location of different receivers can be determined from source location. If the ship is assumed moving in south direction, first receiver coordinate will be (Source X coordinate – 15m, Source Y Coordinate - 33.625 m) and location of different receiver group can be obtained by further subtracting 3.125m from Y coordinate for each receiver group. For ship moving in any other orientation other than south direction, the exact coordinates of different receiver group can be found by taking components of X offset and Y offset along true X and Y directions. The study area is extended across two different UTM coordinate zones. So before the navigation data can be added to data headers, all coordinates need to be converted into a uniform system. This was carried out in GTM converter and the updated navigation file can be added into the geometry database. Ensuring all coordinates are in the same zone is crucial; otherwise the line appears to be broken by a  $3^\circ$  margin. Once the “Marine Geometry Input” module is run, it will show the number of traces and shots on which geometry has been applied. If there are any shots or traces that are discordant with the navigation file, a dialog box will appear indicating the number of shots or traces affected.

Filtering and quality control is used to improve the signal/noise ratio. The filter used for this data set is a simple band pass filter (25-40-400-500). A band-pass filter is applied at both pre-stack and post-stack phases. A spherical divergence amplitude correction and exponential correction with 3dB/ms are applied next. The spherical divergence correction takes into account the reduction in amplitude of the signal as it radiates spherically from a source. Exponential correction takes into account the intrinsic attenuation. In this way, channels farthest from the source are improved, as well as deep reflections in near channels.

Common depth point (CDP) binning is a process whereby data points with coordinates that fall into boxes (bins) of pre-defined size are grouped together. The subsurface can be broken up into an infinite number of slices; it is not possible to perfectly image the Earth’s subsurface. Therefore, the more data points per CDP bin, the better will be the quality of the data. CDP bin size should not be so small that the number of data points cannot appropriately cover the bin, so the CDP bin size is often defined as half of the channel spacing. But only 2-4 traces fall in each

CDP bin with 1.625m bin size (half of the channel spacing). So a bin size of 3.125m is selected to have an adequate number of traces per CDP. In RadExPro, to perform binning of the data, each data point must have source and receiver coordinates, a source (shot) number and the data must be sorted in order of source number.

Normal Move-Out (NMO) is the process of correcting the data set for arrival time variance due to the offset of channels away from the airgun. This correction is based on velocity of the subsurface. For this data set during the on-board processing, a simple, 1D velocity model of  $1500\text{ms}^{-1}$  is used as this is the velocity of sound through water, and we can assume that the sediments are very saturated, at least in the shallow subsurface. Once NMO has been corrected, traces can be stacked. Some traces may not have been assigned a CDP bin, due to either falling outside of the bin range, or a coordinate problem. These traces are assigned a CDP value of -1, and so we have used a data filter to exclude these traces from the stacking process.

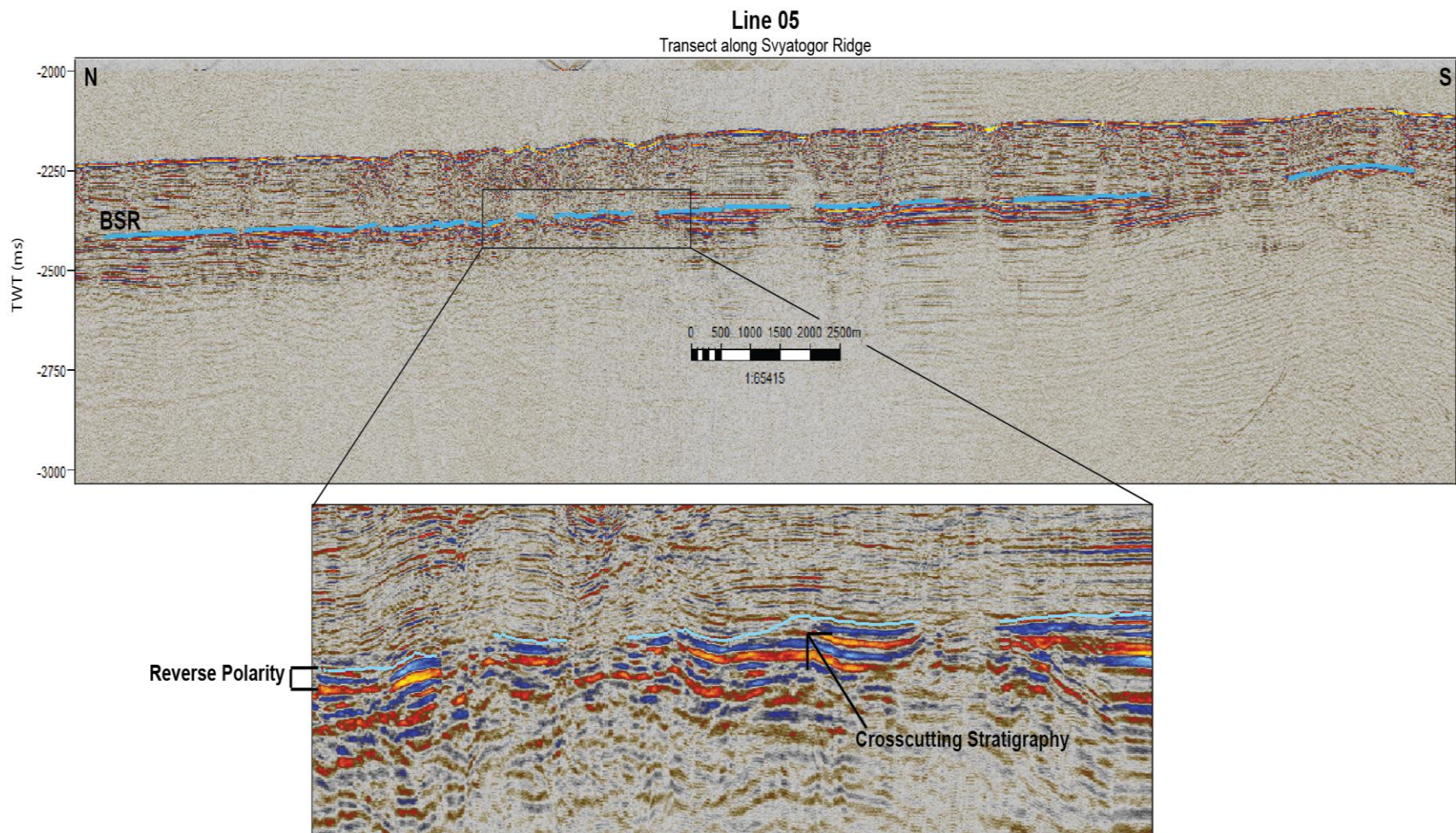


Fig. 3.5 Line 05 (transect along Svyatogor Ridge) showing the interpreted BSR (blue interpreted horizon). This high amplitude feature is interpreted as a BSR because it is discordant with pre-existing stratigraphy and is opposite polarity to the seafloor.

### 3.3. Interpretation

The objective of the seismic acquisition during CAGE 14-1 was to test the potential of the Svyatogor Ridge (Fig. 3.2; Fig. 3.3) for gas hydrate and free gas reservoirs. Prior investigation of the shallow sub-seafloor features in this area is limited to one seismic line ending at the apex of the ridge, showing a strong BSR (Johnson et al., submitted). It is hypothesized that the Svyatogor Ridge began forming as part of the Vestnesa Ridge further north, and then became offset by the Molloy Fracture Zone (Johnson et al., submitted). Interpretation of the seismic lines collected during CAGE 14-1 is carried out in Petrel Software Platform. First-pass interpretation of the seismic data is performed which excludes advanced seismic data analysis methods like seismic facies and attribute analysis.

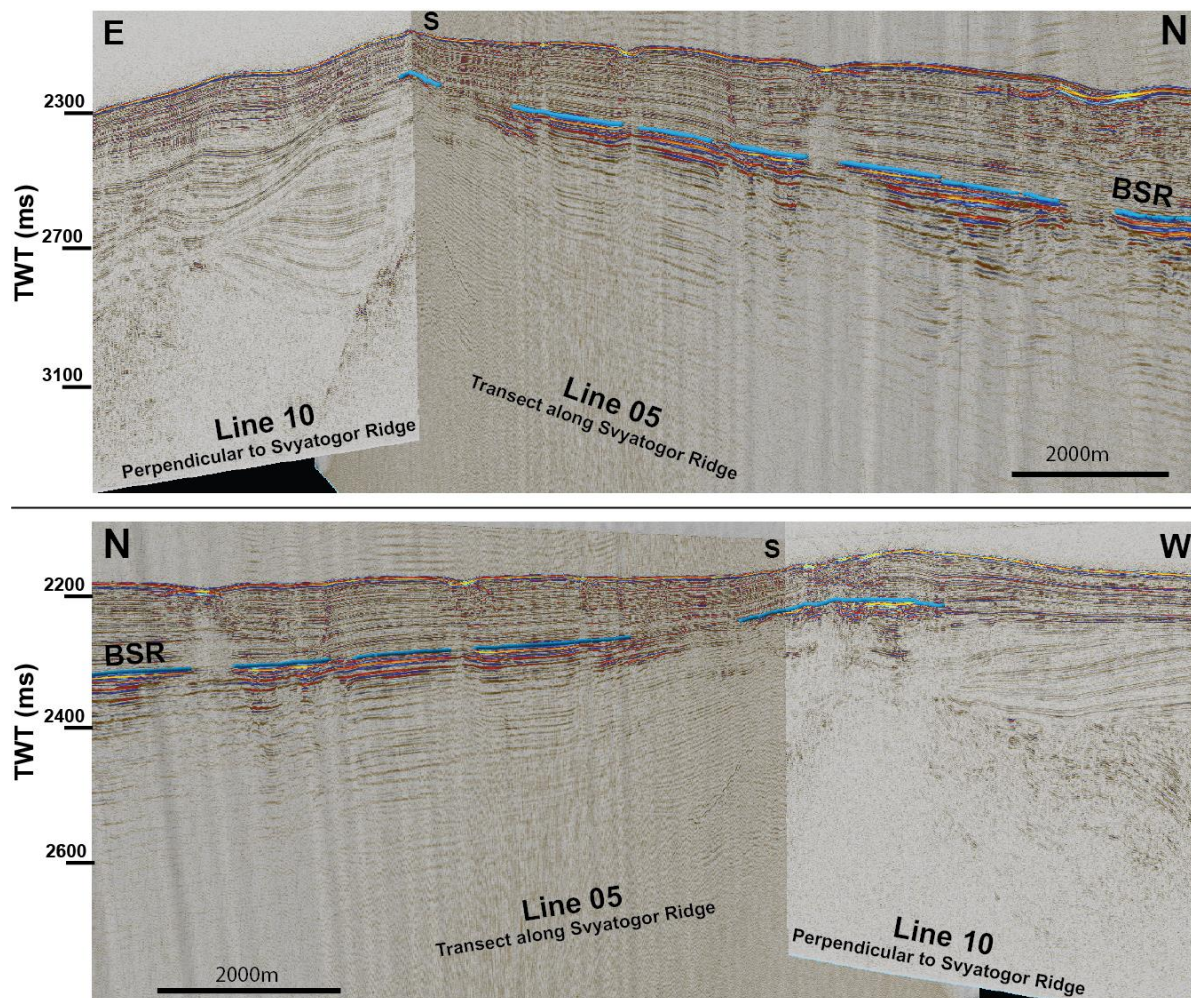


Fig. 3.6 The BSR (blue horizon) extends along the Svyatogor Ridge, however it does not extend significantly off the ridge, it is confined to the axis of the Svyatogor Ridge.

### 3.4. Evidence for gas hydrate and free gas reservoirs on Svyatogor Ridge

Typically, in seismic data the presence of gas is evidenced by a BSR reflector, which is caused by a density contrast between different materials (i.e. solid vs. fluid) filling pore space [Pecher *et al.*, 2001]. In the case of a BSR reflector, the density contrast is created by interface between solid gas hydrate and fluid free gas. Such an amplitude anomaly can also occur when pore fill changes from free gas to water, water to air, gas to air etc., although the anomaly should be less pronounced than in the solid-fluid case [Pecher *et al.*, 2001]. The BSR occurs at the base of the hydrate stability zone, which is governed mostly by pressure and temperature conditions. Due to this control, the BSR often mimics the seafloor and therefore, cross-cuts the sedimentary strata [Berndt *et al.*, 2004; Maslin *et al.*, 2012; Pecher *et al.*, 2001]. A continuous high amplitude reflection parallel to the sea floor reflection is observed in all the lines that intersect the Svyatogor Ridge. These reflections have a polarity opposite to the polarity of the sea floor reflection and are found to be discordant with the pre-existing stratigraphy; therefore they have been interpreted as a BSR (Fig. 3.5). In this case, the BSR has its highest amplitude right at the top of the Ridge, and disappears very quickly with distance from the topographical high (Fig. 3.6).

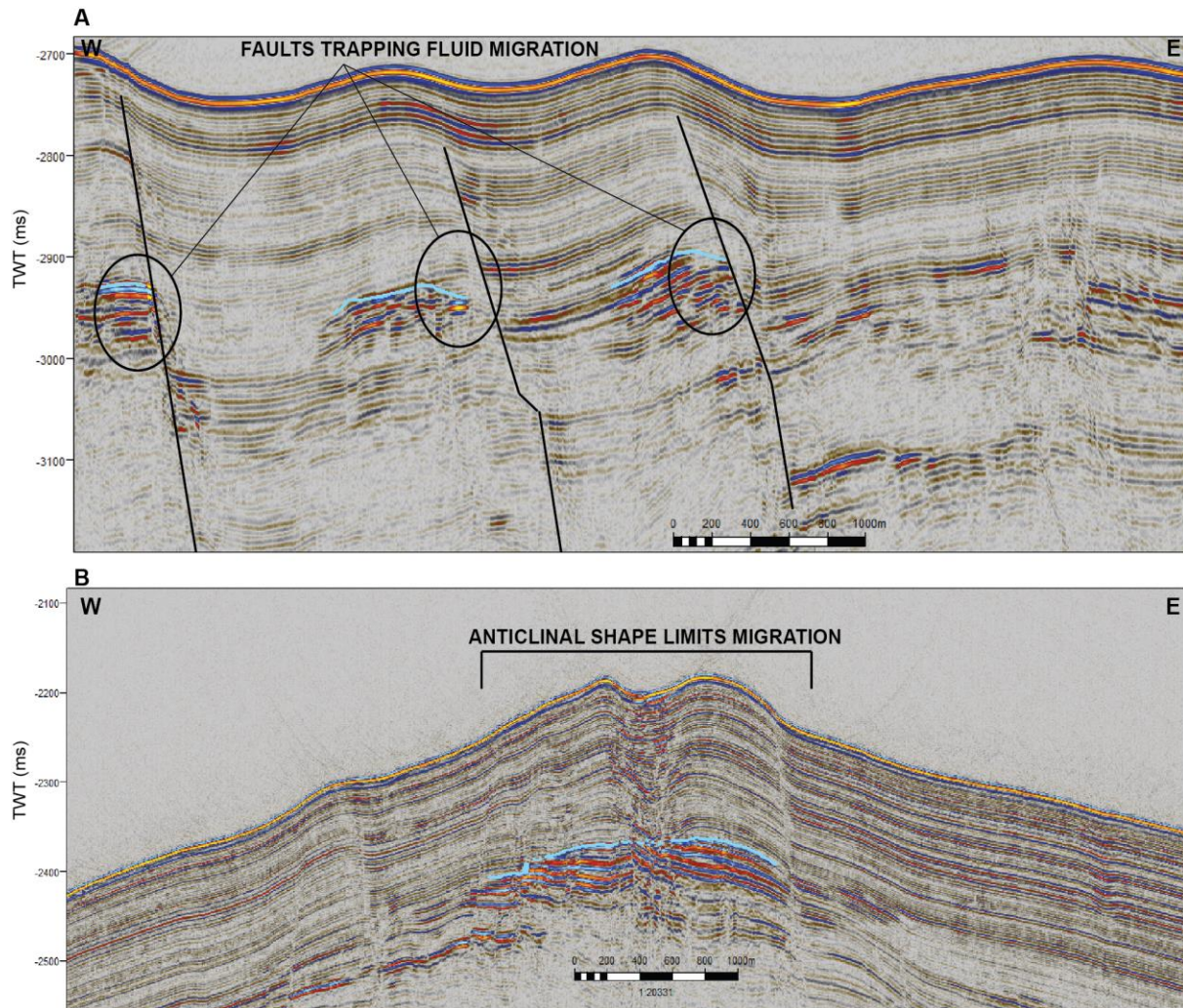


Fig. 3.7 A) Faults act as traps, stopping further migration of fluid. This is shown by a high amplitude reflector, which is observed truncating against a fault. B) Upwards migration stops when a fluid has reached the apex of an anticlinal structure. In this scenario, the reservoir must be overlain by a cap rock with limited porosity/permeability. In this case, the cap may be gas hydrate.

As well as a BSR, there is other evidence of gas accumulation on the Svyatogor Ridge. There are small areas of increased amplitudes in structural anomalies, which is often diagnostic of trapped hydrocarbons [Biddle and Wielchowsky, 1994; Brown, 2004]. In this data, traps include faults (Fig. 3.7a) and anticlinal structures limiting further upward migration (Fig. 3.7b). Along the Svyatogor Ridge itself, there are small circular/elliptical seafloor depressions imaged (Fig. 3.8). These features appear to be related to gas escape as they are higher in amplitude than the surrounding undisturbed seafloor, and they have regions of disturbed, hummocky reflections, or complete blanking beneath (Fig. 3.8). The BSR beneath these features is also discontinuous (Fig.

3.8). All these features are diagnostic of pockmarks caused by gas release [Heiko Sahling *et al.*, 2008]. In some cases, the high amplitude depression structure is buried by a lower amplitude seafloor, but the seafloor still maintains concordance with the depression (Fig. 3.8), resulting in a bathymetry that still shows circular depressions.

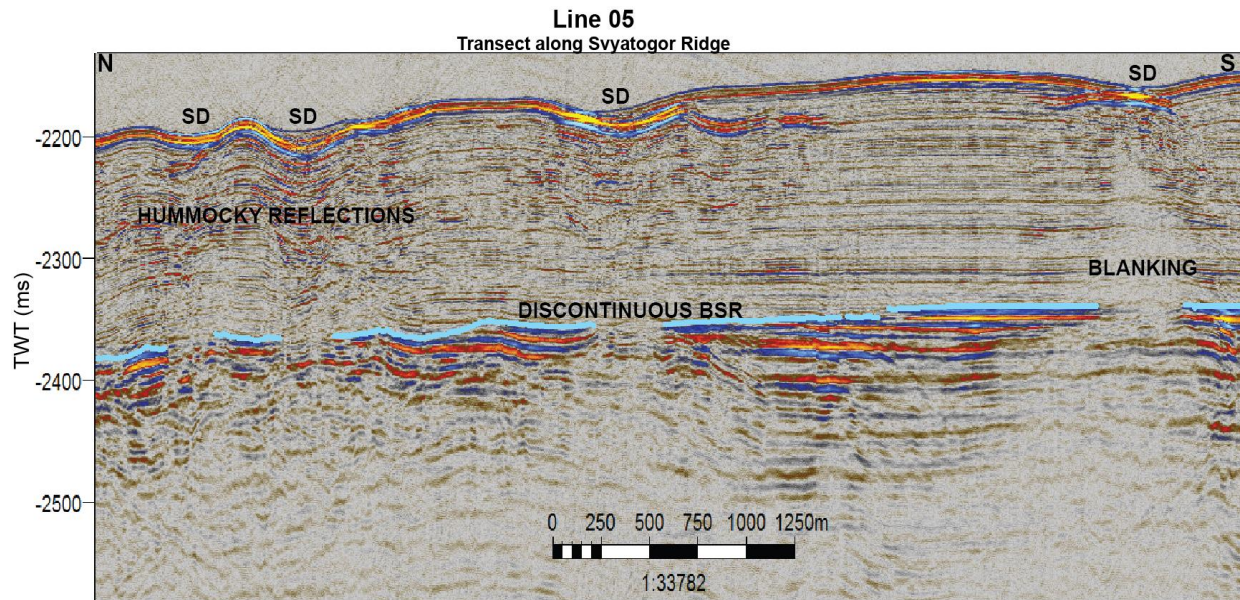


Fig. 3.8 A number of seafloor depressions (annotated 'SD') were observed along the Svyatogor Ridge. Beneath these circular depression structures are regions of blanking or hummocky reflections, and a discontinuous BSR. The depressions themselves have a higher amplitude than the seafloor. In some cases, the amplitude anomaly is buried, but the seafloor reflection maintains concordance with the depression structure.

### 3.5. Faults and their origins

There is a variety of faults imaged in the seismic lines acquired during CAGE 14-1. The regional tectonic regime is quite complex; to the east of Svyatogor Ridge is the Knipovich Spreading ridge and to the north is the Molloy Fracture Zone. This implies that there are potentially two stress regimes interacting across the Svyatogor Ridge.

Faults identified in the seismic data from Svyatogor Ridge appear to fall into two categories; large scale, steep dip normal faults and small normal faults with a variety of dip angles (Fig. 3.9). An initial hypothesis for the variation in fault type is that the large normal faults are detachment faults related to spreading in the Knipovich spreading ridge. The large normal faults appear to only be observed in the south of the Svyatogor ridge, coincidentally where there the BSR reflection is comparatively lower amplitude. This effect is most likely related to the reduced free gas quantities – seismic energy is able to penetrate further when there is a reduced quantity of

gas present in the sub-surface. Therefore, we are able to better image the basement and other features below the gas reservoir at the south end of Svyatogor Ridge better than the north.

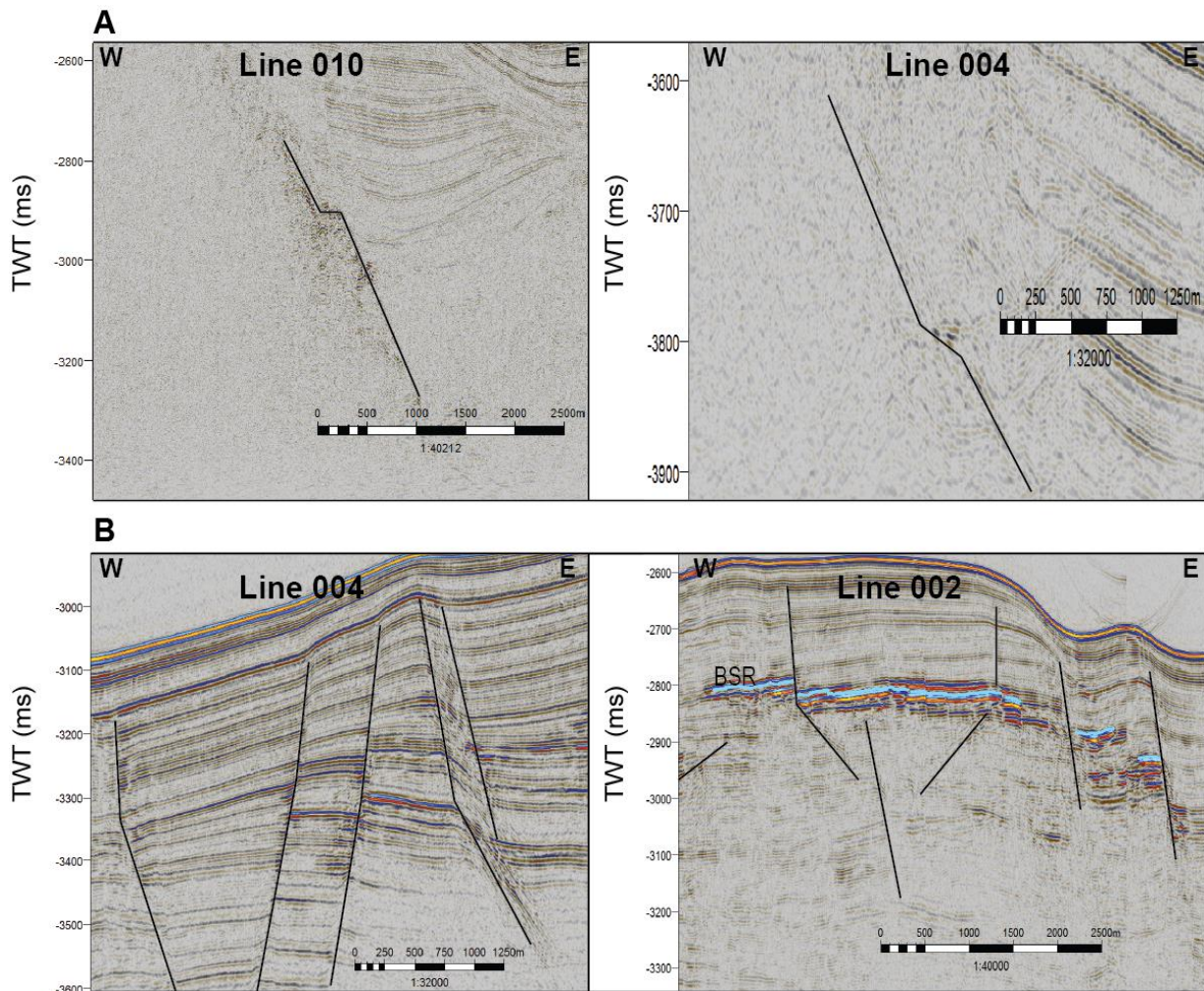


Fig. 3.9 A) Examples of large steep dip normal faults. These features are interpreted to be detachment faults related to spreading along the Knipovich spreading ridge. As these faults are deep within the seismic data, they are not well imaged, especially where the BSR amplitude anomaly is high. B) Smaller normal faults with a variety of dip angles are common in the top second of the data set. These faults appear to increase in offset with depth. Fault terminations are mostly buried.

Towards the north of Svyatogor Ridge, confined within certain seismic reflections are small pockets of increased amplitude immediately beside faults (Fig. 3.7A). These features are interpreted as gas pockets trapped from further lateral migration by faults. In the south of Svyatogor ridge, however, there are similar fault structures, yet these faults do not have the same

amplitude anomaly nearby (Fig. 3.10). Fault seals can be created through a number of mechanisms [Yielding *et al.*, 1997]:

1. When a coarse grained (reservoir) unit becomes juxtaposed against a fine grained (seal) unit across the fault [Yielding *et al.*, 1997]
2. When clays are entrained in the fault and create a high entry pressure barrier to fluids entering the fault zone [Yielding *et al.*, 1997].
3. When mineral grains are crushed in the fault zone creating an overall finer grained texture inside the fault zone [Yielding *et al.*, 1997].
4. When diagenesis occurs along a fault, removing any primary porosity [Yielding *et al.*, 1997].

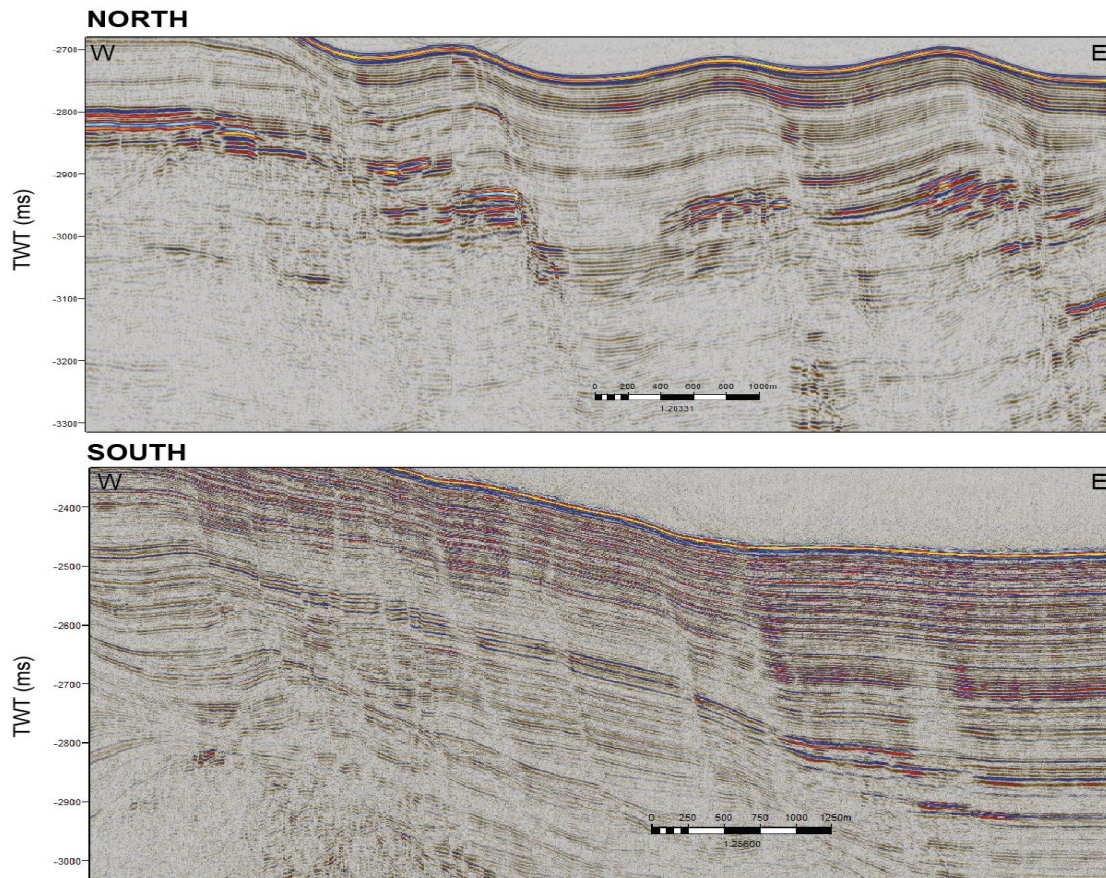


Fig. 3.10 In the north, faults have an amplitude anomaly in some horizons immediately next to the fault. This is interpreted as trapped gas as it synchronizes well with where we expect the BSR. In the south, however, even though there is evidence of gas charged sediments (a BSR), similar faults do not have regions of anomalously high amplitudes beside them. The faults in the north are interpreted to be sealing faults, while the faults in the south may either be leaking, or there is simply no fluid for the fault to trap. As there is still evidence of gas (a BSR) in the south,

it is unlikely that there is completely no fluid to trap, however there is no evidence of gas escape in the past or present at the top of the faults in the south, so this issue will need further investigation.

### 3.6. Paleo-depression features along the Svyatogor Ridge

There are a number of interesting enigmatic features observed in the seismic line running directly down the Svyatogor ridge (Fig. 3.11). These features could be interpreted as either paleo-channel structures or paleo-gas escape features. Topography of the region alone would suggest that these features are not channels, as to cut a channel perpendicular to the ridge would imply the channel incising mechanism flowed up the ridge on one side. Additionally, Svyatogor Ridge is across the Knipovich spreading ridge from land, and at 1800m water depth makes a flow with enough energy to flow uphill and incise channels on the apex of Knipovich ridge highly unlikely. Therefore, these features are interpreted as paleo gas release features. This is supported by the underlying seismic data; there are regions of blanking and/or disturbed, hummocky reflections beneath these features, they are higher amplitude than the surrounding reflections, and finally they appear connected to the current day seafloor depression structures. Interestingly, these features appear to migrate significant lateral distances, as well as migrating vertically (Fig. 3.11).

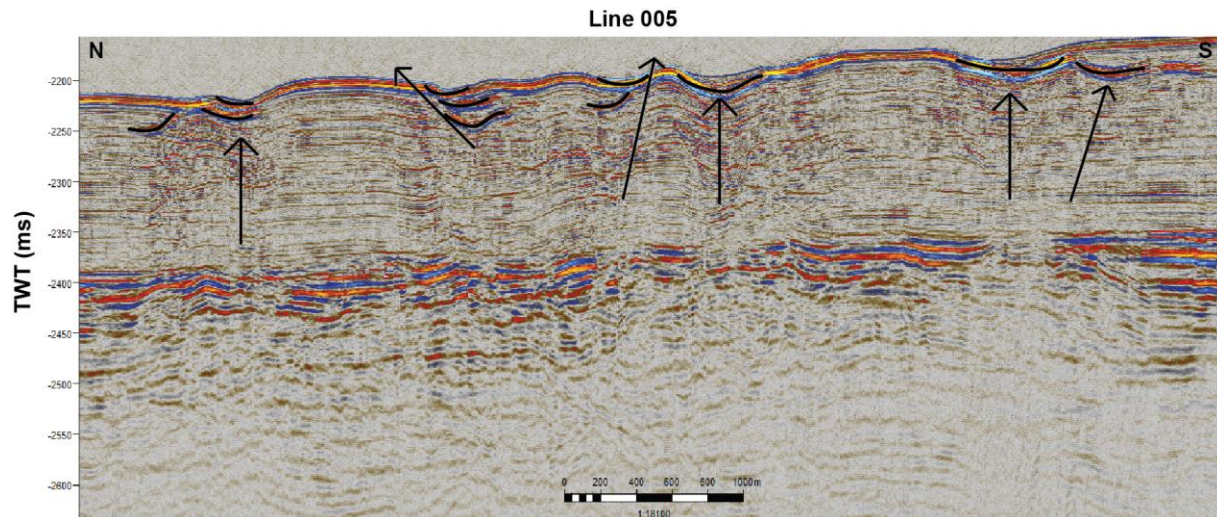


Fig. 3.11 Along the transect of Svyatogor Ridge, there is a region with numerous paleo depressions. The interesting thing about these paleo depressions is they do not necessarily migrate directly upwards, rather there is some lateral migration as well. Additionally, some of the features (rightmost two) are buried under a lower amplitude seafloor reflector.

## 4. Hydrographic survey

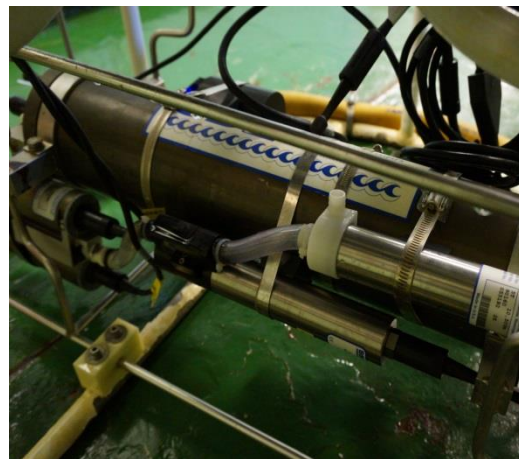
### 4.1. Instrumentation and procedures for data collection

The research Vessel Helmer Hanssen is normally well equipped for ocean surveys, and on this cruise additional instrumentation was brought onboard for a very broad array of measurements, ranging from marine biology, oceanography and atmospheric data to seismic and sediment core data.

Some of the measured water column data were available for immediate processing, while other data depends on sample analyses which can only be performed in specialized laboratories. A total of 95 hydrographic stations were performed at the West Svalbard Margin (Fig. 1.1, 4.5a).

### 4.2. Conductivity, temperature, depth (CTD survey)

A Seabird 911+ CTD, attached to a water sampler rosette (Fig. 4., left), was used for acquiring water column data. Sensors for temperature, pressure, oxygen concentration, turbidity, fluorescence and electric conductivity, giving salinity are attached to the CTD, which is lowered and heaved through the water column while sampling at 25 Hz. Post processing of the water column data includes conversion of raw data (voltage) using polynomes for each sensor into physical parameters, spike removal, low pass filtering, loop editing to compensate for ship heave and finally bin averaging over 25 cm bins [*Seabird*, 2013]. The CTD's water unit (Fig. 4.) communicates through a wire and closes bottles for water sampling (nutrients and gas analyses) given a command from the PC in the instrument room via a deck unit.



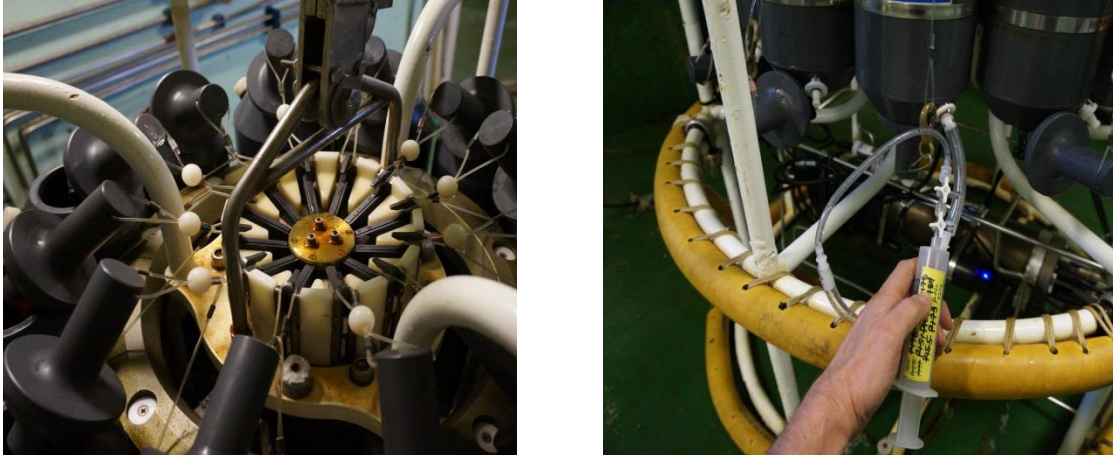


Fig. 4.1 The rosette with Niskin bottles for water sampling at different depths in the water column (top left). The water unit of the CTD (top right), the release mechanism for closing Niskin Bottles (bottom left) and the syringe-tube-valve system for sampling dissolved methane (bottom right).

Prior to the cruise, we checked calibration protocols for all sensors and deck unit. Sensors were replaced and calibrated in January 2014 according to the log files.

### **4.3. Sampling of dissolved methane gas in the water column**

Niskin bottles on the rosette (Fig. 4.) were closed by remote control and samples were taken to analyze the methane concentration at different water depths. A 60 ml water sample from each Niskin bottle was taken, using syringes and silicone tubes with double valves (Fig. 4., bottom right). The syringes were flushed three times with sample water to ensure no air could invade the sample and no residual water from previous samples remained. 5 ml of the water was tapped from each syringe and replaced with nitrogen gas and the syringes were brought into a refrigerator, kept at +2°C. The samples were shaken for two minutes and gas in the head space, now in equilibrium with the water sample, was analyzed in gas chromatograph equipped with a flame ionized detector (FID GC) provided by GEOMAR. Carrier gas ( $H_2$ ) brings the gas sample to a flame ionizer after passing through a capillary column (Fig. 4.) that separates gas species with different molar masses in time (light gas is transported faster than heavy gas). Hence peaks in detector responses after certain times are associated with specific gas species. To measure the gas concentration, a 1 ml gas sample was injected and the resulting flame ionizing detector profile integral corresponding to methane was calculated. The GC calibration line (Fig. 4.) was updated after each station, using gas

samples with known methane concentrations. A total of 95 stations, consisting of 8 -12 samples each, comprise our water column methane dataset.

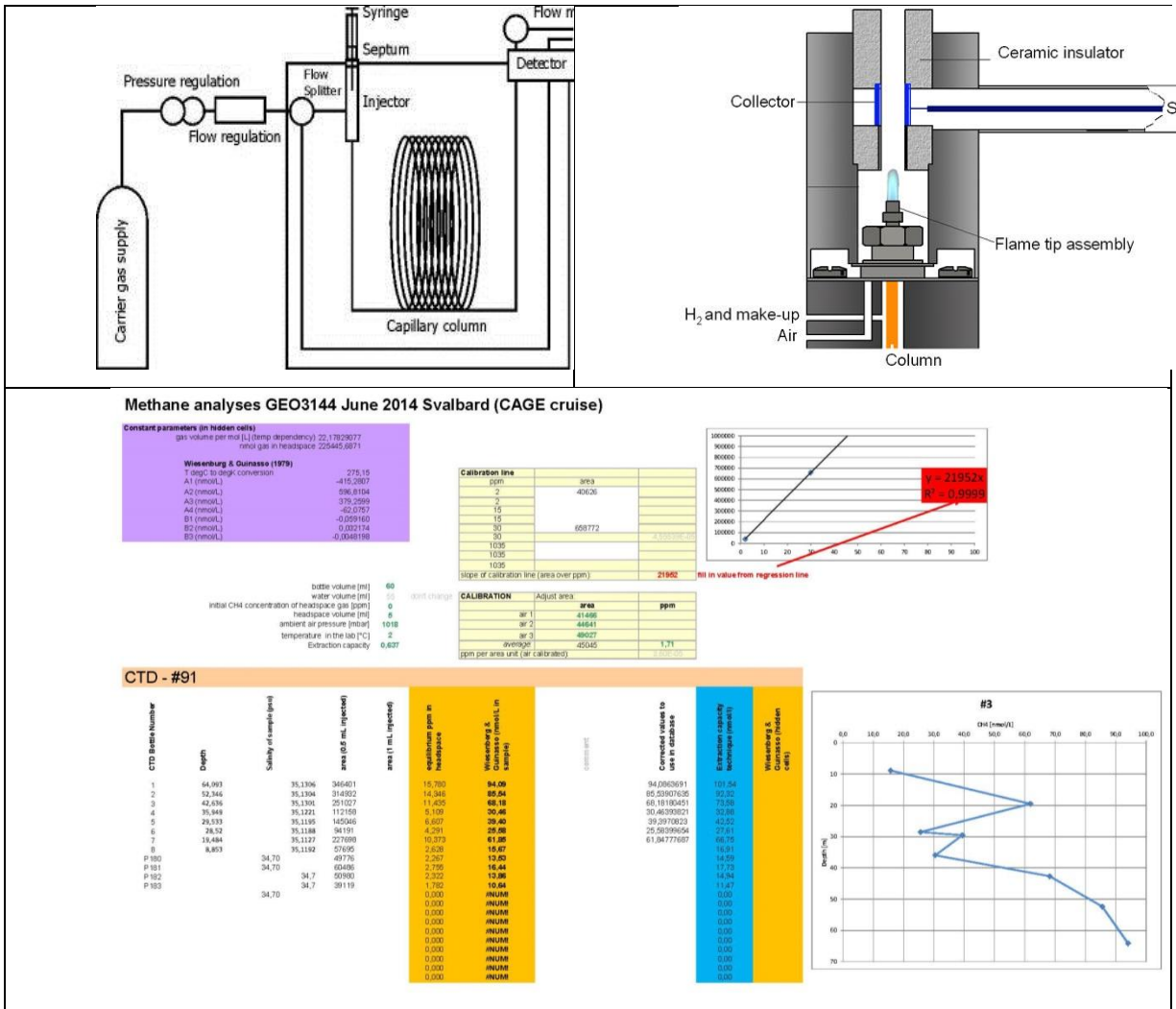


Fig. 4.2 Sketch of FID GC setup and flame ionization detector (top). Methane concentration calculation from FID GC analysis spreadsheet that was used (bottom), (pictures from <http://services.leatherheadfood.com> and <http://www.chem-agilent.co>)

#### 4.4. Nutrient sampling

We sampled water from the Niskin bottles at some of the stations, focusing on the long East-to-West transect from the deep to the shallow end of our survey area (Fig. 1.1). Plastic vials were used for the samples, and were flushed three times with sample water before they were filled and chloroform was added. The samples were stored in closed boxes (dark) in the ship's

labrefrigerator. We expect that results from these measurements will be analyzed in a laboratory in August.

#### 4.5. ADCP

The ship is equipped with a traditional “Ocean Surveyor” Acoustic Doppler Current Profiler (ADCP) from Teledyne RD, operating at 75 kHz. The setup consists of an ADCP-transducer/receiver mounted on the lowered keel (**Error! Reference source not found.**), 7 meters below the sea surface, a deck unit, communicating with the device and a standard PC in the Instrument room.

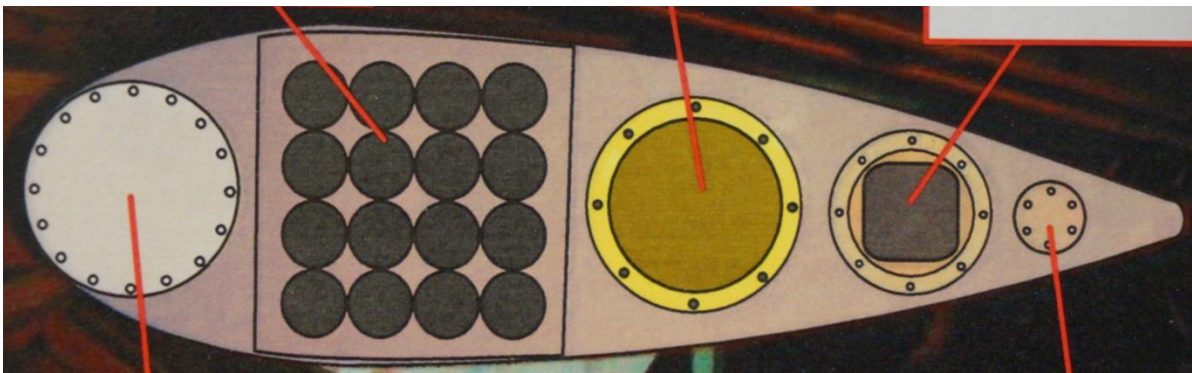


Fig. 4.3 The lowered keel (“senkekøl”) instrumentation on r/v Helmer Hanssen. The ADCP is mounted in the front, followed by a multibeam array and three single-beam echosounders.

After a week of trying to get the installed ADCP software to work, we installed new (free trial) software (ViSea from AquaVision) to record and process the data stream from the ADCP and the ships Navigation system. This software is much more intuitive and easy to operate than the old software (Vmdas and winADCP), which was last updated in 2010. Therefore we suggest that the software should be permanently updated to the new ViSea and the setup should be calibrated and tested.

#### 4.6. Split beam echosounder

RV Helmer Hanssen is equipped with the Simrad EK60 scientific echosounder system. Simrad EK60 is a single-beam echosounder primarily designed for the fishery research, however traditionally used for detecting the gas bubbles in the water column during the scientific research cruises. Gas bubbles releasing from the seabed dramatically change the physical properties of water. The signal backscattered from the bubbles appears on the echosounder record as a distinct hydro-acoustic anomaly, so called “gas flare”. During the cruise we operated 3 different

frequencies, provided by the echosounder – 18, 38 and 120 kHz. Potentially the higher-frequency record is aimed to also detect the bubbles of smaller size; however we noted that 38 kHz is the most appropriate frequency. The methodology of detection and analyzing hydro-acoustic anomalies from the single-beam echosounder data and distinguishing between the gas bubbles and fish is widely used and described by e.g. *Nikolovska et al.* [2008], *Weber et al.* [2014], [*Granin et al.*, 2012].

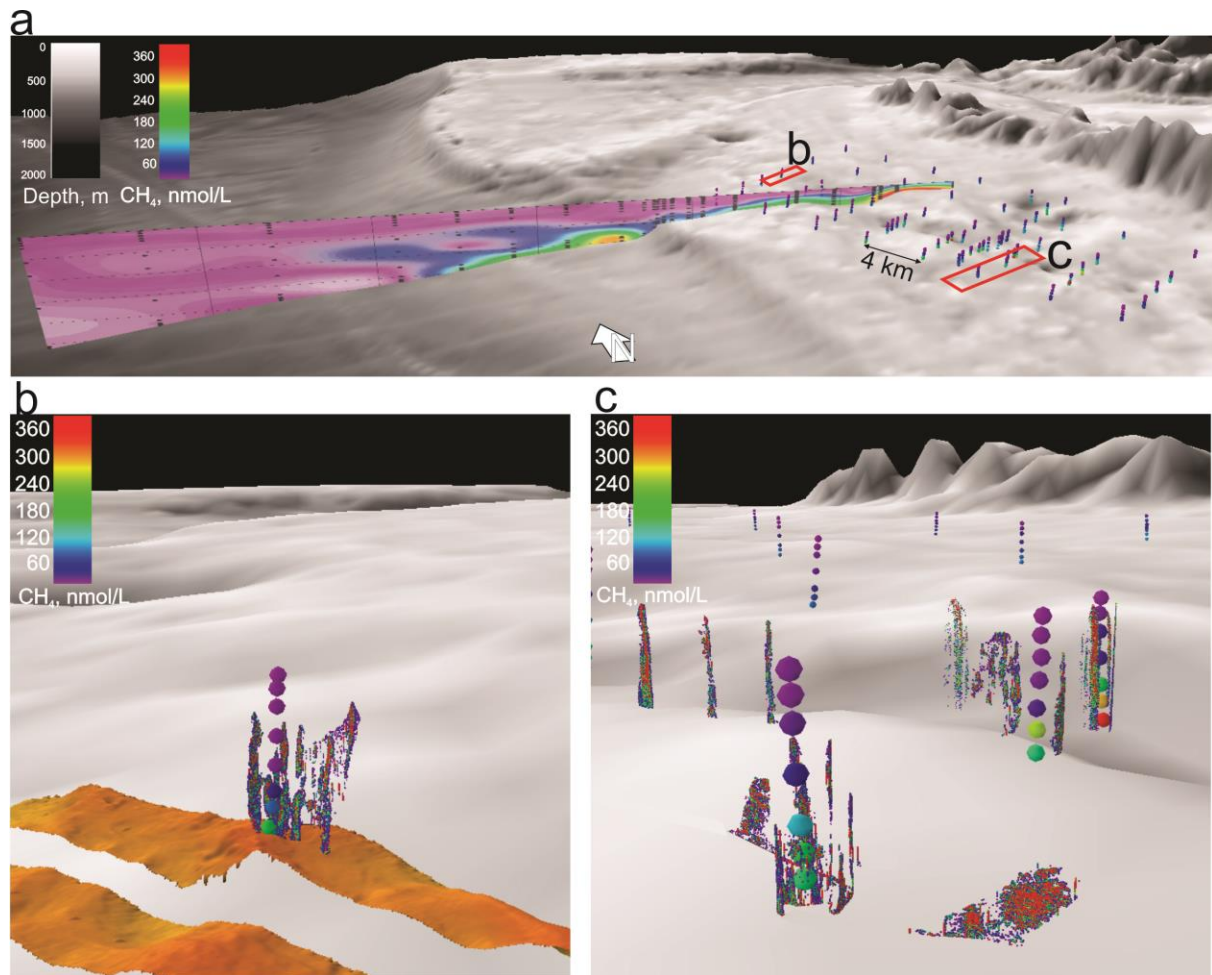


Fig. 4.4 (a) Location of the CTD stations at the West Svalbard margin. Bathymetry is from IBCAO v.3 grid. Colored vertical “curtain” shows interpolated methane concentration between the stations along the deep-water transect. CTD stations at the shallow-water site are shown as vertical chains of balls, where each ball marks the exact location of the single water sample (b, c). The colour of the balls defines methane concentration in each water sample. Methane concentrations show significant increase in the bottom water samples, acquired in the gas seepage spots. Coloured point clouds rising from the seafloor represent gas flares at the seabed.

#### **4.7. USGS-GAS (US Geological Survey – Gas Analysis System)**

Prior to the cruise, a research-team from United States Geological Survey (USGS) installed equipment for measuring methane and carbon dioxide concentrations in the ocean surface and atmospheric boundary layer (Fig. 4.5). Air intakes and sonic anemometers were installed at approximately 10, 15 and 23 m above the sea surface. Tubing from the intakes and cable from the anemometers were run from the ship exterior into the laboratory. During the cruise, methane and carbon dioxide concentrations in the air from each level was measured for 1.5 minutes during a 4.5 minute cycle using a Picarro G2301-f cavity ring-down spectrometer (CRDS). Data from each level is to be used to determine if methane and CO<sub>2</sub> concentration gradients were present in the marine boundary layer.

Surface water from approximately 5 meters below the sea surface was also continuously delivered to the laboratory. Methane and CO<sub>2</sub> were extracted from the incoming stream in a modified Weiss-type gas equilibrator and analyzed for concentration and stable isotopic content using a Picarro G2201-i CRDS. Surface water methane and CO<sub>2</sub> concentrations calculated with the headspace data and sonde data (temperature and salinity) are used in combination with the atmospheric data to calculate methane and CO<sub>2</sub> fluxes into or out of the surface water.

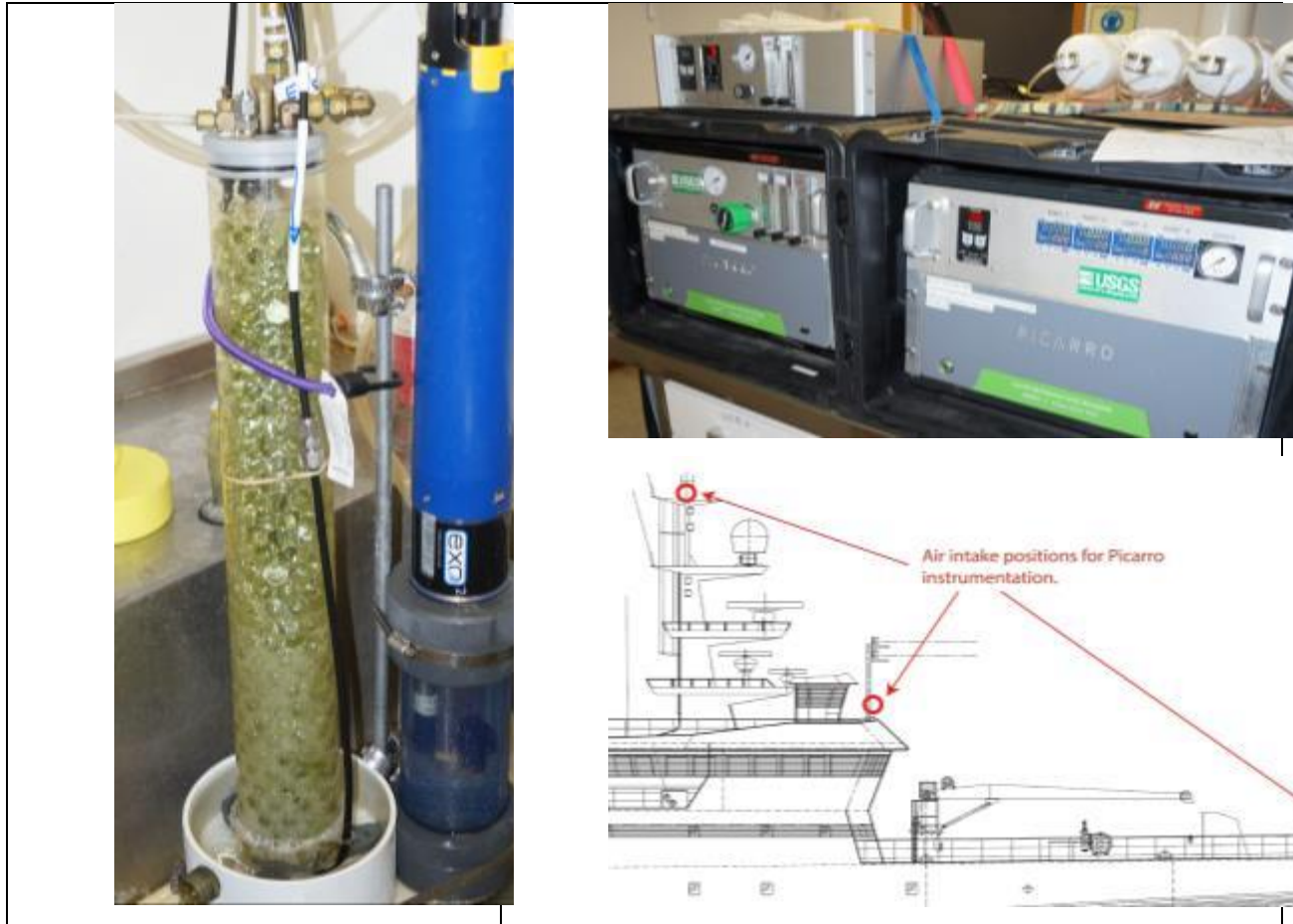


Fig. 4.5. The Picarro setup, showing the position of air intake (bottom right), the equilibrator and attached salinity/temperature sensor (left) and the cavity ringdown spectrometer (CRDS) -cases (top right).

#### 4.8. Preliminary results

##### *CTD*

The CTD data was collected from 95 stations and subsequently compiled in a database, using Ocean Data View (ODV) developed by Alfred Wegener Institute, Germany. ODV simplifies data display of the different parameters by allowing the user to specify a transect (series of stations). Using the positions of the stations and depths, a “curtain” can be drawn by interpolating between the stations. Here we show such plots of salinity and temperature data from the long transect that was included in the survey, ranging from the deep end of the margin (approximately 1200 meters) offshore Prins Karls Forland to the shallow shelf (80 meters). Obviously many more transects can be defined and plotted and we here only present a fraction of the data collected.

The top left panel of Fig. 4.6 shows the depth-dependent salinity over the transect. We observe a small range of salinity (34.9 – 35.2 PSU) and higher salinities in the upper part of the water column. This is possibly caused by evaporation, enriching the remaining water in salinity. It could be expected that river runoff would reduce the salinity of the upper layer, but apparently the river runoff is small or cold enough to penetrate deeper into the ocean. The salinity differences are very small and exhibit a negative salinity stratification implying that stable stratification must be sustained by the temperature difference in this area.

The temperature is highest in the surface a distance away from the coast (Fig. 4.6, top right panel), indicating that the water close to the coast is affected by the east Svalbard current (ESC), bringing cold water from the Barents Sea or by river runoff. However salinity data shows no fresh signal, expected from both Barents Sea water and river runoff. Nutrition data may support the hypotheses that this is Barents Sea water if the water is not enriched in nitrate and phosphate.

Levels of oxygen concentration are high close to the surface at the shore, indicating primary production and/or strong vertical mixing (Fig. 4.6, middle left panel). We also see a local low offshore at 100 meters depth. Here, the temperature is high, which decreases the solubility of oxygen.

Turbidity is expectedly high in the productive area close to the surface at the shore (Fig. 4.6, middle right panel). There is also a high, close to the bottom from 200-250 meters depth (35-50 km from the outer station), and another local high, at 400-600 meters depth (15-25 km). Interestingly, this coincides with high bottom-concentrations of methane. We hypothesize that local ebullition of sub-bottom methane causes re-suspension of sediments.

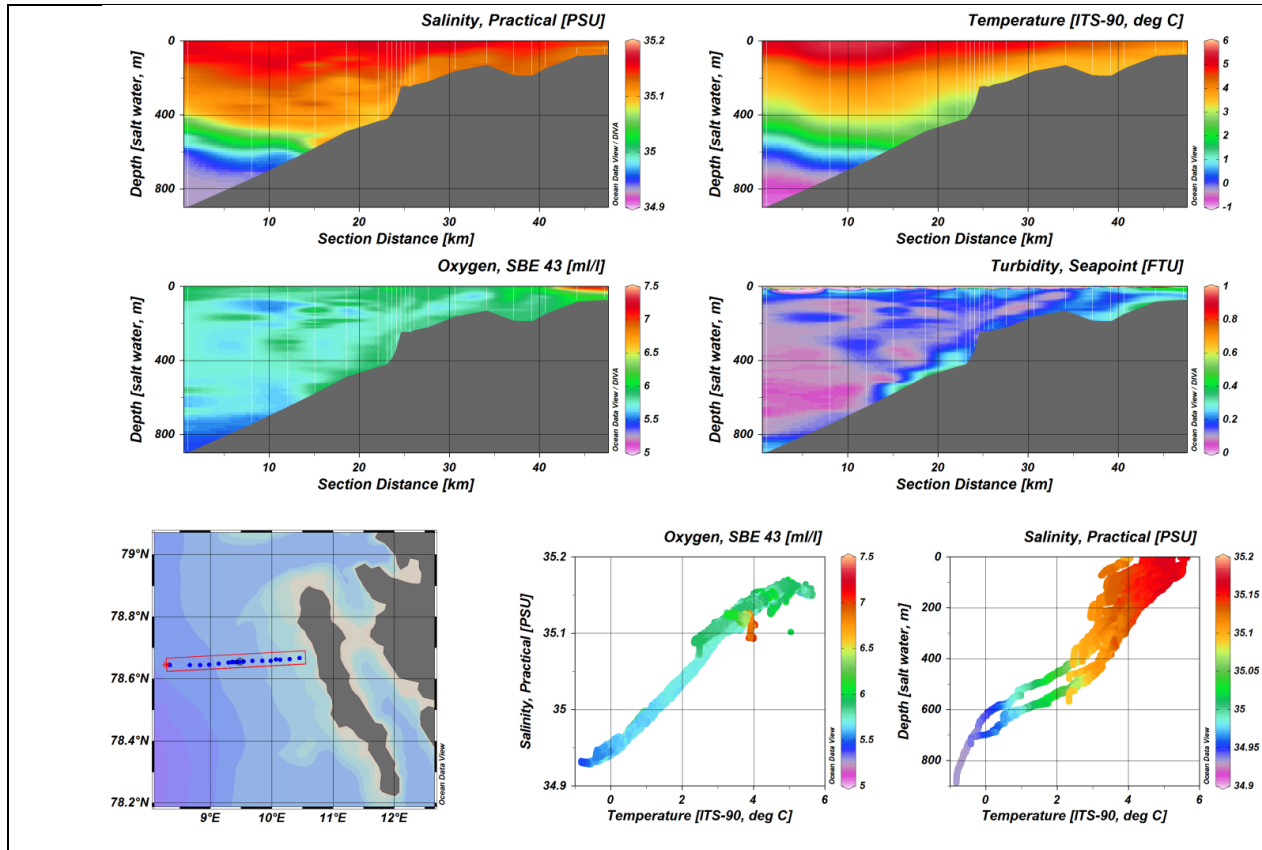


Fig. 4.6. The transect from the deep end of the margin to the shallow shelf (bottom left panel). ODV-data shows salinity, temperature, oxygen concentration and turbidity. We note overall small negative salinity stratification. The temperature shows a local low near the surface close to the shore, probably caused by a contribution of fresh cold water from the Barents Sea via the ESC. The turbidity is high in the surface, close to the shore, where oxygen levels are also high, indicating high primary production. We also see increased turbidity close the bottom at approximately 200 meters and 400 – 600 meters. This coincides with high levels of methane (section 4.6), indicating that local benthic methane release causes re-suspension of sediments in this area. Oxygen levels are high in the productive surface layer near the shore of Prins Karls Forland and shows a local low where the temperature is high, lowering the solubility of oxygen.

### Nutrients

From the Niskin bottles, we collected samples to analyze nutrient contents as described in section 2.2. Samples were taken along a transect ranging from the deep end to the shallow end of the margin in the northern part of the survey area. At the time of writing this report, we haven't received the nutrient data, which has to be provided by a land based laboratory.

## Dissolved Methane

At the time of our cruise, methane sampled from the water column was high at two distinct locations close to the bottom and concentrations show sharp vertical and horizontal gradients. The top panel of **Error! Reference source not found.** shows the same transect as the CTD-data (**Error! Reference source not found.**) and the lower panel shows a 2-dimensional map of concentrations at the deepest level for each station (approximately 5 meters above the seafloor) in the shallow-water survey area near Prins Karls Forland.

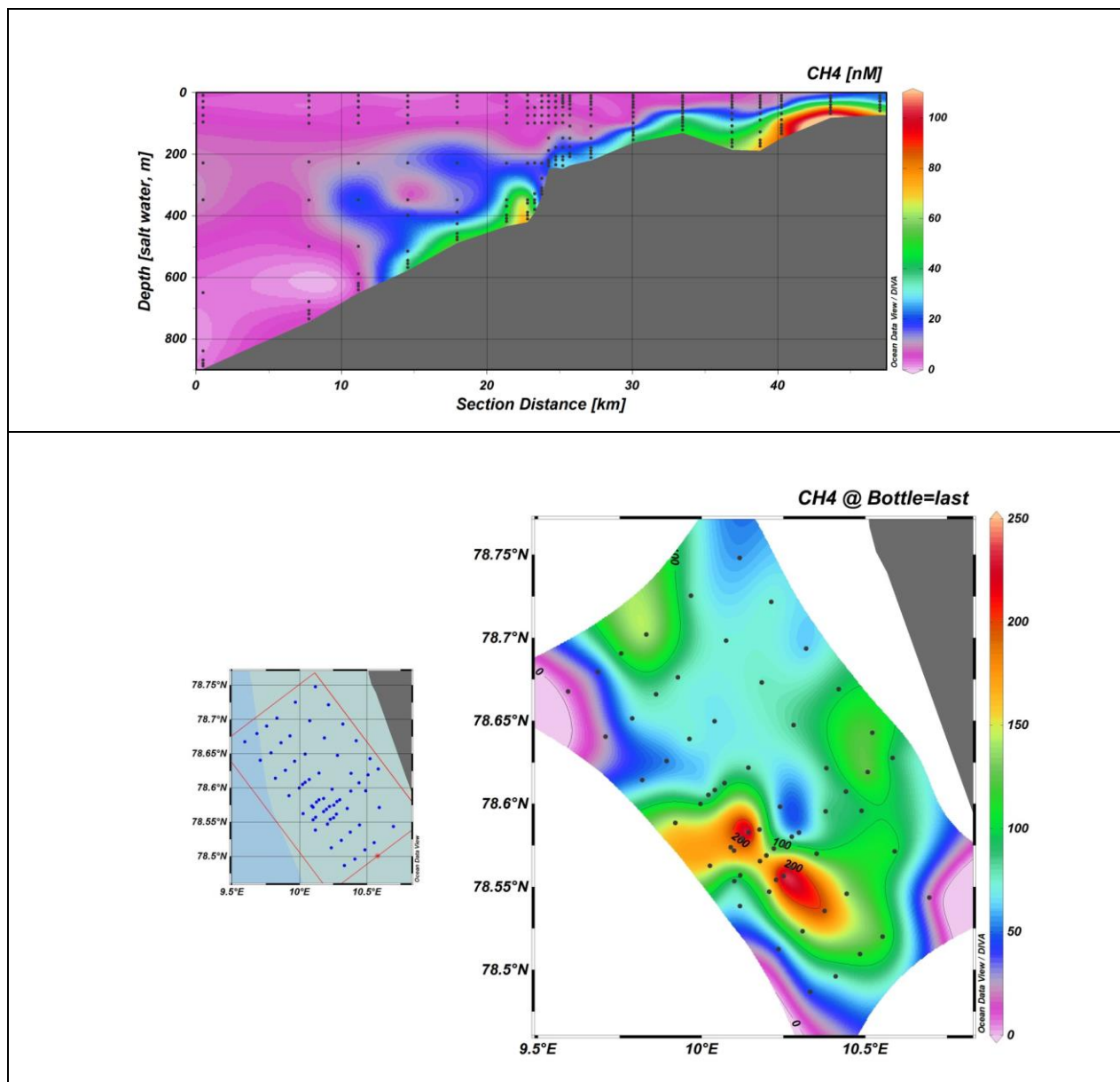


Fig. 4.7 Top panel: Methane distribution along the transect from the deep end of the margin (900 m) to the shallow shelf (80 m). Two distinct sources of methane can be inferred. One at ~150 meters depth and one at ~400

meters. Bottom panel: Methane concentrations in the sample closest to the bottom (typically 5 meters above the bottom) show two methane sources close to each other at approximately 90 meters depth.

### *ADCP*

Although great effort was put into collecting ADCP-data, we have only scattered data with spurious quality. This is due to our limited experience in configuring the ADCP, operating the software, and communicating with the ship navigation system.

Here we present data from a 17 minute period when we received non-blank current data (**Error! Reference source not found.**). We interpret the orange parts of the contour plot as being noise, which is always seen in ADCP-data close to the surface and bottom. The average velocity (green) is approximately  $2.5 \text{ ms}^{-1}$ , which corresponds to 5 knots, which approximately matches the survey speed of the vessel. The ADCP-software normally corrects for the ships navigation (speed and direction) as well as heave, pitch and roll data from the ships gyro. This requires data communication through the com-ports of the PC in the instrument room. Unfortunately this was not working well for us and the raw data is basically useless unless we recreate the navigation (NAV) and gyro (ENV) files and correct the raw ADCP-data, using these ancillary data files. This task, however that would require considerable effort and that may not be fruitful, since most of the ADCP-data is blank anyway.

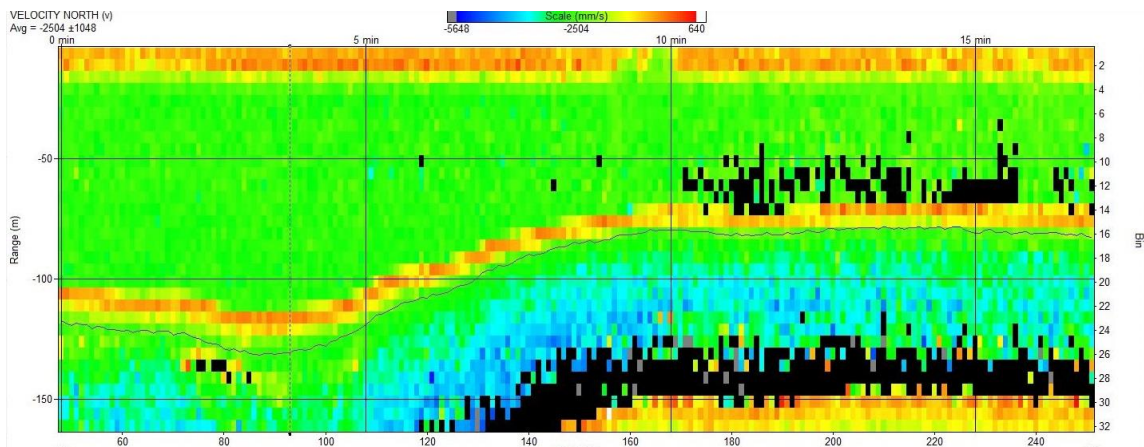


Fig. 4.8. A snapshot of ADCP data originating from a 17 minute period when the ship traveled from 120 meters to 80 meters depth. The Orange part of the contour is noise and the solid black line is the bottom contour. Black dots are faulty data (NaN-values)

### *Echosounder*

We worked in the area of previously discovered and documented seafloor gas expulsion [G K Westbrook *et al.*, 2009] which left us no doubt that we were dealing with the gas flares but not the fish schools. We imported the raw echosounder data into Fledermaus software – FMMidWater module, where we implemented the simplest processing procedures, adjusting the backscattered amplitudes to enhance the target values, which simplified the following interpretation process. High-amplitude reflections from the gas bubbles were cut out from the data and exported as \*.txt files, containing the spatial coordinates (XYZ) and amplitude as an attribute value. Later these text files were imported in the 3D environment of Fledermaus software and appeared as vertical point clouds (flares) colored according to the attribute values. Combined with the multibeam echosounder data and CTD locations it provided a solid overview of the hydro-acoustic survey in the water column within the study area (Fig. 4.4).

#### *USGS-GAS*

The Fig. 4.9 depicts the concentration (ppmv) of methane in the surface water equilibrator during a transect across the shallow-water seep (90 meters). In addition to demonstrating supersaturation of methane in the surface water, isotopic data (as  $\delta^{13}\text{C}$  values) is useful for determining the origin of the methane. In this case, the  $\delta^{13}\text{C}$  of the methane overlying the seep is significantly lower than the background data appearing on the right side of the graph. Background values are in equilibrium with the atmosphere, where the  $\delta^{13}\text{C}$  of methane is  $\sim -48\text{‰}$ . Over the seep the methane consists of greater than 80% seep derived methane and has a  $\delta^{13}\text{C}$  of approximately  $-55\text{‰}$ . Interpreting the source based on that value is difficult as it is intermediate between typical microbial ( $-65$  to  $-75\text{‰}$ ) and thermogenic values ( $> -50\text{‰}$ ) [Whiticar, 1999]. To fully characterize the origin of this methane source additional isotopic analysis (e.g.,  $\delta\text{D-CH}_4$ ) is required. Nevertheless, the ability to provide first order gas source interpretations in real time is a powerful and heretofore unprecedented tool for ocean going expeditions. Based on this  $\delta^{13}\text{C}$  data only, we can speculate that the source of methane is predominantly biogenic at this shallow site.

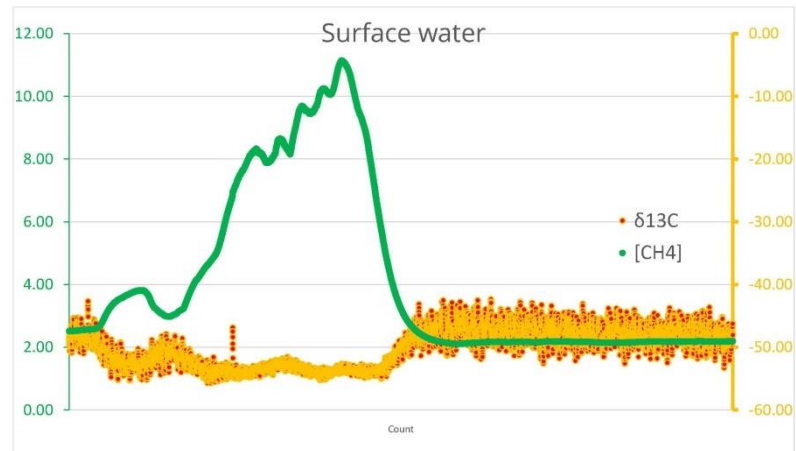


Fig. 4.9. Methane concentrations measured in ppmv (parts per mil (thousand)), volume (green) and  $\delta^{13}\text{C}$  isotopes (red/yellow). Low levels of  $\delta^{13}\text{C}$  correlates with high methane concentrations, implying a biogenic source of methane. Also, the signal-to noise ratio is larger due to better isotope-measurements with higher concentrations.

## 5. Micropaleontology and pore water sampling

One of the goals of the cruise was to collect sediment samples in order to characterize benthic foraminifera assemblages associated with methane seep sites, and compare these to records of sites that are unaffected by methane seepage. Benthic foraminifera live directly on the seafloor or a few cm within the surface sediment. Therefore, they have a great potential to trace methane emissions from the seafloor. In order to explore the link between active methane seepage and the geochemical composition of the foraminifera tests, analyses of dissolved constituents of the pore water like e.g. sulfate ( $\text{SO}_4^{2-}$ ), dissolved inorganic carbon (DIC) and methane are combined with the benthic foraminifera record. Furthermore, sediment properties will be determined while dating of the surface sediments will reveal sedimentation rates.

This chapter presents an overview and baseline information of the micropaleontological and pore water sampling sites, a description of the applied sampling scheme, and preliminary outcomes of the study.

### 5.1. Study sites

Material from 14 shallow and deep water sites offshore NW Svalbard has been collected as box- or multicore during the cruise. The sites are listed according to the sampling date with a brief description of the sampling activities, the seafloor characteristics, and linked sampling activities such as CTDs,  $\text{CH}_4$  measurements and gravity cores (Table 5.1). The sampling sites are shown in Fig. 1.1.

A shallow-water site in Kongsfjorden Trough (KongHau long-term biological monitoring site, termed V 12 in this report) as well as shallow sites offshore Prins Karls Forland (PKF 1; PKF 2) with water depths between 200 and 380 m have been sampled. Grab samples for biological analyses and CTDs were taken from this area (Table 5.1).

A Box-core transect has been sampled (PKF 3 - 9) parallel to a CTD-Transect and  $\text{CH}_4$  measurements in surface water and air (Table 5.1) across the Forlandet Moraine Complex offshore Prins Karls Forland. Here, seven sites were chosen for box coring in 80 to 160 m water depth.

Furthermore, a multicore was deployed onto the northern Vestnesa ridge in 1200 m water depth. We also sampled Vestnesa south (VS) in around 1580 to 1700 m water depth. The location is a sediment drift that is a potential southern extension of the Vestnesa ridge with a similar genetic background. Both sites are ridges composed of sediment drifts located on ultraslowly

spreading ridges (REF). When the Fram Strait was opening about 33 Ma ago (e.g. Engen et al. 2008), possibly former transform faults turned into an ultralow seafloor spreading zone and disrupted the Vestnesa Ridge into its well-known northern and its less studied southern part. Gravity cores and CTDs were taken from this area as well (Table 5.1).

Table 5.1. Overview and brief characteristics of the sampling sites for micropaleontological sampling, porewater and methane measurements in boxcores (BC) and multicores (MUC). VS – Vestnesa south. PKF – Prins Karls Forland. PoreW – Pore water. F – Foraminifera. D – PB 210 dating. S – Sedimentology (Total Organic Carbon; Grain size; Porosity). B – Benthic sampling at the site. GC – Gravity core.

Site	Date	Ship station no.	Coordinates	Water depth (m)	Seafloor characteristics	Core type	CH <sub>4</sub> , PoreW	F	S	D	B	Other activities / Remarks
<b>V 12</b>	20/06	646	78°59.766 N 09°29.634 E	216	Silt/clay with pebbles	BC		X	X	X	X	Reference site Kongsfjorden, KongHau control site biology
<b>VS 1</b>	23/06	656	78°18.265 N 05°48.063 E	1578	Silt/clay	BC	X	X			X	GC 663
<b>VS 2</b>	23/06	658	78°21.342 N 05°42.125 E	1614	Silt/clay	MUC	X	X			X	GC 664
<b>VS 3</b>	23/06	659	78°30.224 N 05°42.631 E	1706	Silt/clay	MUC	X	X			X	GC 660, GC 661
<b>VR 1</b>	28/06	676	79°00.452 N 10°15.518 E	1205	Silt/clay	MUC	X	X	X		X	CTD 410, Replica over 1 core GC 677; GC 678; GC 679; GC 680,
<b>PKF 1</b>	22/06	653	78°39.339 N 09°26.010 E	244	Silt/clay with pebbles & cobbles	BC	X	X	X	X	X	
<b>PKF 2</b>	22/06	654	78°37.594 N 09°24.298 E	376	Silt/clay with pebbles & cobbles	BC	X	X	X	X	X	Sampling for microbiological analyses and Chlorophyll analyses
<b>PKF 3</b>	25/06	667	78°33.222 N 10°05.777 E	116	Silt/clay with pebbles	BC	X	X		X	X	CTD 353, CH <sub>4</sub> -survey, Replica over 1 core
<b>PKF 4</b>	25/06	669	78°33.442 N 10°07.438 E	107	Sand with shell fragments	BC		X			X	CTD 354, CH <sub>4</sub> -survey, Forams from surface
<b>PKF 5</b>	25/06	670	78°33.672 N 10°08.925 E	86	Sand with shell fragments & pebbles	BC / Grab 6	X	X			X	CTD 360, CH <sub>4</sub> -survey, Forams from surface, Sampling for Chlorophyll analyses
<b>PKF 6</b>	25/06	672	78°33.832 N 10°10.084 E	99	Sand with shell fragments & pebbles	BC / Grab 6		X			X	CTD 365, CH <sub>4</sub> -survey, Forams from surface
<b>PKF 7</b>	26/06	none	78°34.179 N 10°11.647 E	103	Sand with shell fragments & pebbles	BC / Grab 6		X			X	CTD 370, CH <sub>4</sub> -survey, Forams from surface
<b>PKF 8</b>	26/06	673	78°34.369 N 10°13.718 E	157	Silt/clay with pebbles	BC	X	X	X	X	X	CTD 375, CH <sub>4</sub> -survey, 1 Archive core
<b>PKF 9</b>	26/06	674	78°34.527 N 10°15.518 E	159	Silt/clay with pebbles & cobbles	BC	X	X		X	X	CTD 381, CH <sub>4</sub> -survey

## 5.2. Methods

### *Boxcoring*

The box corer is a sampling device for soft and hard seafloor, even with clasts (pebbles or cobbles). The corer lands on the seafloor and the chamber sinks into the sediment, the slicer tilts and cuts out a block of surface sediment that is excavated together with the bottom water directly above the sediment surface. The boxcorer can recover the uppermost ca. 30 cm of sediment and preserves the stratigraphy during its way upwards through the water column (Fig. 5.1).



Fig. 5.1. a) The box corer gets deployed from the side of the ship with its chamber open. b) After taking the box corer on board again, multicore tubes were pushed into the sediment in the chamber. The core with black tape has predrilled holes for methane and pore water sampling. c) Cross section through the sediment in the chamber.

Once onboard, the surface water in the box corer chamber is removed with a hose. An inspection of the surface sediment allows characterizing the surface of the seafloor (soft or clasts), its biology, and the decision if subcores (multicore tubes) can be retrieved. If the surface conditions are soft enough, several core tubes (diameter 10 cm) are pushed into the sediment in the box core chamber carefully in order to preserve the original stratigraphy. In case of pebbles on the surface, these were removed prior to pushing in the multicore tubes. Finally, the chamber is lifted, the core tubes taken out, sealed on both ends, and stored in an upright position.

### *Multicoring*

The multicorer is a sampling device that can recover six core tubes (diameter 10 cm) parallel from the same spot on the seafloor. It is suitable for soft bottom conditions. The core tubes are loaded with open ends. The multicorer lands on the seafloor, the tubes are pushed into the soft

sediment by lead weights, and closed on both ends. Up to 60 cm of surface sediment and the immediate overlying bottom water can be sampled (Fig. 5.2). Once onboard, the core tubes filled with water and sediment are carefully taken out of the sampling device, the ends sealed, and the cores stored in an upright position. They are labelled and subsampled immediately.

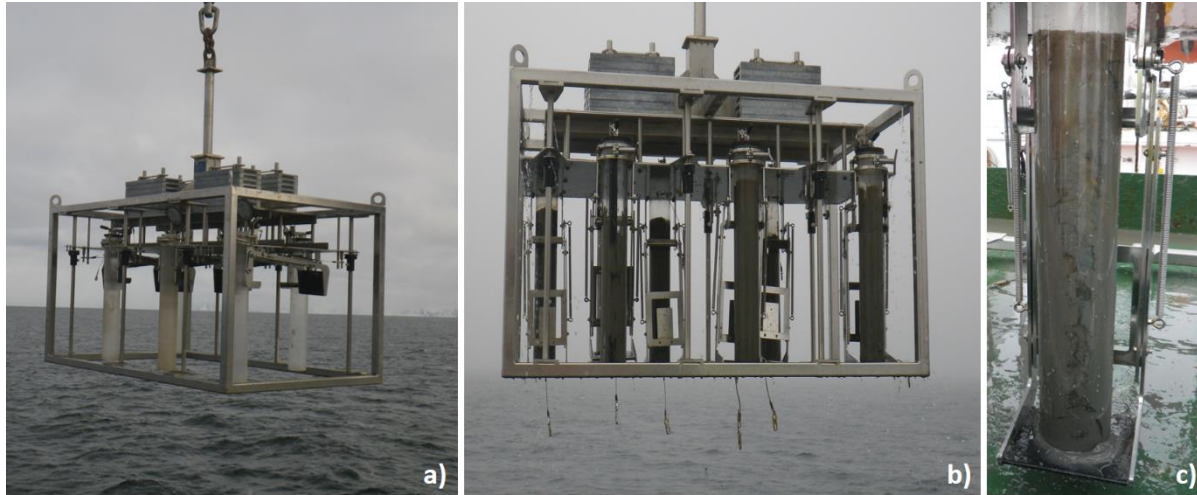


Fig. 5.2. a) The multicorer gets deployed from the side of the ship with its chamber open. b) Multicorer with filled tubes. c) Filled coretube with a vertical disturbance that probably formed during coring.

### 5.3. Subsampling the core material

According to a sampling scheme (Fig. 5.3), one core from each sampling site is sampled for methane, pore water and water content analyses onboard the ship. Samples for methane, DIC in the pore water and water content analyses were kept in the refrigerator, while samples for Sulfate analyses in the pore water were frozen. Parallel, samples for foraminifera analyses were taken from the same core in 1 cm intervals over the entire length of the core. We stained samples from the uppermost 10 cm with Rose Bengal to distinguish living from dead foraminifera. Rose Bengal is a pink-coloured powder that is dissolved in distilled water. It is added to the sample and mixed through careful stirring or shaking. It stains the cytoplasm in living organisms in pink colour. Samples from the depth below 10 cm were not stained. The core slicing in the given intervals was done onboard. All samples were transferred into pre-labelled sample bags or vials, and preserved in the fridge.

A second core was dedicated for geochronology ( $^{210}\text{Pb}$  dating) and establishing sedimentation rates. Here, the uppermost 10 cm were sampled in 1 cm intervals, 2 cm sampling

intervals were used until 20 cm, and below 20 cm we sampled in 5 cm intervals. The samples were preserved in the fridge without any further treatment.

From the third core, samples for sediment properties (TOC, grain size, porosity) were taken in 1 cm intervals in the uppermost 10 cm, in 2 cm intervals below 10 cm, and in 5 cm intervals below 20 cm. The samples were preserved in the fridge without any further treatment.

If more core material was available, material was dedicated for the following purposes:

- a second core for foraminifera analyses according to the same scheme as above
- qualitative biological (fauna) sampling,
- sampling for chlorophyll analyses (sampling interval was 1 cm for the uppermost 10 cm, the samples were frozen in a light-tight container),
- sampling for microbiological studies (pilot study of microbial DNA and RNA, the samples were kept in the refrigerator or freezer),
- magnetic susceptibility logging on the ship,
- replica or bulk sampling,
- as an archive core.

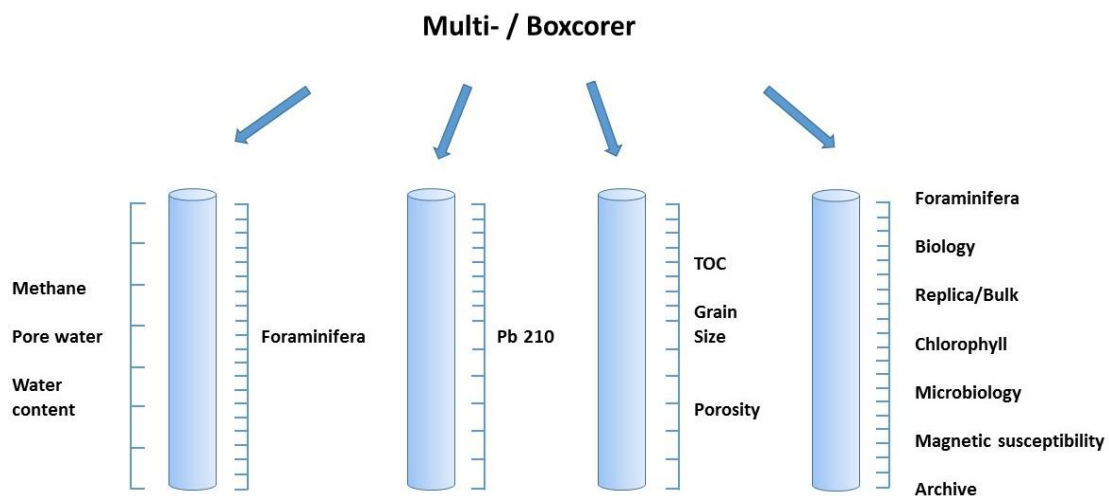


Fig. 5.3. Sampling scheme of box and multicores.

The sampling scheme at the selected stations was combined with CTDs and sampling for methane analyses throughout the water column, flare mapping, Van Veen grabs to learn about the benthic macrofauna, gravity coring in order to obtain long records, bathymetric and seismic data collection.

## 5.4. Sampling for methane in sediments

All cores were sampled for methane analyses within 15 min after retrieval. For multicores, subcores of box cores, and gravity cores we predrilled (15mm diameter) and taped the liners. The sampling interval for multi and box cores was mostly 3cm, and for gravity cores 30 cm.

After core retrieval we sampled between 1.5 and 4 ml sediment using a 5ml syringe with a cut off tip through the pre-drilled holes. The sediment was immediately transferred to a 20 ml serum vial that contained two glass beads and 6 ml of 2.5% NaOH solution to prevent any further microbial reaction (Fig. 5.4). The vial was then sealed with a rubber plug, crimp sealed, shaken well and stored in the fridge (app. 2°C). After taking the sediment plug, the holes were sealed with tape.

Methane concentration in the headspace was then measured on board with a gas chromatograph (GC). We used a Thermo Scientific FOCUS GC run with direct injection. Hydrogen was used as carrier gas as well as zero air and zero N<sub>2</sub> to run the flame ionization detector (FID) (N<sub>2</sub> was the mask gas which helps to keep the flame stable). The injector temperature was set to 150°C and the septum was constantly purged to avoid septum bleeding into the column flow. The FID temperature was set to 170 °C and the oven temperature was ramped from 40°C to 120°C in steps. The flow through the column (RESTECK Packed Column HS-Q 80/100, 2 m length 2 mm inner diameter) was set to a constant pressure of 40 kPa and the entire injection was run in a split-less mode. The software used for recording the data and integration was Chrome Card 6.01.

A calibration curve was produced (Fig. 5.5) with gas standards of known methane concentration to determine methane concentration in the headspace of the samples (in ppm). Standards were run on average after 10 samples.

Using the ideal gas law ppm was converted to number of molecules (mol):

$$n \text{ (mol)} = \frac{P * V}{R * T}$$



Fig. 5.4 Photo of filled and empty vials

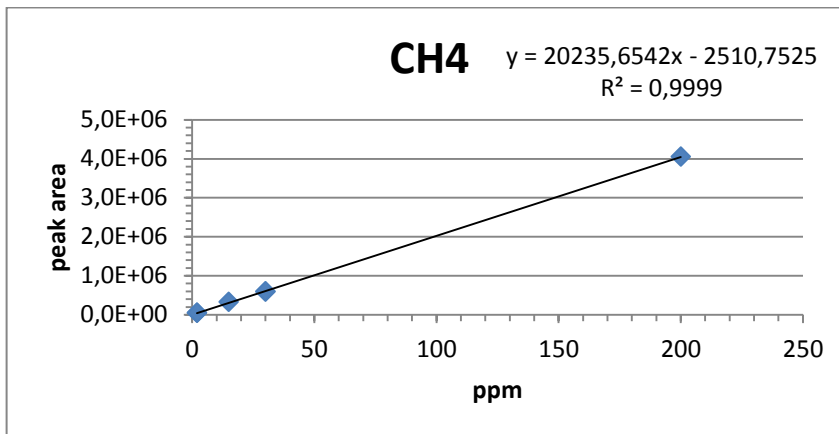


Fig. 5.5 Example of calibration curve in the 0-200 ppm range vials for methane samples.

Were P is pressure (101.325 kPa), R is the gas constant ( $8.314 \text{ l kPa K}^{-1} \text{ mol}^{-1}$ ), T is the temperature in Kelvin and V the volume of methane in the headspace in litres. Then this was divided by the volume of the sediment sample taken (to get mol/- sediment) and finally multiplied by an assumed porosity of 80% to get mol/l of porewater. The actual porosity (water content) will be determined later. Sediment samples (3-4ml) were collected with cut off syringes from the same depths as the methane samples were taken, and stored in plastic bags for later on shore analysis. The water content will be determined by weighing the sample before and after drying. Analyses of stable carbon and hydrogen isotopes of methane ( $\delta^{13}\text{C}_{\text{CH}_4}$  and  $\delta^2\text{H}_{\text{CH}_4}$ ) will be performed on samples that contain high enough concentrations of methane in the headspace. Those results will help distinguish between different sources of methane (microbial, thermogenic, abiotic).

## 5.5. Porewater sampling

Porewater from gravity, box and multicores was sampled using the rhizone technique. Holes with a diameter of 3.9 mm were drilled into the liner through which the rhizones were inserted. 10ml syringes were attached to the rhizones and kept open to create a vacuum using a wooden spacer (Fig. 5.6). It took between 10 minutes and several hours to fill the syringes. After taking the samples the holes were sealed with tape.



Fig. 5.6 Photo of rhizones inserted to a gravity core with 10 ml syringes attached that are kept open with a wooden spacer.

Then a split of the pore water was filled into a 2ml glass vial without headspace and closed with a septum and screw cap and stored at 2°C for later onshore analysis of stable carbon isotopes of dissolved inorganic carbon ( $\delta^{13}\text{C}_{\text{DIC}}$ ). The remaining porewater was left in the syringe and frozen. This will be analysed for the anions sulphate and chloride with an Ion Chromatograph (IC) and for the major cations (Mg, Ca, Si, K, Na, Sr, Ba) with inductively coupled plasma optical emission spectroscopy (ICP-OES) at the NGU in Trondheim.

## 5.6. Onboard analyses and preliminary results

### *Sediment descriptions*

During subsampling and from observations of the sediment surface, the sediment properties were described and core logs were drawn for each sampling site. The logs are shown in Fig. 8 (drawn by Giuliana Panieri) and include symbols for foraminifera, methane and pore water sampling. Most of the sampled sites were characterized by brown or grey clay with occasional silt lenses and pebbles and cobbles at the sediment surface. Across the oceanographic transect

offshore Prins Karls Forland (PKF 3 to 9, Fig. 5.15 to 5.18), the sediment from sites shallower than 110 m water depth were characterized by a sandy surface with pebbles as a common feature while at the deeper sites brown and grey clay prevailed. In this area, Knies et al., 2004 discovered microbial mats, which, however, were not observed during the AMGG cruise. In general, very little material was obtained from the sites with sandy material due to coring difficulties? and only a small amount of surface material could be described and sampled.

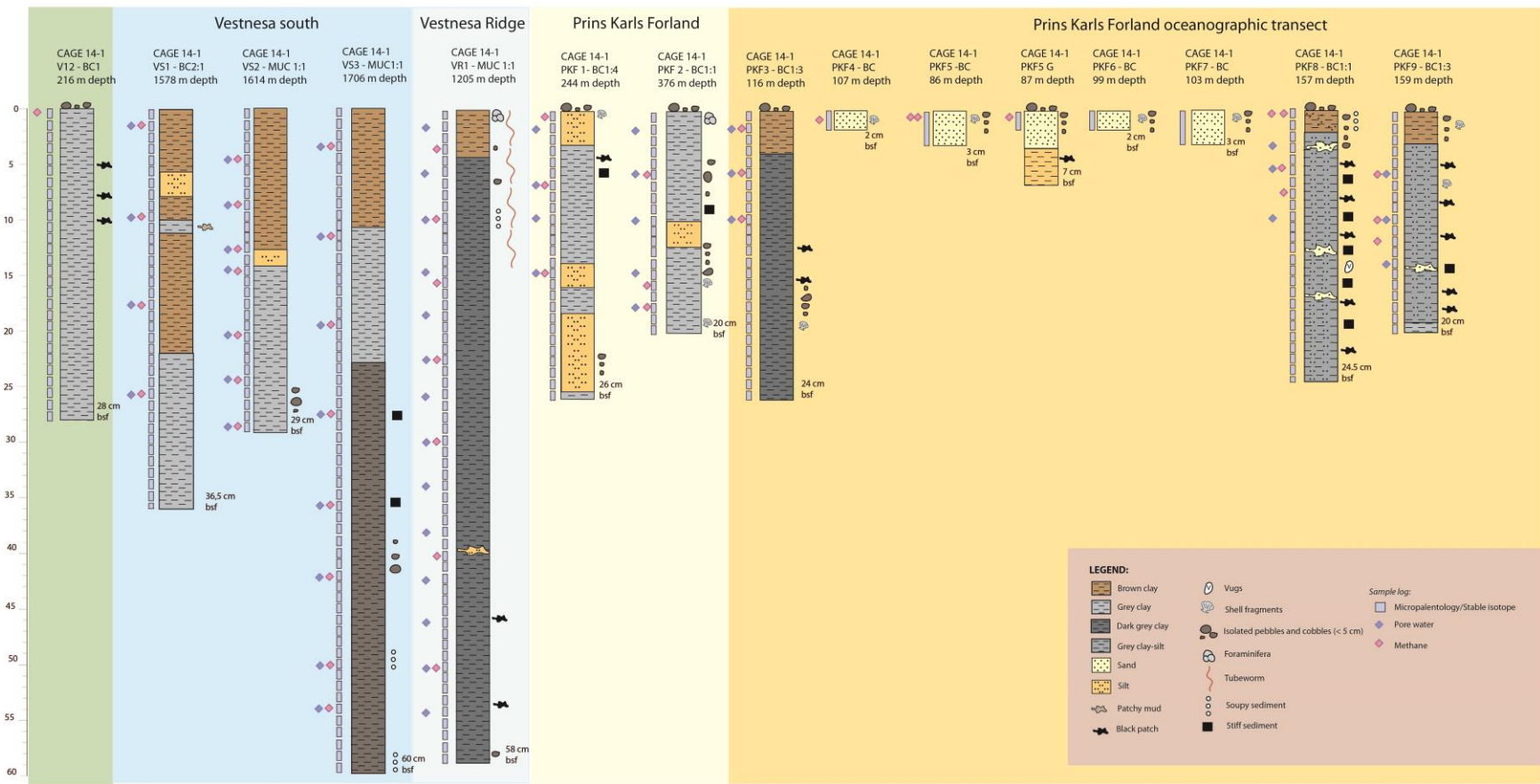


Fig. 5.7 Lithological description of multi and box cores. Fig. drawn by Giuliana Panieri.

*V12 - KongHau control site. Box core*

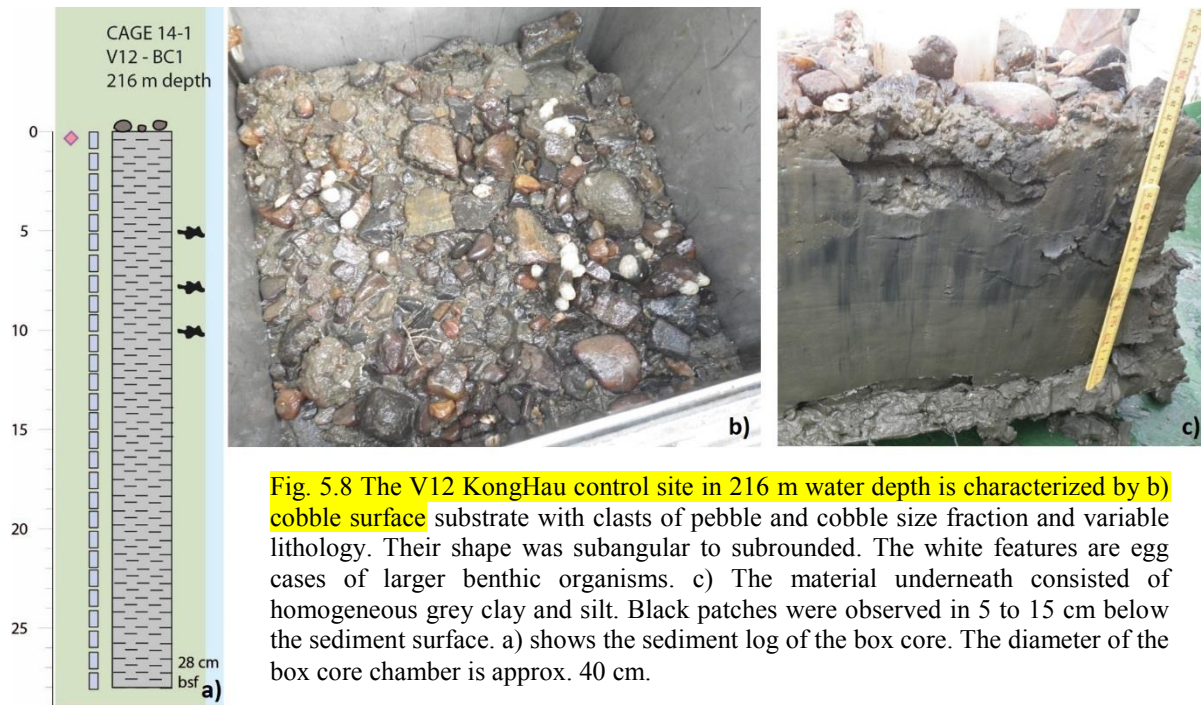


Fig. 5.8 The V12 KongHau control site in 216 m water depth is characterized by b) cobble surface substrate with clasts of pebble and cobble size fraction and variable lithology. Their shape was subangular to subrounded. The white features are egg cases of larger benthic organisms. c) The material underneath consisted of homogeneous grey clay and silt. Black patches were observed in 5 to 15 cm below the sediment surface. a) shows the sediment log of the box core. The diameter of the box core chamber is approx. 40 cm.

*VS 1 – Vestnesa South 1. Box core*

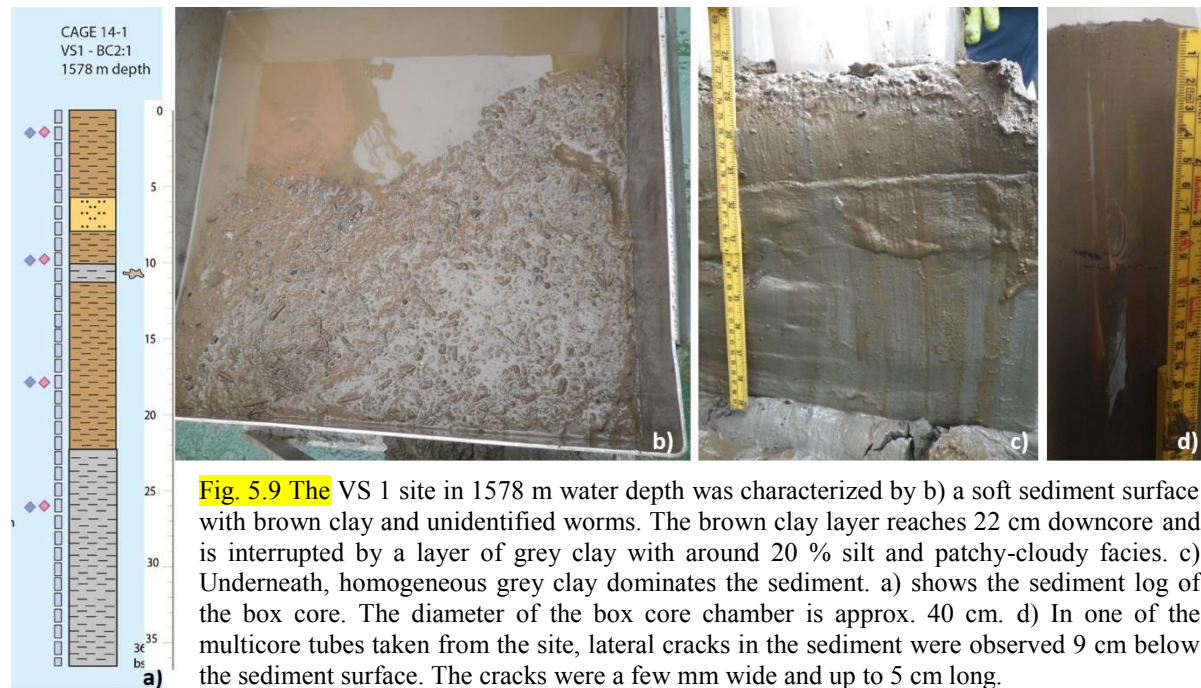
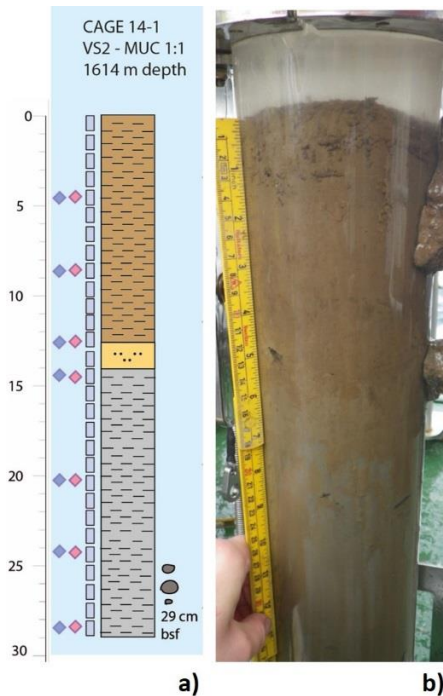


Fig. 5.9 The VS 1 site in 1578 m water depth was characterized by b) a soft sediment surface with brown clay and unidentified worms. The brown clay layer reaches 22 cm downcore and is interrupted by a layer of grey clay with around 20 % silt and patchy-cloudy facies. c) Underneath, homogeneous grey clay dominates the sediment. a) shows the sediment log of the box core. The diameter of the box core chamber is approx. 40 cm. d) In one of the multicore tubes taken from the site, lateral cracks in the sediment were observed 9 cm below the sediment surface. The cracks were a few mm wide and up to 5 cm long.

### VS 2 – Vestnesa South 2. Multi core



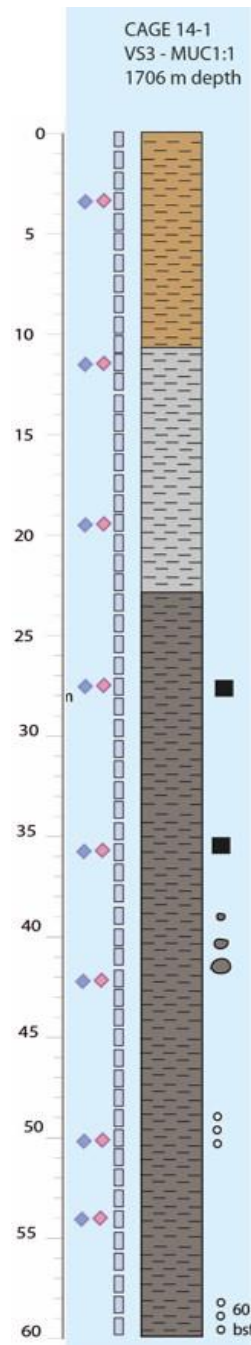
**Fig. 5.10** The sediments at the VS 2 site in 1614 m water depth were characterized by a 12 cm thick soft brown clay layer with a silty layer at its base. In its lower part, the sediment changed gradually into homogeneous grey clay. Isolated clasts were found in the depth of 27 to 28 cm below the sediment surface. a) shows the log and b) a photo of the filled multicore tube.

### VS 3 – Vestnesa South 3 Multi core

**Fig. 5.11.** The surface material of a 60 cm long multicore from the VS 3 site in 1706 m water depth was composed of brown clay. Occasionally, grey spots appeared in the middle of the core from 5 cm depth and downward. Light grey homogeneous clay dominated from 12 to 23 cm. The material changed downcore into dark grey, compact and relatively dry clay below 23 cm. At about 40 cm depth pebbles of 1 to 2 cm in diameter were found. Moreover, in the depth interval between 49 and 50 cm, about 1 mm long white crystals were observed and identified as salt crystals using the binoculars on board.

In 50 and 60 cm below the sediment surface a soupy sediment texture was observed.

In the core MUC 1:1 bubbling mud was observed after coring. No methane was measured in the sediment (**Fig. 5.21**).



VR 1 – Vestnesa Ridge. Multi core

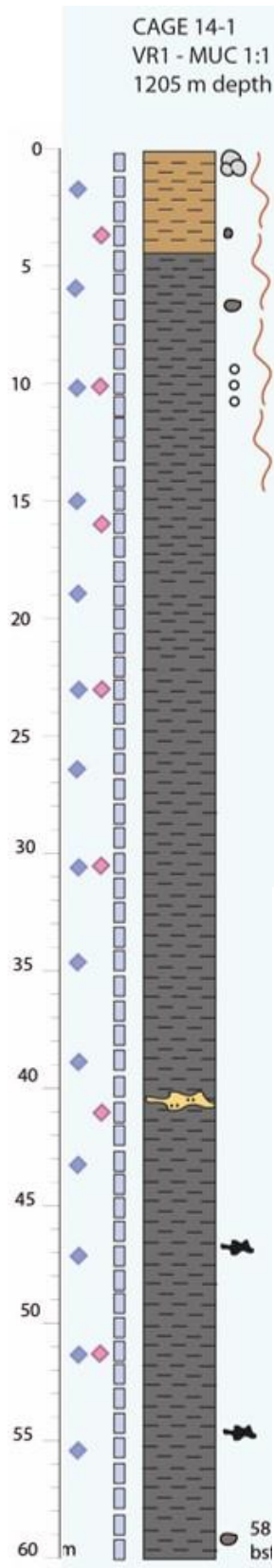


Fig. 5.12 A multicore from the northern Vestnesa Ridge in 1205 m water depth (VR 1 MUC 1:1, Fig. 11) had a unique «fluffy» surface structure with abundant agglutinated foraminifera (see figures 25 and 26) and unidentified orange-red tubeworms (see fig. 28).

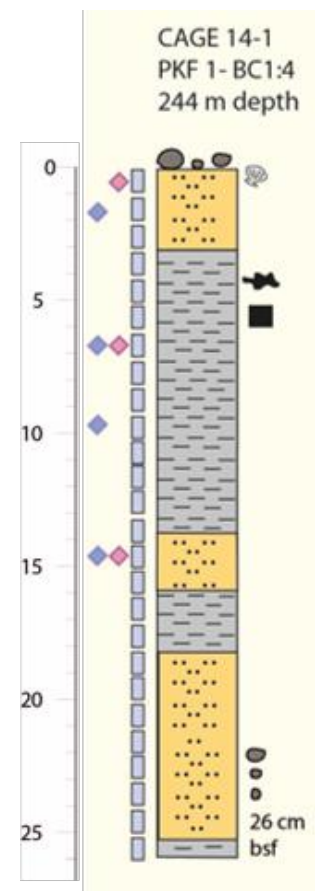
The uppermost 4 cm were composed of brown clay with small pockets of silt which changed into homogeneous dark grey clay further downcore. Abundant tubeworms were found in the top of the core. They were abundant in the first about 10 cm, and became rare around 20 cm below the sediment surface.

An interval with soupy sediment was observed 10 cm below the sediment surface. Occasional silt pockets were found in 40 cm depth. In about 45 cm below the sediment surface black patches occurred in the sediment. Isolated pebbles were found in the uppermost 10 cm as well as at the base of the core.

PKF 1 - Prins Karls Forland 1. Box core

Fig. 5.13 From a water depth of 244m a box core with rounded to subrounded pebbles at the surface was taken. Furthermore, pieces of authigenic carbonate were found. An intact bivalve shell was found at the sediment surface.

The clasts were removed prior to pushing multicore tubes into the chamber. The sediment consisted of silty clay with stiff sections and black patches in about 5 cm depth. Sandy-silty layers occurred in around 15 and 18-25 cm depth below the sediment surface. Pebbles with a diameter of 1 cm were found in 23-24 cm depth.



*PKF 2 - Prins Karls Forland 2. Box core*

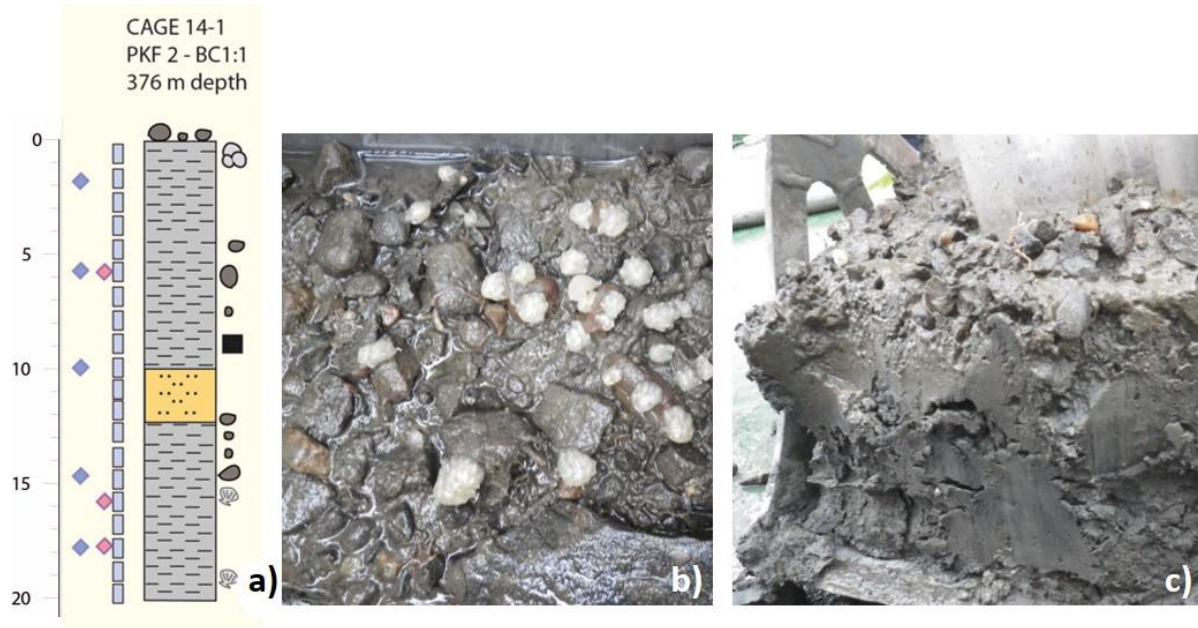


Fig. 5.14a and b) A box core with pebbles at the surface was taken from 376 m water depth. a) shows the sediment log of the box core. c) Cross-section through about 20 cm sediment. In the grey clay below the pebbles, foraminifera were present. Further downcore, pebbles, a compacted and a silty layer occurred. The grey clay contained pebbles and shell fragments. At 18-20 depth, an intact bivalve was found in situ.

*PKF 3 - Prins Karls Forland 3. Box core*



Fig. 5.15 From a water depth of 116m a box core with pebbles at the surface was taken. The uppermost layer of the core was composed of brown clay. The colour changed into grey clay at 4 cm. Black patches, pebbles and shell

fragments occurred further downcore. Living and dead *Macoma calcarea* and *Mya truncata* (empty but complete shells) were found in black patchy areas, the shells were partly black. a) shows the sediment log of the box core.

*PKF 4; 5; 5G; 6; 7 - Prins Karls Forland*

*PKF 4; 5; 6; 7: Box cores,*

*PKF 5G: Van Veen grab*

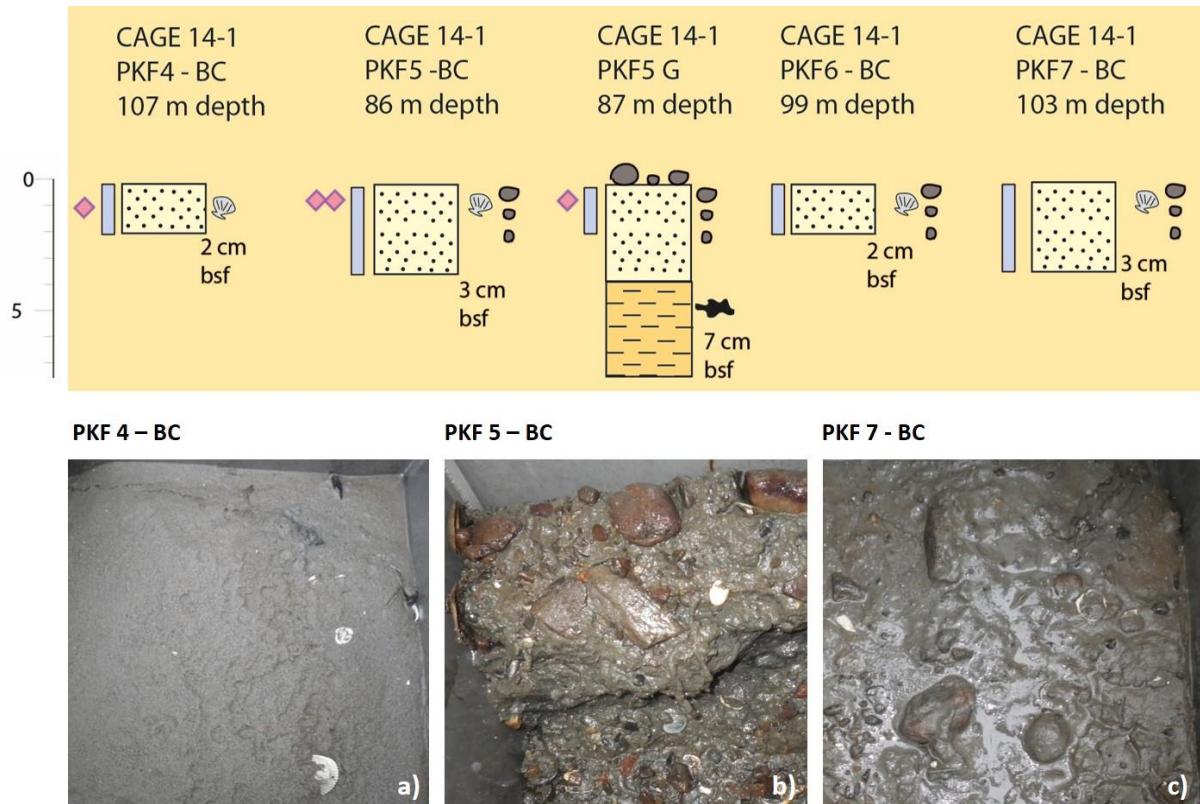


Fig. 5.16 At the site PKF 4 in 107 m water depth, shell fragments were found. Carbonate-cemented sandstone and a cemented *Mya truncata* shell were found. The box core PKF 5 contained little material consisting of brown clay with sand, gravels, pebbles and shell fragments. PKF 5 G was material taken from a Van Veen grab sample. The surface material was characterized by brown clay with sand and shell fragments, gravel and pebbles of several lithologies. In 3-4 cm depth below the sediment surface, the material changed into grey clay with occasional black patches. The box cores PKF 6 and PKF 7 from 99 and 103 m water depth were characterized by sandy surface material with shell fragments and pebbles. In PKF 7, intact *Macoma calcarea* shells occurred.

*PKF 8 - Prins Karls Forland 8. Box core*

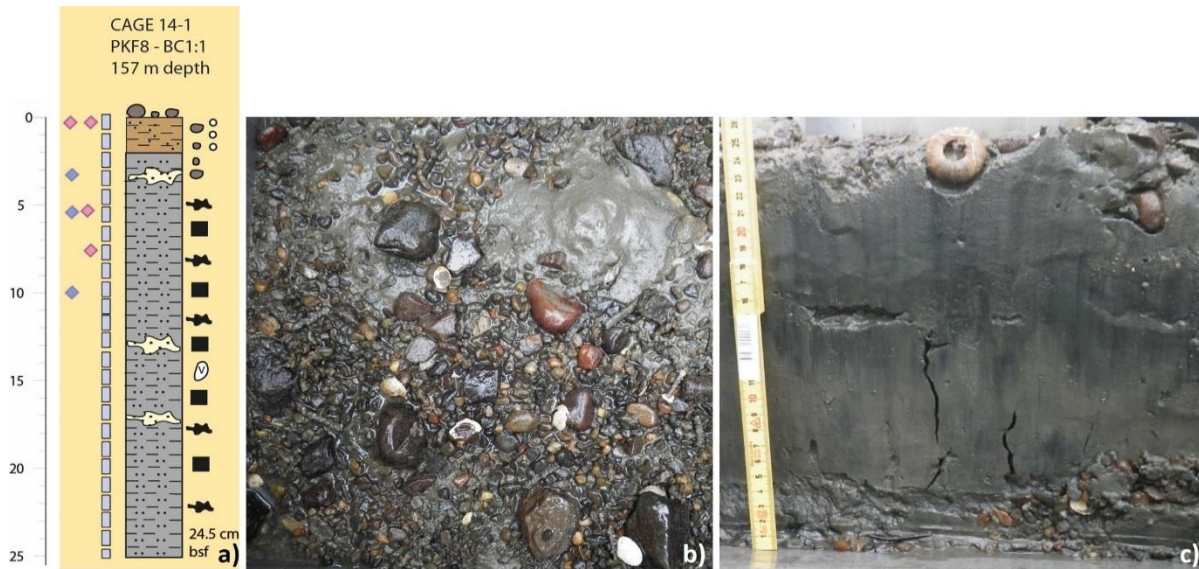


Fig. 5.17 From the site PKF 8 a box core with brown mud, sand and gravel at the surface was recovered from 157 m water depth. The surface facies was soupy below the pebble layer. The pebbles were subrounded in shape, had a diameter of < 2cm, and were composed of different lithologies. The sediment changed into grey clay 2 cm below the surface. Black patches, sand lenses and compact, stiff areas occurred sommonly within the grey clay. A void with a diameter of 1.5 cm was found in 14-15 cm depth below the seafloor surface. a) shows the sediment log of the box core.

*PKF 9 - Prins Karls Forland 9. Box core*



Fig. 5.18 A box core from the area PKF 9 in 169 m water depth was sampled. On the surface, pebbles of different lithologies and subangular to subrounded shape were found and removed prior to pushing in the multicore tubes. The sediment in the first 3 cm below the pebble layer was brown clay with shell fragments and clasts. The

colour of the sediment changed into grey clay. Furthermore, a small amount of sand, sand lenses and black patches occurred. Within the black patches, living *Macoma calcareata* were found and sampled for biological and stable isotope analyses. The lowermost cm of the core consisted of grey silty-clay. The black patches disappeared. a) shows the sediment log of the box core.

### 5.7. Methane and porewater

Dissolved constituents of sediment porewater are determined to study the biogeochemical activity in the sediments which is mainly controlled by the amount of organic matter deposited at a site, the sedimentation rate, the sediment composition or the influence of hydrocarbon or other fluid seepage.

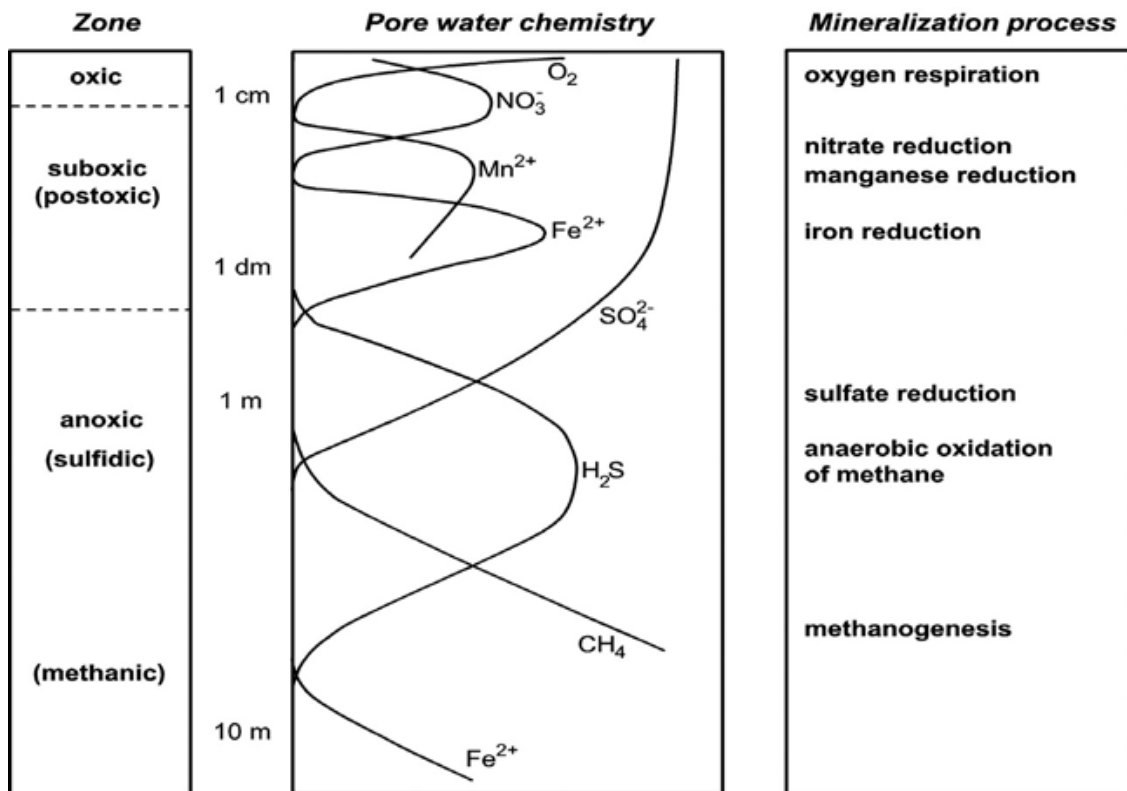


Fig. 5.19 Schematic representation of the biogeochemical zonation in marine sediments (modified from Froelich et al. [1979]).

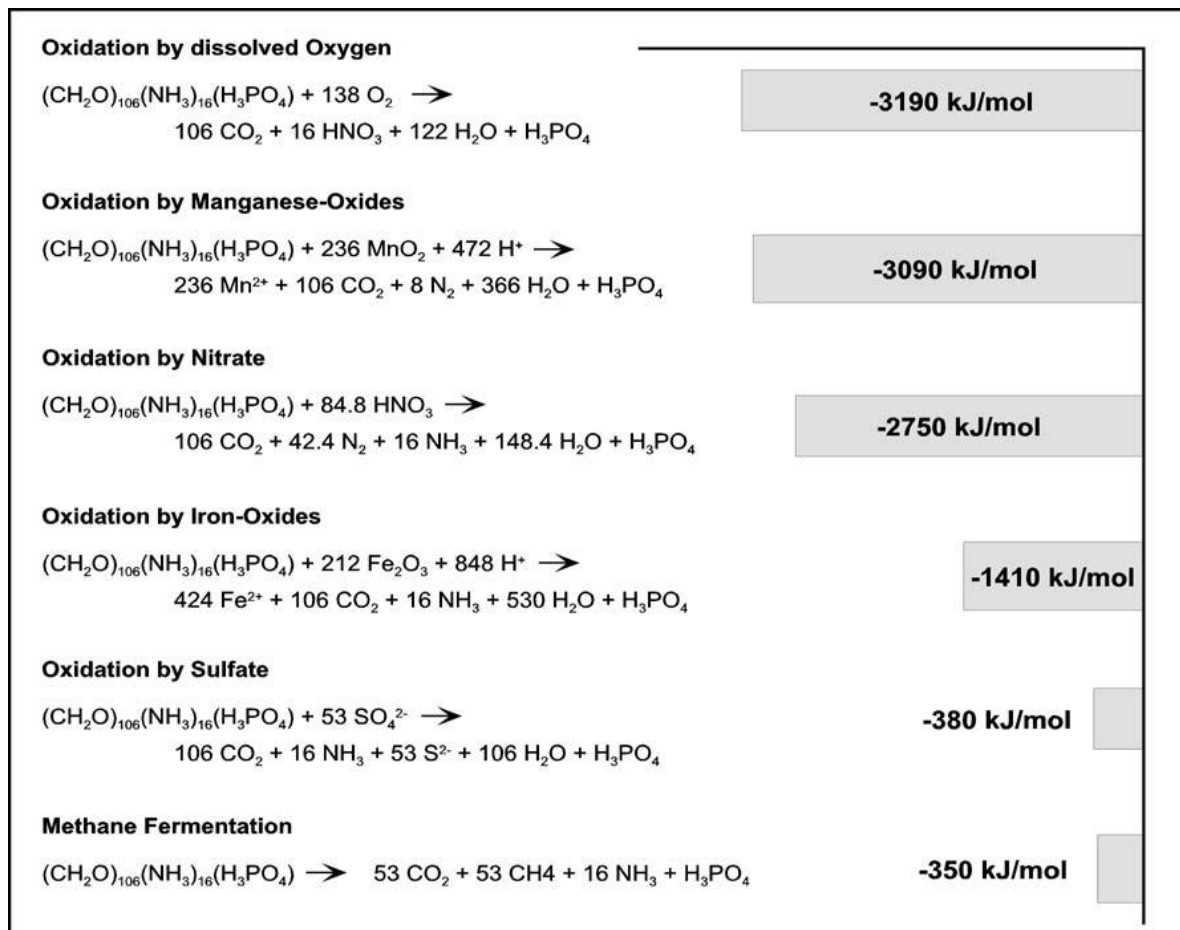


Fig. 5.20 Degradation of organic matter with different electron acceptors (modified from Froelich et al. [1979]).

The generalized porewater profiles and the reactions producing these are shown in Fig. 5.28 and 5.21. The sequence of the different electron acceptors with depth is determined by the energy yield that the microorganisms receive from remineralising organic matter using these different constituents. The last step is methanogenesis which can only occur when sulphate is depleted to a certain level. The methane produced in the methanogenic zone diffuses upward and is oxidized by sulphate. This anaerobic oxidation of methane (AOM, Fig x) produces the sulphate-methane-transition-zone (SMTZ).

The net reaction is:



At a non-seep site with only diffusive transport the depth of the SMTZ is mostly influenced by the organic matter content of the sediment. In the case of high organic matter content sulphate reduction starts earlier (closer to the seabed) because all the other electron

acceptors are used up faster. This means also sulphate will be depleted earlier and methanogenesis can start in shallower depths producing a SMTZ closer to the seafloor. On the other hand, in sediments with low organic matter content sulphate can penetrate to much greater depths.

At sites with advective transport of methane rich fluids from deeper sources the depth of the SMTZ is mainly controlled by this fluid flow. Strong fluid flow “pushes” the SMTZ upward [Borowski *et al.*, 1996].

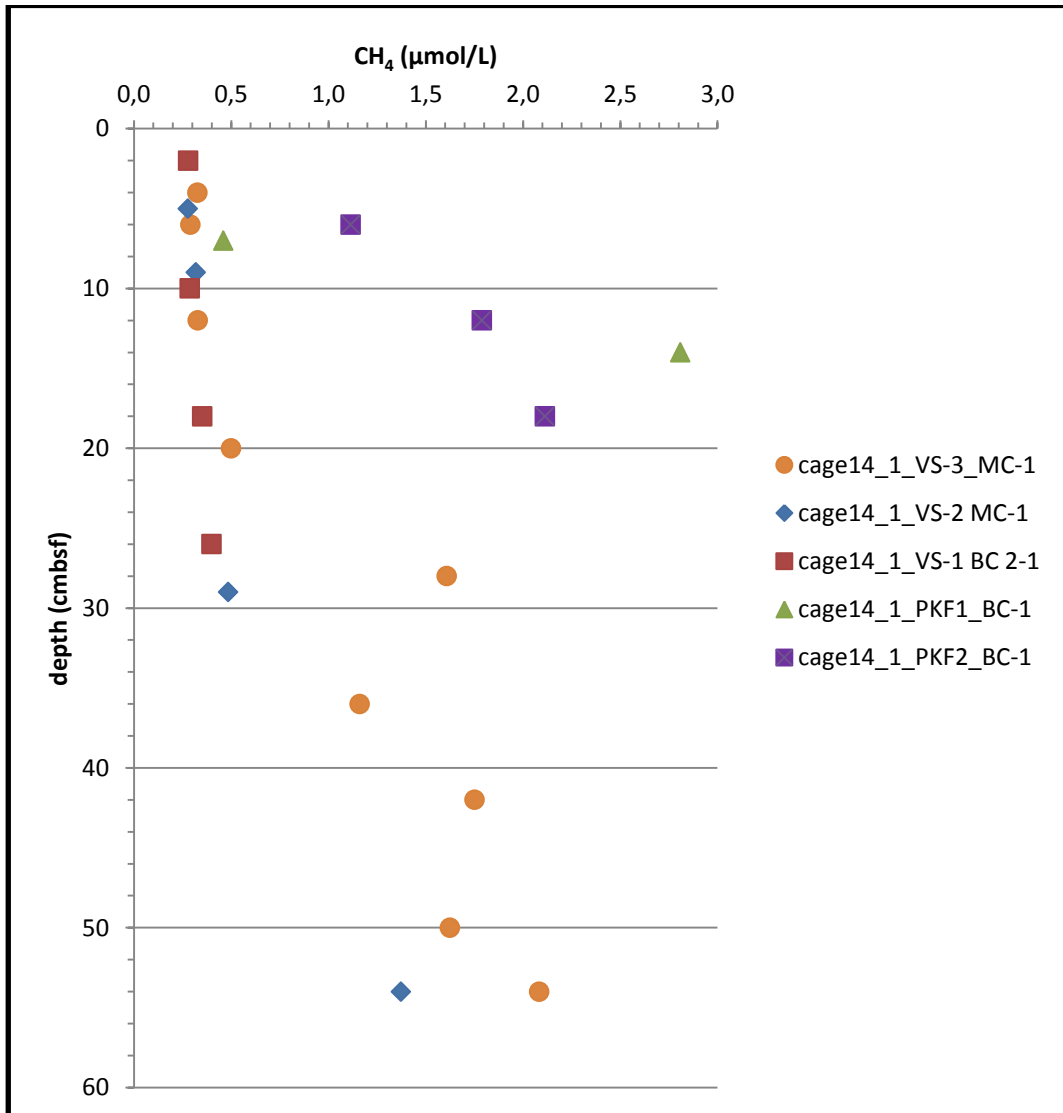


Fig. 5.22 Methane concentration in sediments from box core and multicore samples.

All samples from box and multicores shown in Fig. 5.21 contained methane concentrations in the  $\mu\text{mol/l}$  range, which means the SMTZ was not reached in any of the cores as methane concentrations below the SMTZ generally increase up to several  $\text{mmol/l}$ . However the profiles from Prins Karls Foreland (PKF1 and PKF2) show a steeper increase in methane with depth which indicates a shallower SMTZ at these two sites than compared to the sampled sites located on the Vestnesa Ridge (VS1; -2; -3).

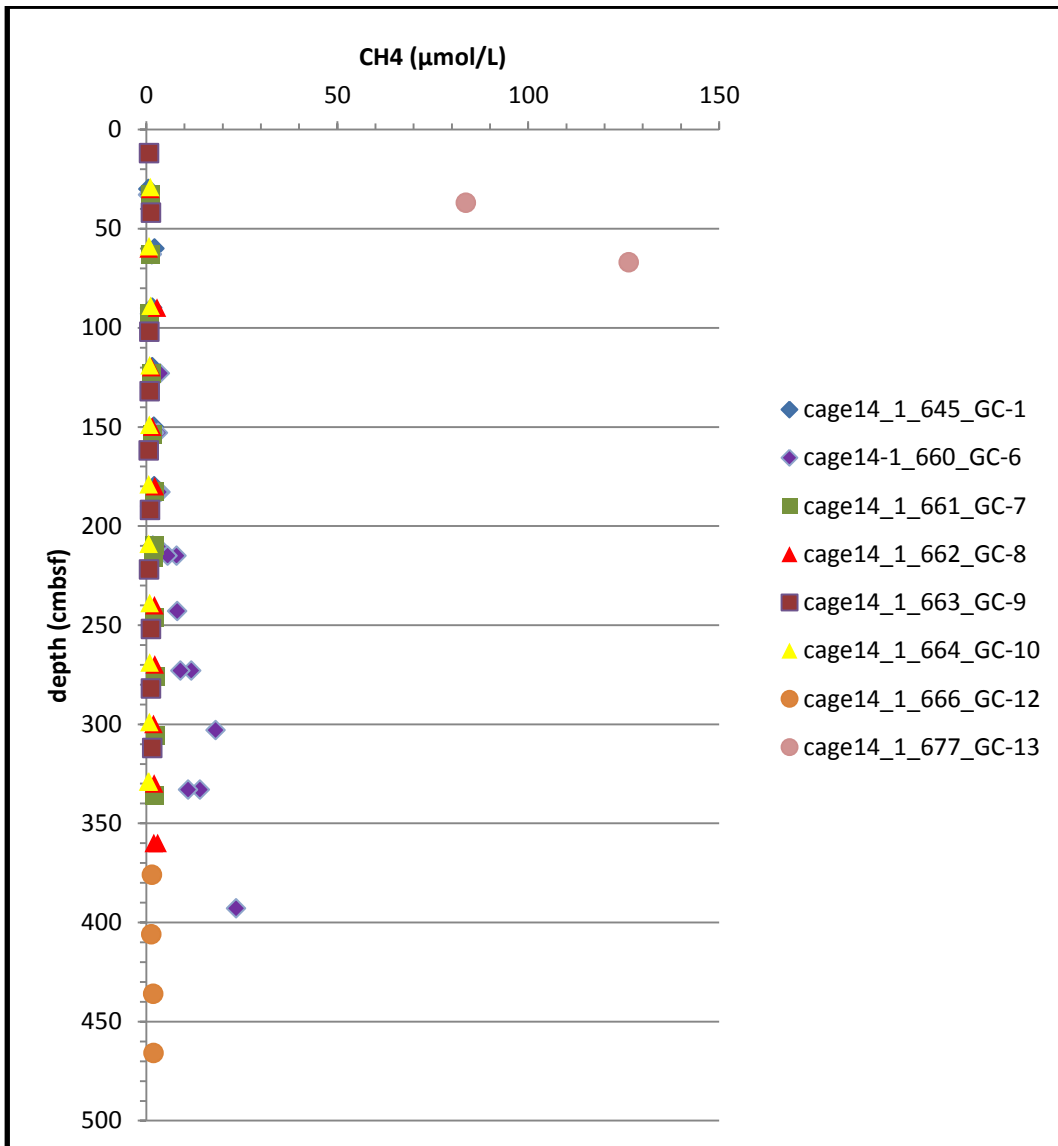


Fig. 5.22 Methane concentration in gravity cores from areas with low to no methane seepage (for locations see Fig. 1.1, 2.1a, 2.1b).

The methane concentration in the gravity cores plotted in Fig. 5.22 also show low methane values in the  $\mu\text{mol/l}$  range. Such low values down to depths of 3-4 m below the sediment surface

indicate the absence of methane seepage at these sites. Only in GC-13 slightly higher CH<sub>4</sub> values were measured, however so far only two samples from this core have been analysed.

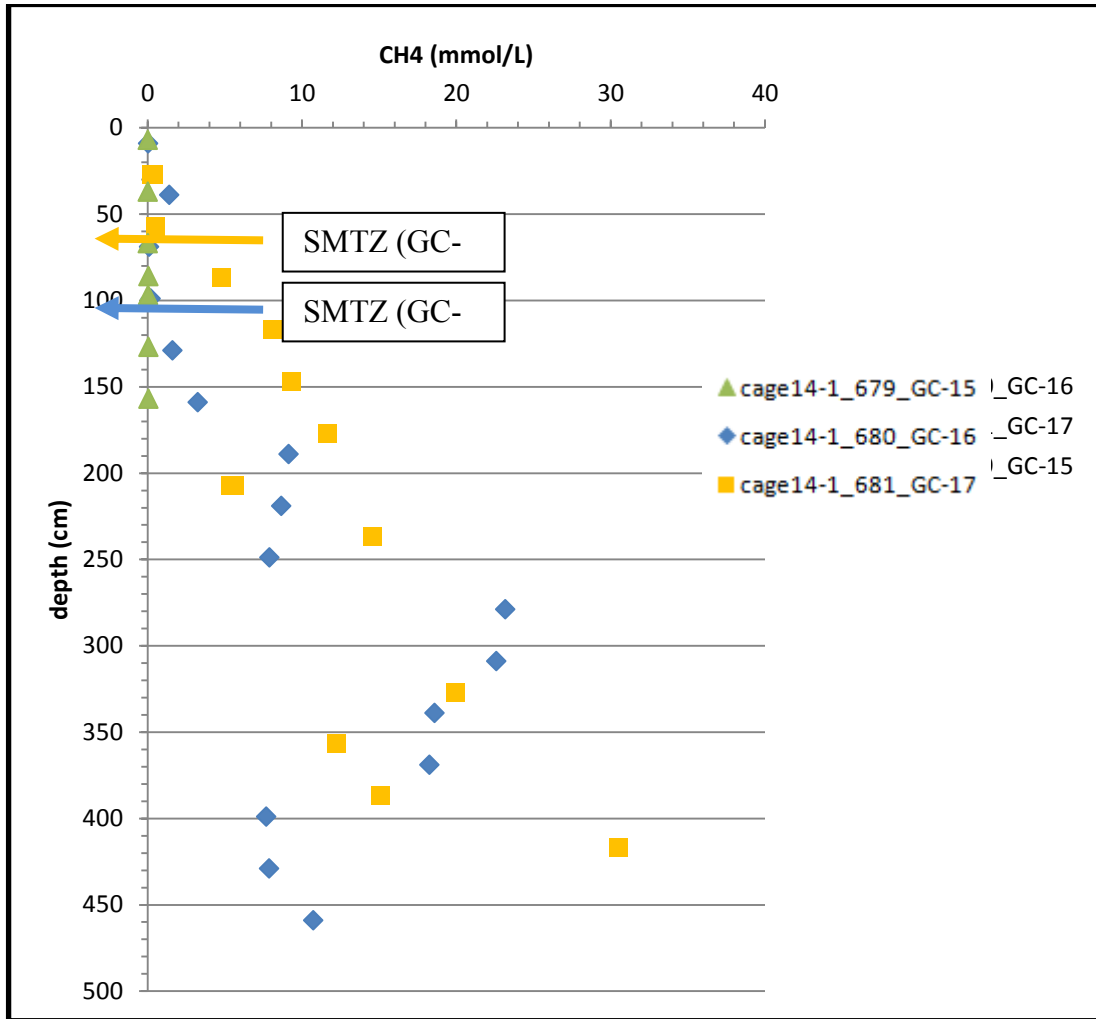


Fig. 5.23 Methane concentrations in gravity cores from Vestnesa ridge. Note that the concentration is in mmol/l. The arrows indicate the depth of the SMTZ.

The methane profiles shown in Fig. 5.23 are all from gravity cores taken on Vestnesa ridge (see Fig. 1.1). These are the only samples with methane concentrations in the mmol/l range. In core GC-16 the SMTZ is at 90 cm bsf and methane concentrations increase to above 20mmol/l at around 300 cm bsf. In core GC-17 the SMTZ is at 60 cm bsf and methane concentrations increase up to 30 mmol/- at around 400 cm bsf. This indicates high methane flux at these sites. Furthermore, gas hydrate has been observed in both cores.

## 5.8. Agglutinated foraminifera and authigenic carbonates in active vent sites

Tubes on the surface of box core PKF 2 BC 1 from Prins Karls Forland 2 (PKF 2) and the Vestnesa ridge (VR 1) were first thought to be worm tubes, but were later identified as tests of the agglutinated foraminifera (figures 5.24 and 5.25). At both sites, the surface of the sediments was covered with foraminifera tests.

This is the first observation of agglutinated foraminifera in active methane seep sites in the Arctic Ocean. So far, those species are not described from active methane seep environments, but from hydrothermal vents (pers. comm. Prof. Giuliana Panieri). During the AMGG cruise, agglutinated foraminifera tests were found on active seep sites with soft and hard bottom conditions. The species identification is still in progress, but probably the active methane seepage is a common characteristic for both sites and may be reflected in the presence of agglutinated foraminifera.



Fig. 5.24 Agglutinated foraminifera tests of the species *Bigenerina ramosa* on the seafloor surface of box core PKF 2 BC 1 offshore Prins Karls Forland. The tubes are around 2 cm long.



Fig. 5.25 Agglutinated foraminifera tests on the seafloor surface of multicore VR 1 MUC 1:1. Arrows indicate tests, they are up to 3 cm long and have several chambers. Diameter of the core liner is 10 cm.

## 5.9. Authigenic carbonates

At the site Prins Karls Forland 1 (PKF 1), a large piece of authigenic carbonate was found in a box core from 244 m water depth (Fig. 5.26). A carbonate test with hydrochloric acid (HCl, 10 %) was performed with a positive result. The carbonate crust piece is ca. 15 cm long and up to 7 cm wide, and light and dark grey in colour. It cements sand grains and dark pebbles up to 1 cm in diameter. The crust contains shell fragments and a worm tube with the worm still living in it (Fig. 5.27). The worm tube was removed for taxonomic analyses of the worm and stable carbon isotope analyses of its tube. The crust piece may originate from carbonate precipitation at the seafloor linked to active methane seepage. Further analyses of the carbonate as well as dating of the carbonate itself (U/Th dating) and the shell fragments (Radiocarbon dating) are a possible approach to characterize the material and to determine its age.

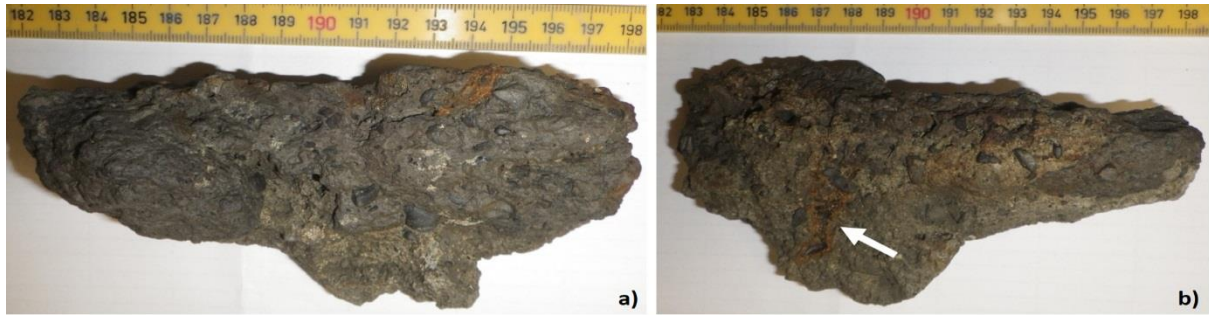


Fig. 5.26. The carbonate piece from PKF 1 seen from both sides. The scale is in cm. The arrow in b) points to a brownish worm tube.

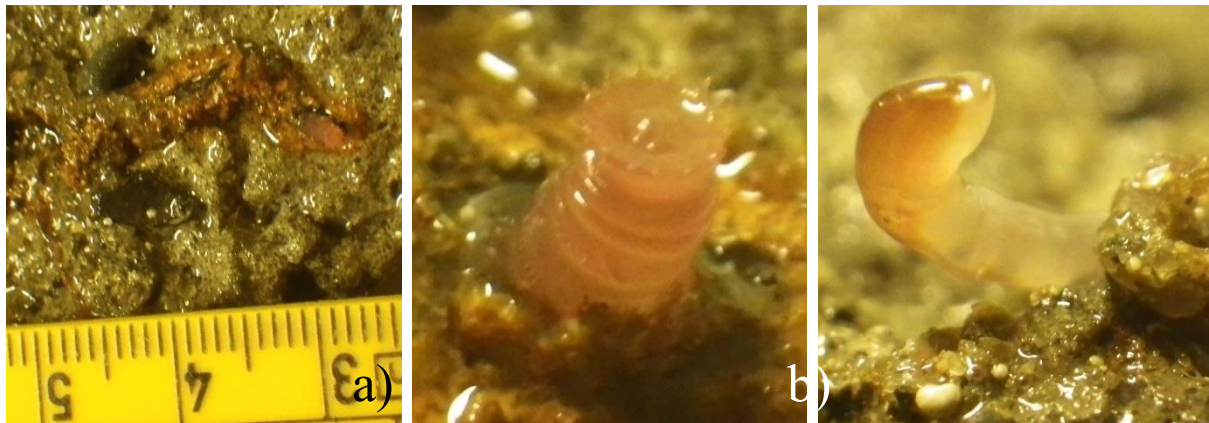


Fig. 5.27 Close-up of the worm tube in a). The scale is in cm. The next fotos show the b) anterior and c) posterior end of the worm that was still living in its tube.

At the site Prins Karls Forland 4 (PKF 4), carbonate-cemented sand grains and a carbonate-cemented *Mya truncata*-shell with both valves were found (Fig. 5.28). A carbonate test with hydrochloric acid (HCl, 10 %) was performed with a positive result. Here, possibly an outcrop of Eocene rocks at the seafloor near the sampling site is responsible for the findings (pers. comm. Joel Johnson).



Fig. 5.28 a) Carbonate-cemented sand grains and b) a carbonate-cemented *Mya truncata*-shell with both valves from Prins Karls Forland 4 (PKF 4). The scale is in cm.

## 6. Benthic macro fauna analysis

The aim with the work is to determine:

- I. *What are the faunal characteristics (diversity and functional groups) in methane seep areas in this region?*
- II. *To what extent does benthic macro fauna use chemosynthesis as an alternative energy source?*
- III. *What is the trophic relationship in an Arctic macro faunal seep community?*
- IV. *Is it possible to detect temporal/spatial variation in methane release in arctic bivalve shells by sclerochronology?*

### 6.1. Benthic community structure

In Arctic regions it is well documented that marine benthic communities can serve as long term bio indicators for physical and environmental changes [Ambrose *et al.*, 2012; Carroll *et al.*, 2009; Clark and Rowden, 2009; Cochrane *et al.*, 2012; Nilsson and Rosenberg, 2000]. Along with proceeding climate change [ACIA, 2005; Stocker *et al.*, 2013] and scientific research bringing better understanding to the function of Arctic ecosystems, there is a continues need of future studies in these previously pristine areas. Anthropogenic disturbance and exploration in Polar Regions is believed to escalate when shrinking sea ice and prolonged ice free summers will open up new waterways in the Arctic [Anisimov *et al.*, 2007; Christiansen *et al.*, 2014; Clarke and Harris, 2003; Tynan and DeMaster, 1997]. In high latitudes, Arctic benthic organisms have to deal with physical parameters as strong seasonal variations, sub-zero water temperatures and sea ice, implications that are not occurring at lower latitudes. Months of continues polar night and midnight sun are two concrete examples of what might regulate marine life in the Arctic. Macro faunal studies in Svalbard shelf and fjords shows how organisms have adapted to different physical influences and disturbances creating diverse marine ecosystems. Sub seabed gas seepages and hydrothermal vents are two natural occurring disturbances that may cause changes in the environmental conditions on the sea floor. Recent fieldwork and previous studies in Svalbard waters and Barents Sea have discovered gas plumes emerging from the sea floor and elevated gas concentrations in the water [Long *et al.*, 1998; G Westbrook *et al.*, 2008; G K Westbrook *et al.*, 2009]. Gas leaking from sub seabed reservoirs provides the possibility for chemosynthetic derived

ecosystems to form around these geomorphological features. Studies all over the world have seen ecosystems partly or fully driven by chemoautotrophs formed around hydrothermal vents, seeps or mud volcanoes, instead of photosynthesis which is usually the main energy source [Boetius and Suess, 2004; Joye et al., 2010; Lösekann et al., 2007; Niemann et al., 2006; Vanreusel et al., 2009]. With new evidence of hydrothermal deposits and gas release from sub seabed reservoirs in Svalbard waters it is likely to believe that this physical disturbance can change the local environmental conditions and influence the present ecosystem structure and faunal diversity.

## **6.2. Stable isotopes**

Constructing a food web, or to determine the trophic relationship within the benthic community and detecting the origin of digested carbon, stable isotope techniques is a useful tool. With use of  $^{13}\text{C}$  stable carbon isotope analyses, the trophic relationship between organisms in seep communities may be determined. It will also reveal whether the main energy source is derived from photosynthetic detritus matter or chemosynthetic autotrophs. Stable isotope techniques make it possible to trace compounds as methane since it has a distinct depleted signal of  $\delta^{13}\text{C}$ , which has been documented from methane associated ecosystems worldwide [Lösekann et al., 2007; Thurber et al., 2010; Vanreusel et al., 2009; Zapata-Hernández et al., 2014].

Another useful tool for determine trophic relationships in a marine food web is the use of stable isotope  $\delta^{15}\text{N}$ . Generally,  $^{15}\text{N}$  is enriched by 3-4 % for each trophic level in the marine food chain which gives possibility to document the diet of an organism (consumer). Documentation of trophic food web analysis in Svalbard waters has been successfully studied and developed by Søreide and collaborators [Søreide et al., 2013; Søreide et al., 2006; Tamelander et al., 2006]. By combining these two tools, a first step to construct a food web is possible to carry out. This will reveal the basic relationship between collected animals and also give an indication of which carbon source the organisms mainly is feeding from.

### **6.3. Sclerochronology**

Sclerochronology is a method that can be applied in organisms creating a hard shell or skeleton i.e bivalves, foraminifera and corals. Generally explained, sclerochronology is used to count lines and relate them to different environmental events, or seasonal changes. Compounds from the surrounding environments incorporates in the shell during the lifetime of an organism and this geochemical information could be used to determine local conditions on the sea floor [Jones, 1983]. By collecting both living bivalves and empty valves we want to use sclerochronology and relate this to methane release in the target areas. Our wishes is to document if there is any connection between growth, incorporated compounds in the shells and spatial and temporal release of gas from the sea floor.

The combination of all three methods, diversity and faunal structure, stable isotopes and sclerochronology, will serve as an important tool to reveal the structure and function in Arctic seep ecosystems associated with methane.

### **6.4. Materials and methods**

In total 14 stations where sampled in four different locations, shallow Prins Karls Forland, shelf Prins Karls Forland, Vestnesa south and Vestnesa ridge. Detailed information is given in Table 6.1.

*Sampling took place in three different key areas; coastal shallow, shelf break and deep sea margin, Fig. 6.1. A control station was used in the mouth of Kongsfjord as a reference site for non-methane impact.*

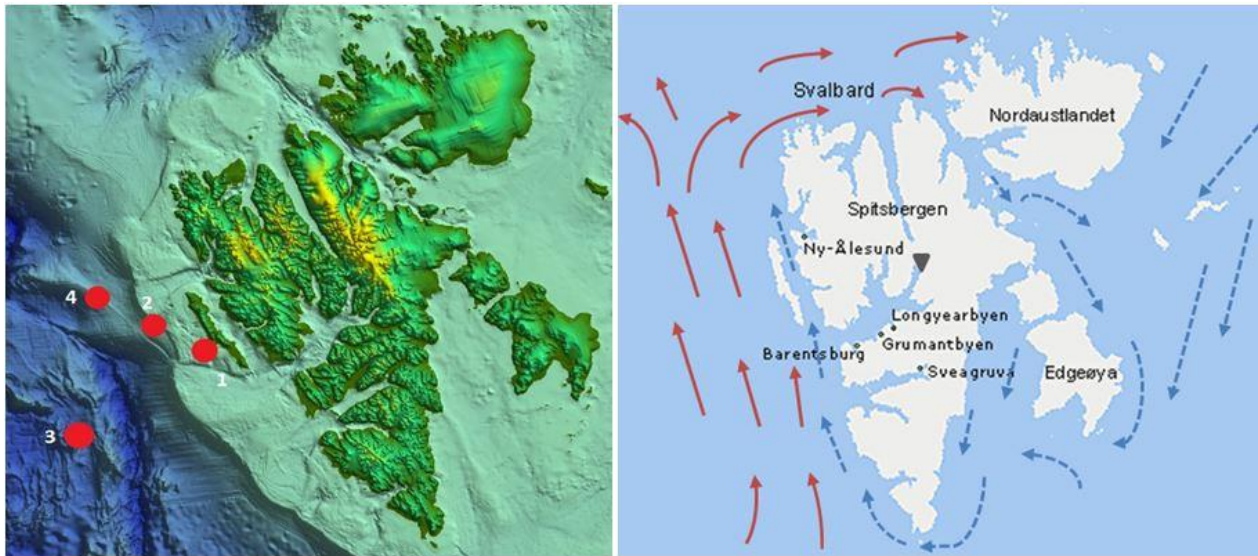


Fig. 6.3 To the left, benthic sampling locations during the cruise in June, shallow shelf stations 1 (80-150 m deep) and 2 (240-350 m deep, and Vestnesa deep continental margin slope, 3-4 (approx. 1200-1500 m deep). Illustration map modified E. Piasecka and author CAGE. To the right, current regime around Svalbard. Dashed, blue arrows show Arctic cold water and red, solid arrows warm Atlantic water. Modified from *Ingvaldsen and Loeng* [2009].

## 6.5. Sampling

For quantitative benthic sampling a van Veen grab  $0.1 \text{ m}^2$  (Fig. 6.2) were used in three different stations with five replicates each. An additional sixth qualitative replicate was taken for sediment analysis and collection of fauna for isotopic analysis. The weight of the grab was adjusted to fit the sediment conditions. Before accepting a grab, it was inspected so the jaws were closed, the grab was filled and had an undisturbed surface layer to avoid miss-placed grabs. For both quantitative and qualitative analyses, a box corer, were used in the majority of the locations, ten in total, because of stony and gravelly bottom substrata.

Sub cores ( $\emptyset$  13 cm), were taken from box, - and multi core for analysing the characteristics of the sediment and for collecting qualitative material for isotope analysis. In the deep sea stations, sub cores were used for quantitative sampling. Multi corer were used for sediment characteristics in addition to quantitative sampling were the suitable bottom substrata allowed this. Hydrography data collection, provided by a CTD rosette, was operated nearby the benthic faunal stations, to record characteristics of surrounding water masses i.e. conductivity, temperature and density. The rosette was equipped with 12, 10 L, Niskin bottles used for vertical

sampling in the water column to analyses content of methane and nutrients, (N, P and Si). The different benthic sampling techniques were used in regard to environmental conditions on the sea floor. For quantitative analysis, it would have been desirable to have van Veen grabs from as many stations possible. But due to stony, hard bottom and time-depth limited sampling, some stations were replaced with either box corer or multi corer.

Quantitative sampling with van Veen and multi corer were treated in accordance to ISO 16665:2014 field work assignments as far possible and sieved for mesh size 0.5 mm. Sub cores sampled from the Box corer and tubes from the multi corer were brought into the wet lab where they were sliced in relevance to the aim of the sample. In total, sediment samples will be analysed for Pb <sup>210</sup>, TOC (Total organic carbon), porosity, chlorophyll and grain size from different coring stations. In addition, organisms were collected for isotopic analysis C<sup>13</sup> and N<sup>15</sup> by sieving left over material from the Box corer, miss-cast or rejected grabs, see Table 6.2 in. This data will serve a base for constructing a food web over a methane seep community in the Arctic and we will be able to see links and relationships between the organisms in the ecosystem.



Fig. 6.4 Van Veen grab (0.1 m<sup>2</sup>) in open mode (Photo, private)

Table 6.1: Detailed sampling information, location, depth, time and oceanographic parameters (T, S and water mass according to *Nilsen et al.* [2008]; *Svendsen et al.* [2002]).  
Abbreviations for sampling tools refers to: Grab = van Veen grab 0.1 m<sup>2</sup>; BC= Box corer and MC

Location	Date	Sampling	Station #	Latitude °N	Longitude °E	Depth (m)	Time (UTC)	Salinity (psu)	Temp. bottom (C°)	Water mass
Kongsfjord control site	20.06.2014	Grab/MuC	V12	78° 59.5'	09° 29.5'	212	10:00	35.1	2.2	TAW
Shelf break	21.06.2014	Grab	PKF1 G	78° 39.3'	09° 26.2'	248	18:32	35.1	3.0	AtW
Shelf break	22.06.2014	BC	PKF1	78° 39.3'	09° 25.9'	245	00:20	35.1	3.0	AtW
Shelf break	22.06.2014	BC	PKF2	78° 37.6'	09° 24.5'	350	07:41	35.1	3.4	AtW
Shallow shelf	25.06.2014	BC	PKF3	78° 33.2'	10° 05.7'	113	09:34	35.1	3.8	AtW
Shallow shelf	25.06.2014	BC	PKF4	78° 33.4'	10° 07.4'	107	12:29	35.1	3.6	AtW
Shallow shelf	25.06.2014	BC	PKF5	78° 33.6'	10° 09.1'	85	17:58	35.1	3.8	AtW
Shallow shelf	25.06.2014	BC	PKF6	78° 33.8'	10° 10.0'	79	21:19	35.1	3.6	AtW
Shallow shelf	26.06.2014	BC	PKF7	78° 34.1'	10° 11.6'	97	02:20	35.1	3.8	AtW
Shallow shelf	26.06.2014	BC	PKF8	78° 34.3'	10° 13.6'	157	06:14	35.1	3.6	AtW
Shallow shelf	26.06.2014	BC	PKF9	78° 34.5'	10° 15.2'	162	11:33	35.1	3.3	AtW
Shallow shelf	27.06.2014	Grab	PKF5 G	78° 33.6'	10° 09.0'	86	21:00	-	-	No CTD
Vestnesa ridge	28.06.2014	MuC	VR1	79° 00.4'	06° 54.1'	1205	07:45	34.9	-0.8	WCW
Vestnesa south	23.06.2014	MuC	VS1	78° 18.2'	05° 48.6'	1577	15:24	34.9	-0.8	WCW
Vestnesa south	23.06.2014	Muc	VS2	78° 21.3'	05° 47.1'	1618	16:57	-	-	No CTD
Vestnesa south	23.06.2014	Muc	VS3	78° 30.2'	05° 42.6'	1706	18:58	-	-	No CTD

## 6.6. Results

### *Hydrography*

The hydrography on the different sampling sites differed from the shallow shelf and shelf area compared to the deep sea. The CTD-data showed that Atlantic water is dominating the shallow shelf area (Table 6.1). The control station, V 12 has transformed Atlantic water (TAW) on the seafloor at 212 m depth. It is slightly colder compared to the Atlantic water but have the same density. The deep sea stations are characterized by cold water, -0.8 C which refer to winter cooled water according to *Nilsen et al.* [2008]; *Svendsen et al.* [2002]. These two stations are off the shelf, in the mid oceanic ridge zone below 1000 m depth. Elevated concentrations of methane from the water column were seen at particularly two locations, Prins Karls Forland shelf, and shallow Prins Karls Forland site, Fig. 6.3.

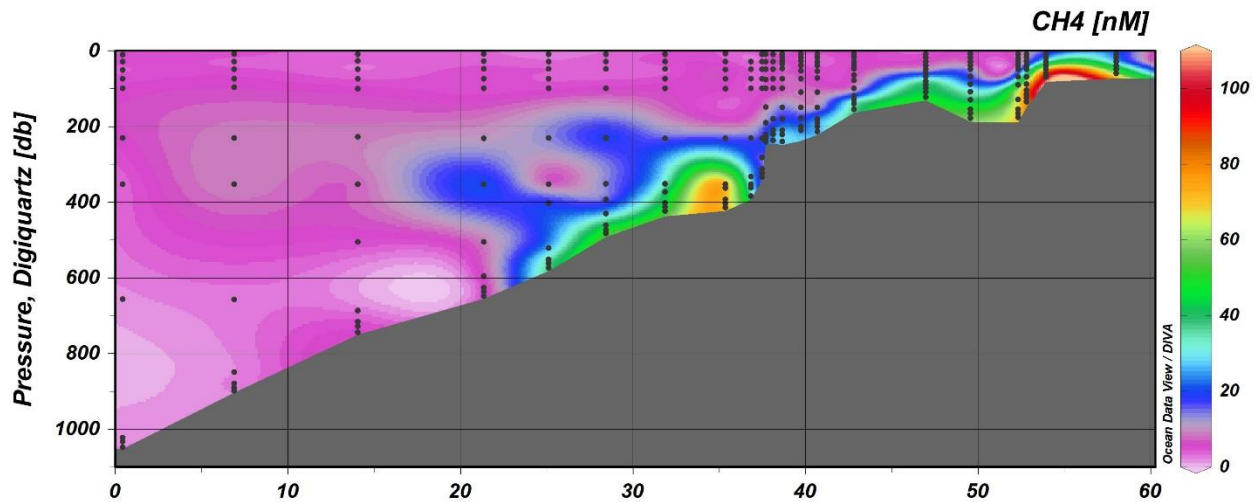


Fig. 6.5 Methane concentrations in the water column from Western Svalbard margin CTD-transect, 20-21 of June 2014.

### *Characteristics of sediment and faunal sampling*

Three quantitative grab sampling stations were conducted during the cruise, one from the control station V12 and two from the shelf area where methane plumes were detected, one shallow and one deeper (PKF 5 and PKF 1). The control station varied in sediment characteristics compared to the shelf stations, Fig. 6.3, where the sediment core contained grey silt and hemiplegic mud, Fig. 5.7 Five quantitative replicates were taken, all in soft sediment, clay and hemi pelagic mud with gravel, stones and surface water on top. The two shelf stations were

characterized by more gravel, sand and stones,  $\varnothing$  2-3 cm and additional weights had to be attached to the grab to be able to penetrate the sediment for receiving a full grab. Based on what was seen in the grab samples and box corer, Prins Karls Forland had several typical hard-bottom associated species, e.g. sea-urchins, scallops, ophiurids and chitons, (Fig. 6.4 and Table 6.2). A box core transect was made in combination with an oceanographic CTD-transect in shallow Prins Karls Forland during the 25-26<sup>th</sup> of June. Main objective was to get an overview over the bottom and sediment characteristics in the strongest flare field area. Stations sampled were PKF3-PKF9 but sufficient sediment cores were just given in PKF 3, PKF 8 and PKF9, see Fig. 5.7. Left over material from this transect was rinsed and larger visible organisms were picked for isotopic analysis. This material cannot be used quantitatively since the box corer had uneven amount of sediment inside from time to time. Also, the selection of organisms is subjective as they were elected in consideration of isotope analysis, i.e. size and presumable trophic niche. Shells from dead bivalves, both complete and single valves were selected from box-core material to be able to do sclerochronological analysis in regard of methane. At PKF 2, empty shells from a so far unknown bivalve were found, it was confirmed that this bivalve belongs to the family of Thyasiridae, but it is not familiar to any species yet, (pers.comm. Jesper Hansen Akvaplan-niva).

Multicorer and box corer were used in the deep sea stations. In Vestnesa south, three stations were sampled with the multi corer and sieved for faunal characteristics. The seabed surface was characterized as a typical deep sea soft bottom with few organisms on top of the sediment. The first station differed to the other two, containing biogenic sand, composed by dead foraminifera causing a reddish, yellow colour of the sediment. VS 2 had more brown clay as well as VS 3. In the last station (VS 3) bubbles venting from the core were seen, no particular smell but bubbles were transported from the bottom of the core up to the surface.

In the faunal samples, sieved on board, few larger organisms were seen, and they were mainly polychaetes. In Vestnesa ridge (VR 1) a record of seep polychaetes were found which later were confirmed by taxonomist as worms in the family Siboglinidae, clade Frenulata (*pers. comm.* Jesper Hansen and Andrei Sikorski, Akvaplan-niva).



Fig. 6.6 Two images from the box-core. To the left, Prins Karls Forland station 3 (PKF 3) depth 116 m, sample is stony with pebbles and larger boulders. Larger macro fauna as sea urchins, chitons, brittle stars and calcareous tubeworms visible at the upper layer of the sediment. To the right, samples from Vestnesa south (VS 1) 1577 m deep with soft sediment and biogenic sand. Predominately agglutinated and calcareous foraminifera were seen on top of the sediment. (Photos private).

Table 6.2: Overview and taxon list for species collected for isotope analysis  $\delta^{13}\text{C}$  and  $\delta^{15}\text{N}$ .

Taxa	VS12	PKF1	PKF2	PKF3	PKF4	PKF5	PKF6	PKF7	PKF8	PKF9	PKF 5 grab
Amphipoda indet	0	0	0	0	0	0	0	0	2	3	0
<i>Astarte borealis</i>	0	0	0	0	2	0	0	1	0	0	0
<i>Astarte crenata</i>	0	0	0	0	0	0	0	0	1	0	0
<i>Astarte elliptica</i>	0	0	0	0	4	3	0	1	0	0	6
Bivalvia indet	0	0	0	1	4	1	0	0	0	1	0
<i>Brada villosa</i>	0	0	0	0	0	1	0	0	0	1	0
<i>Chlamys islandica</i>	0	1	0	0	0	0	0	0	0	0	0
<i>Ciliatocardium ciliatum</i>	0	0	0	0	0	0	0	2	0	0	0
<i>Diplocirrus glaucus</i>	0	0	0	0	0	1	0	0	0	0	0
Golfingia	3	0	0	1	0	0	0	0	0	0	0
<i>Lepeta caeca</i>	0	0	0	0	0	0	0	0	0	1	0
Lumbrineridae	0	0	0	0	1	0	0	0	1	1	2
<i>Macoma calcarea</i>	0	0	0	7	0	15	0	2	13	6	0
Maldanidae indet	0	1	0	3	0	0	0	0	1	5	5
Natacidae ( <i>Naticia clausa</i> )	0	0	0	1	0	1	0	0	0	0	0
Nemertea indet	0	0	0	0	1	2	0	1	1	0	1
<i>Nephtys sp.</i>	1	0	1	0	0	0	0	1	1	0	0
<i>Niomache lumbricalis</i>	0	0	0	1	1	1	0	0	1	1	0
<i>Notomastus latericeus</i>	0	0	0	0	0	0	0	0	1	0	0
<i>Ophiopholis acuelata?</i>	0	0	0	0	0	0	0	0	0	3	0
Ophiura indet	2	0	6	3	3	6	0	0	1	5	9
Phyllodocidae	0	0	1	0	1	0	0	0	0	0	0
Polynoid	0	0	1	0	0	0	0	0	0	0	0
<i>Priapulus caudatus</i>	0	0	0	0	0	0	0	0	0	1	1
Rissoidae?	0	0	0	0	0	1	0	0	0	0	0
<i>Scoletoma fragilis</i>	0	0	0	3	0	0	0	2	0	1	0
<i>Scoloplos armiger</i>	0	0	0	0	2	0	0	1	0	0	1
Sipunculid	0	0	0	0	0	0	0	0	1	4	1
<i>Spirontocaris spinus</i>	0	1	0	0	0	0	0	0	0	0	0
<i>Strongylocentrotus droebachiensis</i>	0	0	0	3	0	1	0	0	1	2	2
Terebellomorpha	0	0	2	0	1	0	0	0	2	0	0
<i>Terrebellides stroemi</i>	0	0	1	0	0	0	0	0	0	5	0
<i>Thyasira sp</i>	0	0	0	0	0	0	0	0	0	2	0
<i>Tonicella rubra</i>	1	0	1	0	0	0	0	0	0	1	2
<i>Travesia forbesi</i>	0	0	0	0	4	0	0	0	0	0	0
Unidentified	0	0	0	0	0	0	0	1	0	0	0
<i>Virgularia mirabilis</i>	0	0	0	0	1	0	0	0	0	0	0

## 6.7. Discussion

### *Hydrography*

The CTD – data showed that the conditions on the sea floor differed in terms of water mass and its characteristics whether it was located at the deep continental slope or the shallower shelf. Sub-zero temperatures occurred at the two deep stations sampled with the CTD, (station VR 1 and VS 1). It is also likely to believe that the two other deep sea stations (VS 2 and VS 3) had sub-zero temperatures on the sea floor due to similar depth and bathymetry. The cold water is probably locally produced winter water since it highly saline and dense, rather than pure Arctic water (which is less saline). Winter cooled water is formed when heat transports from the water surface to the colder air combined with sea ice formation resulting in a convection where brine accumulates and dense water sinks. [Nilsen *et al.*, 2008; Svendsen *et al.*, 2002]. According to Cottier *et al.* [2005] winter cooled water may occur in Kongsfjorden and be pushed of the continental shelf down to the deeper depressions. The cold temperature and the large depth is most likely why solid gas hydrates is found in the area since they are stable related to high pressure and low temperature.

The shelf and the shallow Prins Karls Forland showed very similar bottom water masses with almost identical temperature and salinity. In western Svalbard, there are two stronger current systems that flows northwards. One of them is the extension of the Gulf Stream which here is referred to the West Spitsbergen Current (WSC), bringing warm and salty Atlantic water into the Arctic Ocean [Seager *et al.*, 2002]. Then there is coastal Arctic water running from the North East Barents Sea and turns northwards again at the southern tip of Spitsbergen (Fig. 6.1). The boundary zone where these two currents meet and separate the ocean from Atlantic to Arctic regime may differ spatially and temporally over seasons [Berge *et al.*, 2005; Cottier *et al.*, 2005; Nilsen *et al.*, 2008; Svendsen *et al.*, 2002]. The pattern of these two currents could have a strong affection of benthic organisms, especially if the life-cycle includes a pelagic state, since it may regulate whether there is chance of Arctic or Atlantic influenced communities to form [Berge *et al.*, 2005; Berge *et al.*, 2009; Gulliksen *et al.*, 1985].

Highly elevated methane concentrations were seen at Prins Karls Forland shelf and shallow area (point 1 and 2 in Fig. 6.1). These values were at some stations tenfold or higher than the background value of methane in seawater in equilibrium to the atmosphere, usually 3.5-4  $\mu\text{m}^3$ . This corresponds well with other research studies conducted recently in the area [Berndt *et al.*, 2014; Gentz *et al.*, 2014; H Sahling *et al.*, 2014; G K Westbrook *et al.*, 2009] and

the areas with elevated concentrations match the areas with gas plumes visible on the echo sonar. The release at 350-400m depth is most likely caused by the boundary of the Gas Hydrate Stability Zone. Whether the origin of gas emissions in the shallow 80-100 m site is from leaking permafrost or sub seabed migrating flows is not yet fully understood and is discussed in *H Sahling et al.* [2014].

#### *Benthic faunal communities*

*It is natural to have different faunal compositions comparing the shallow shelf stations and the deep sea (Fig. 6.4). The depth is a strong physical factor limiting the range of habitats among various benthic organisms since the most natural energy source is originating from photosynthesis and hence comes from the sea surface. It was clearly seen visually that the benthic communities were different in terms of macro faunal diversity and biomass (Fig. 6.4). Deep sea flats are predominantly inhabited by smaller organisms (contributing to a smaller biomass) even if it is now well established that the species diversity may be very high, discussed in the review by Gage [1996] and references herein. Even though no results are available from the density and community structure analysis, the shallower areas were seen being composed by more hard bottom associated species whereas the deep stations had signs of few soft bottom polychaete species.*

*One distinct difference was the record in VR 1 of the methane associated polychaetes, Siboglinids (Frenulata) which serves as an evident sign of chemosynthetically influenced environment. Siboglinids is tube-dwelling polychaetes and directly associated with chemosynthetically communities worldwide as example, hydrothermal vents, whale-falls, seeps and reduced organic sediments [Hilario et al., 2011]. The absence of a functional digestive system (mouth, guts, intestines and anus) in adult siboglinids make them dependent on microbial endosymbiosis to maintain essential needs. Frenulating siboglinids contain thiotrophic/ methanotrophic symbionts and transport of hydrocarbons pass by diffusion between the sediment whereas an uptake occur from the water column of CO<sub>2</sub> and O<sub>2</sub>. The ecology of frenulating tubeworms is not yet fully cleared and is discussed in Dando et al. [2008]; Hilario et al. [2011]; Sommer et al. [2009]. New advances in technology and molecular tools brings new information to the research of deep sea polychaetes and the taxonomy in Siboglinidae has been reviewed continuously since the first discovery 100 years ago [Black et al., 1997; Halanych, 2005; Hilario et al., 2011; Ivanov, 1956; Pleijel et al., 2009; Rouse, 2001] and will probably continue to be debated and change within the nearest future.*

*Another remarkable record were the shells from a so far undescribed species. The characteristic folding at the edge of the valve made it possible to place the species into the family of Thysiridae by taxonomists. It is commonly known that bivalves in this family occur in habitat with geo-hydrothermal activity as mud volcanoes and seeps [Taylor and Glover, 2010]. It is, hereof highly believable to consider this record as sign of chemosynthetic impact even though comprehensive analyses must be done to describe the species.*

#### *Concluding remarks*

*Benthic macro faunal response from methane hydrates and chemosynthetic Arctic ecosystems have so far been poorly studied. Since no data from this year's cruise was analysed on board R/V Helmer Hanssen, it is just possible to speculate around possible results. Although, with the findings of Sibiglonids we can say that methane has impact on the surrounding faunal community in some areas even though it is not yet cleared to what extent organisms are influenced by the gas release. Data from the cruise will be used in one of the first studies of macro faunal community structure from methane associated areas in Arctic regions. These unique ecosystems needs supplementary studies in order to determine their importance in relation to other Arctic ecosystems and the response to future climate change.*

## 7. Sedimentology

### 7.1. Methods

Aiming for subsurface sediment information, sediment cores have been retrieved by the deployment of Gravity Cores (GC). The research vessel Helmer Hanssen is provided with a 6 meter long gravity corer loaded with  $\approx 1800$  Kg weight. It consists of an iron tube that can host a 6 meter long plastic liner on the inside. The core catcher is placed at the bottom of the iron tube. It consists of a metal half-sphere composed of independent metal blades which allow the sediment to flow in the liner and prevent them to fall out during the recovery. The metal tube, the plastic liner and the core catcher are secured by screwing the core cutter at the bottom of them. The function of the core cutter is to help the gravity core to penetrate into the sediments.

The gravity core is placed on one side of the main deck and it lies on a metal half-tube ( $\approx 60$  cm diameter) that can be pulled to a vertical position. Previously attached to a winch, the gravity core can from this position be lowered down through a hole on the main deck all the way down to the seafloor. As the descending of the gravity core might cause some oscillations, the winch stops for some seconds as soon as the gravity core is close to bottom and allows the gravity core to stabilize its position. Potential oscillations are detected by instable values on the rope tension sensor. When the rope tension on the winch is stable, the gravity core is released onto the seafloor. Once it has penetrated the sediments, the gravity core is recovered and taken back on deck.

After having recovered the core, the core cutter and the core catcher have been the first pieces demounted and the sediments have afterwards been sampled, labeled and stored. Then, the plastic liner was extracted from the iron tube and it was placed on a pile of pallets on deck. While it was being cleaned, the recovery was measured in order to cut away the part of the liner that had not been filled by sediments (Fig. 7.1). Once the liner was cut, it was marked and further cut into 1 m sections from the top to the bottom (in case that the deepest section was shorter than 20 cm the second deepest section could be up to 1.2 m long in order to include the deepest 20 cm in it).



Fig. 7.7 The sections with no sediments are cut away from the plastic line lying on the pallets.

If potential gas hydrate occurrence was detected by the thermal scanner, the liner was cut on the area which showed the lowest temperature in order to be able to retrieve the gas hydrate. The cores were later on capped on both ends of each section. In order to avoid mistakes in labeling, 1) the name of the gravity core, 2) the absolute length and 3) the top/bottom information have been written on both the caps and the liner section before moving the sections from the pallets. Once all the information was available on the section surface and on the caps, adhesive tape was stick to the caps. The sections were then moved to the dry lab where the Multi-Sensor Core Logger (MSCL) was mounted (Figure 7.2). Almost all of the cores (Table 7.1) have been run through the MSCL in order to measure the Magnetic Susceptibility (MS) and the bulk density along the cores. The sediment was measured in 1 cm intervals with a count time of 10s. The MSCL results have been processed and MS/Density vs. Depth graphs are available for all the cores logged (see next chapter).



Figure 7.8 The core sections are logged in the Multi-Sensory Core Logger (MSCL).

Once logged, the core sections were moved to another room where a rotational saw was mounted on a table in order to cut the cores into two halves. To avoid loss of labeling information after splitting, the same information had to be written twice on the liner surface before cutting the core. Once the liner had been sawed, the sediment was split into a *work* half and an *archive* half using an osmotic knife (Figure 7.3). *The knife operates on the principle of electro-osmosis, which reduces drag along the blade during slicing and minimizes distortion of the sediment (McMillen et al., 1977).*



Figure 7.9 The sawed core section is split using the osmotic knife.

The split sections were then moved to another room where, after the sediment surface was cleaned, the work part was described. Detailed description is available for core number GC-06, -07, -08, -09, -10, -11, -12, -16 and GC-17 (see next chapter). After the description, some of the cores have been sampled (Table 7.1) for CHNS and Grain size analyzes (Figure 4). In order to avoid future evaporation and facilitate the storing process, the sections were finally wrapped into plastic foil then closed into plastic D-tubes. All the information about the section contained was written on both ends of all D-tubes. Thereby it will be easier to spot the right section once the D-tubes are stored in the refrigerated storehouse at the department. The D-tubes were then moved to the refrigerated room of the ship to temperatures around 4 °C.



Figure 7.10 The core sections have been described and sampled. The coupled holes mark the sampled intervals.

Table 7.3: Gravity core information.

2014 TEACHING CRUISE WESTERN SVALBARD MARGIN GRAVITY CORE LOG						MSC Logged	MSC Logged	CHNS & GS Sampled
BRIDGE STATION #	SITE NAME	CORE #	PENETRATION (CM)	RECOVERY (CM)	DEPTH (MBSF)	MAG. SUSC.	BULK DENSITY	
645	V-12	GC-01	375	228	216	X	X	-
649	PKF-1	GC-02	0	0	244	-	-	-
650	PKF-1	GC-03	0	0	245	-	-	-
651	PKF-1	GC-04	0	0	244	-	-	-
652	PKF-1	GC-05	0	0	245	-	-	-
660	VS-3	GC-06	~500	417	1730	X	X	X
661	VS-3	GC-07	~500	364	1718	X	X	X
662	VS-4	GC-08	~500	382	1691	X	X	X
663	VS2	GC-09	~500	360	1593	X	X	X
664	VS-1?	GC-10	~500	346	1636	X	X	X
665	VS5	GC-11	~500	362	1666	X	X	X
666	VN	GC-12	600	500	1483	X	X	X
677	VR	GC-13	250	91	1207	X	X	?
678	VR	GC-14	220	only core catch	1208	-	-	-
679	VR	GC-15	~300	183	1208	X	X	X
680	VR	GC-16	600	475	1217	X	X	X
681	VR	GC-17	600	440	1207	X	X	X

## 7.2 Core description

Gravity coring was performed at 17 locations. The recovery was good in 12 of them. In the following chapter, the different gravity cores are described. The core logs and MSCL plots of all gravity cores are attached in the Appendix 2.

### CAGE 14-1-GC-06

The brown (and soupy) event at the top is followed by units of different brownish to greyish colors, most of them showing bioturbation (Fig. 7.6a). Except of the lowermost silty unit, the sediment grain size is clayey. The density increases to  $1.6 \text{ g/cm}^3$  within the uppermost meter, and shows values around  $1.6\text{-}1.7 \text{ g/cm}^3$  further downwards, with several peaks up to  $2.0 \text{ g/cm}^3$ . Isolated pebbles in Fig. 7.6b correlated with peaks in density and magnetic susceptibility. The MS values are within an interval of  $8\text{-}24 \cdot 10^{-8} \text{ SI}$ . Foraminifera have been identified in two beds at 130 and 400 cm (Fig. 7.5).

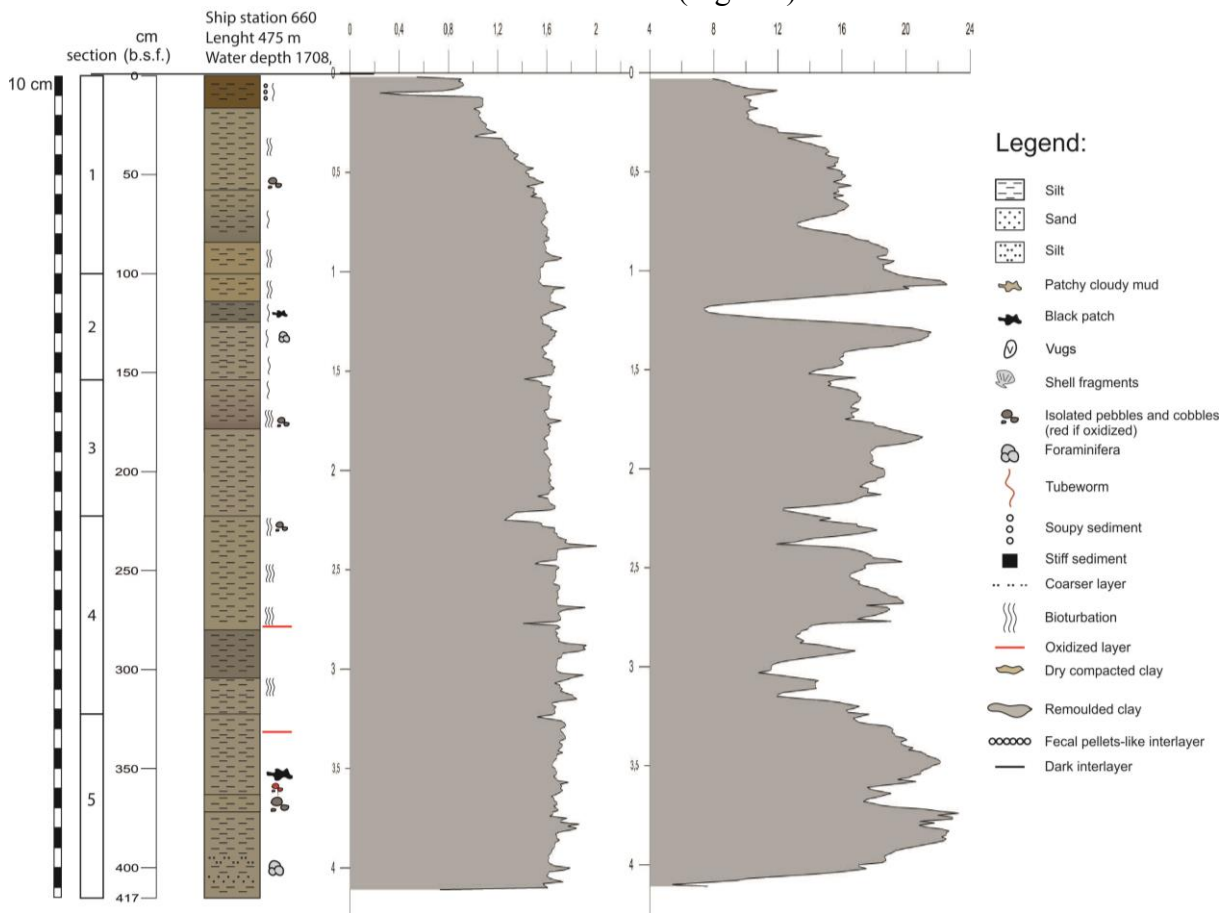


Figure 7.11 Gravity core GC-06, including sediment description, density plot (middle, in  $\text{g/cm}^3$ ) and magnetic susceptibility plot (right, in  $10^{-8} \text{ SI}$ ).

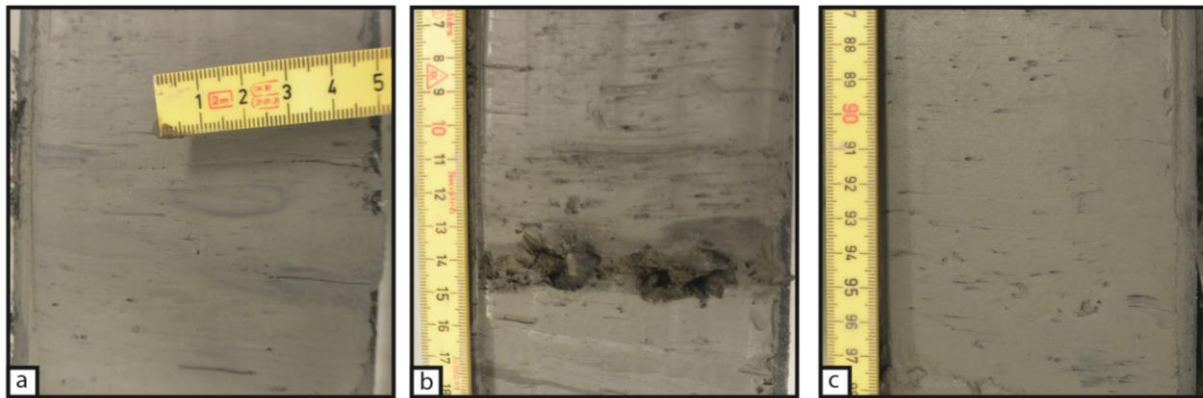


Fig. 7.12 Sediments of gravity cores GC-06 and GC-12. a) Bioturbation at 250 cm core depth in GC-06, b) Isolated pebbles at 230 cm core depth in GC-06, c) Black patches at 190 cm core depth in GC-12.

#### *CAGE 14-1-GC-07*

The sediment units show different greyish-brownish colors. The uppermost sediment package is again characterized by a brownish color, here containing a fecal pellet-like interlayer. The only grain size which has been detected in this core was clay (no silty interlayers). Indication of bioturbation (similar to Fig. 7.6a), several dark interlayers as well as oxidized layers are identified in different units of this core. The density oscillates from 1.5 to 1.8 g/cm<sup>3</sup> and the MS from 10 to 25 · 10<sup>-8</sup> SI. The significant peak in MS and density at about 200 cm core depth can probably be explained by pebbles occurrence. Other identified pebbles are correlating just with the MS-data (at 30 and 60 cm sediment depth).

#### *CAGE 14-1-GC-08*

This core, clayey in grain size, is generally strongly bioturbated. Black patches (similar to Fig. 7.6c) and dark interlayers are observed in areas with lacking bioturbation. In the interval from 220-260 cm, several oxidized layers were observed. The density is increasing from 1.4 to 1.7 g/cm<sup>3</sup>. MS values are generally increasing up to 1 m depth, and the trend is constantly decreasing further downwards.

#### *CAGE 14-1-GC-09*

The core changes its color several times. The different units are bioturbated and 10s of cm in thickness. Around 320 cm core depth, a strong color change in a smaller scale is observed (bioturbation missing in these units, Figure 7.9a). Shell fragments and foraminifera are found in the silty interlayer at 270 cm core depth. A coarser interlayer was detected at a core depth of 170 cm (Figure 7.8a). In addition, pebbles were detected in depths of 150 and 200 cm (Figure 7.8b). Density values are oscillating between 1.4-1.8 g/cm<sup>3</sup> and show abrupt changes, and MS values are measured from 10 to 25 · 10<sup>-8</sup> SI. The highest MS values correlate with the olive bioturbated unit and a density of 1.5-1.6 g/cm<sup>3</sup> (Figure 7.7).

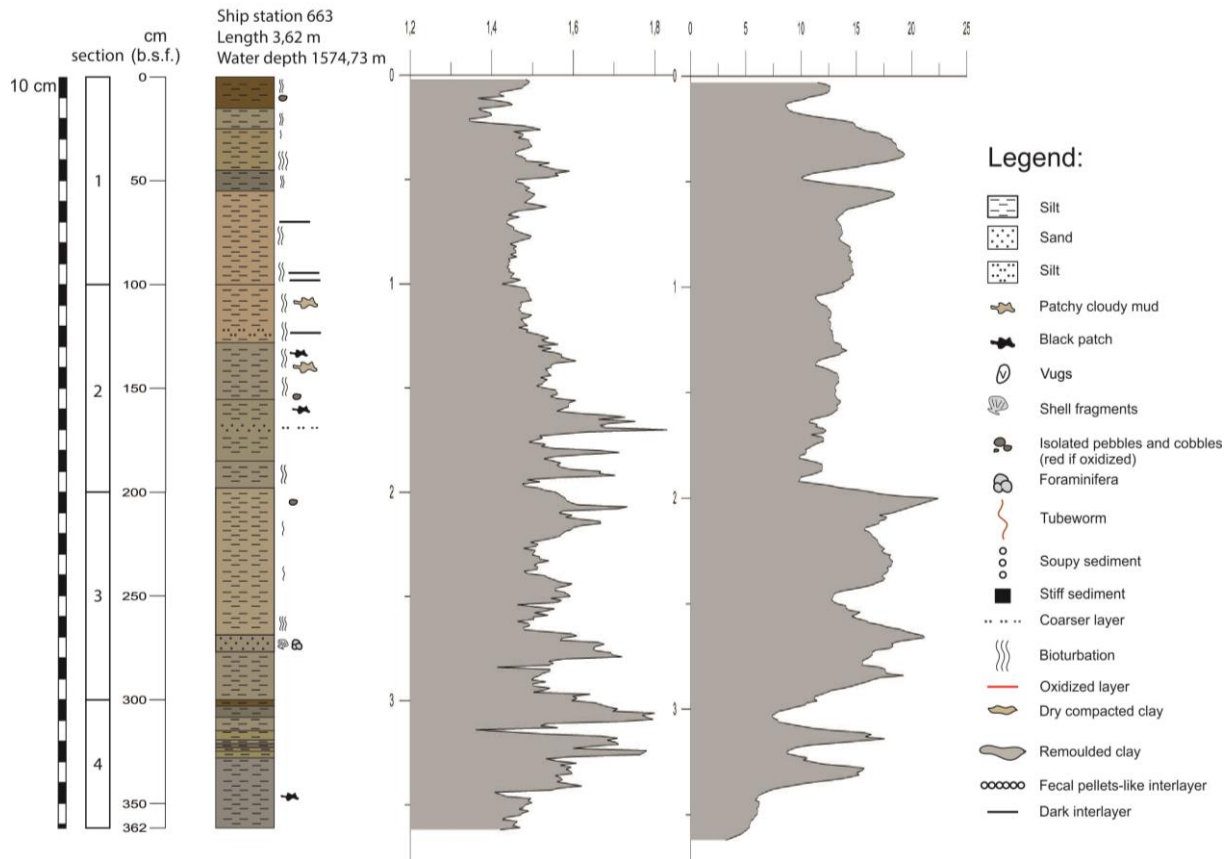


Fig. 7.13 Gravity core GC-09, including sediment description, density plot (middle, in  $\text{g}/\text{cm}^3$ ) and magnetic susceptibility plot (right, in  $10^{-8}$  SI).

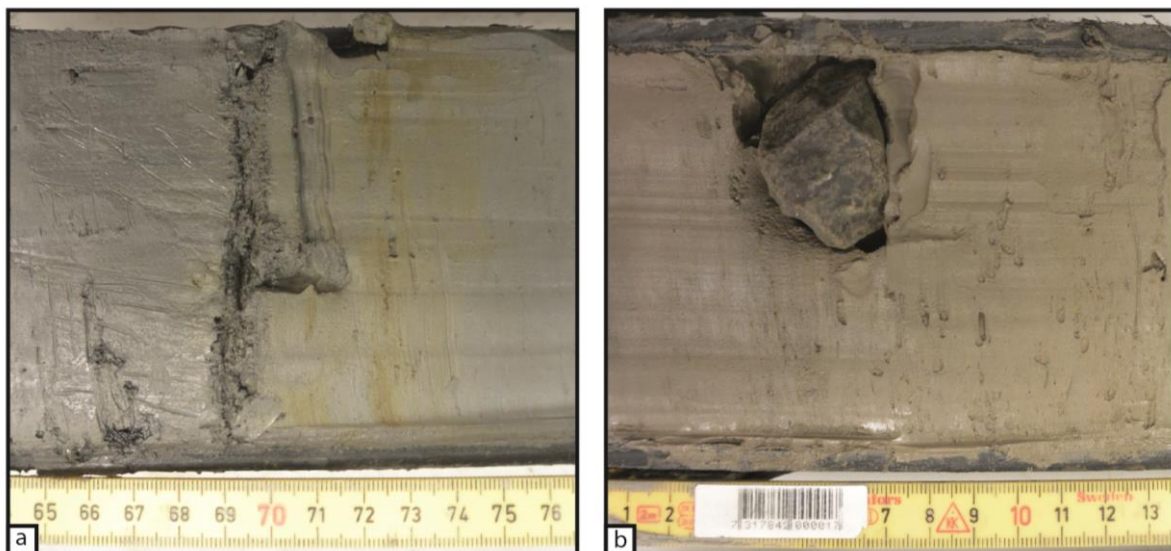


Fig. 7.14 Sediments of gravity core 09. a) Coarser interlayer at 170 cm core depth, b) Pebble in 200 cm core depth.

#### *CAGE 14-1-GC-10*

The core shows a uniform color within the upper 3 m and downward the color changes from grey into olive. Black patches (100-160 and 250-345 cm depth) and patchy cloudy mud (110-150 cm depth) intervals are observed. Overall, the density plot is varying over a wide range ( $1.4\text{-}2.2 \text{ g}/\text{cm}^3$ ), and shows no general trend (no increase in density by

depth). The MS data are generally low ( $5-7 \cdot 10^{-8}$  SI) with two peaks up to  $12.5 \cdot 10^{-8}$  SI and significantly higher values in the lowermost package ( $> 20 \cdot 10^{-8}$  SI). The silty interlayers at around 25 cm and the pebbly interlayer at around 250 cm are probably reflected by peaks in the MSCL-logs. The silty layer at 1 m core depth is just correlating with a peak in the density plot (no peak in MS data).

#### *CAGE 14-1-GC-11*

The color varies between different units from brown to grey. The units from 0-330 cm are of several dm in thickness, and abruptly change into smaller units in the lowermost part of the core (Fig. 7.9b). Lots of black patches are observed in the intervals from 180-230 cm resp. 300-350 cm. Bioturbation is documented in the bottom and top of the sediment core. Dark interlayers are observed in depths of 140, 150, 240 and 310 cm. The density increases from 1.5 to 1.8 g/cm<sup>3</sup> (including few peaks), and the susceptibility varies from  $8-30 \cdot 10^{-8}$  SI with significant changes.

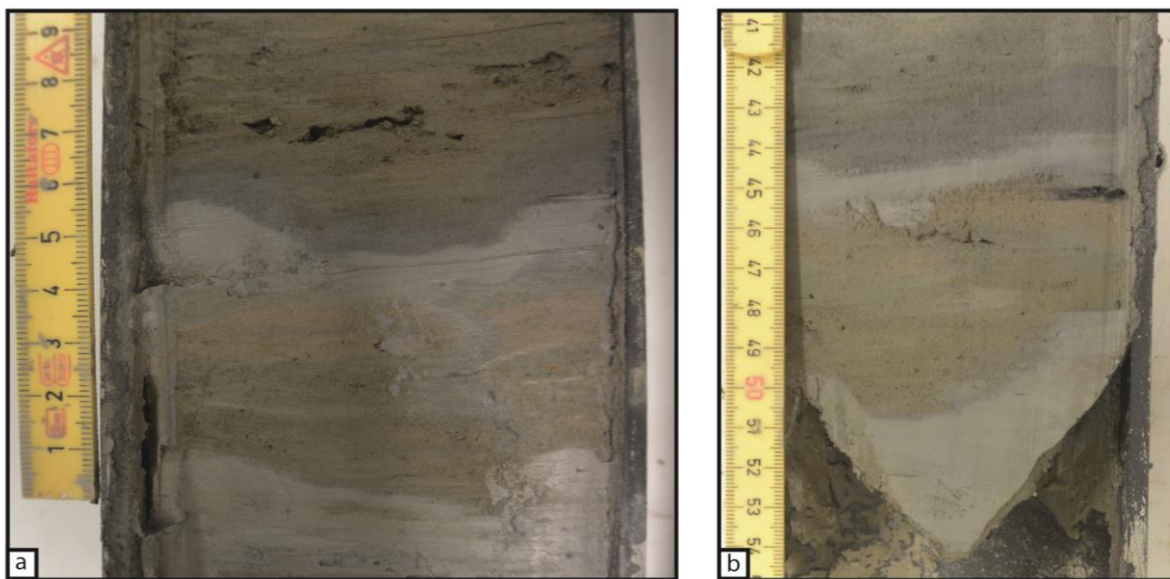


Fig. 7.15 Small-scale color changes in sediments of a) GC-09, 320 cm core depth and b) GC-11, 330 cm core depth.

#### *CAGE 14-1-GC-12*

The core shows a uniform color and contains lots of black patches (Fig. 7.6c), with very high occurrence in the intervals from 190 to 310 and from 360 to 420 cm. Similar to the sediment color, the sediment density is also characterized by low changes (1.3-1.4 g/cm<sup>3</sup>). The MS values show an increasing trend from 17 to  $28 \cdot 10^{-8}$  SI to a depth at about 3 m and decrease constantly down to 17 further downward.

#### *CAGE 14-1-GC-13*

This core was logged by MSCL, but not described in detail. The gravity core, 91 cm in length, has a density of about 1.3 g/cm<sup>3</sup> and MS-values of  $12-18 \cdot 10^{-8}$  SI.

#### *CAGE 14-1-GC-15*

This core was logged by MSCL, but not described in detail. The 183 cm-long gravity core has an increasing density from 1.4 to 1.8 g/cm<sup>3</sup>, interrupted by some peaks. The MS-values are very low ( $2-6 \cdot 10^{-8}$  SI).

#### *CAGE 14-1-GC-16*

The clayey shows a quite uniform sediment color (slightly changing downward from 2.5Y 4/1 to 5Y 3/2 according to Munsell soil color charts. Charts, M. S. C. 1975) with several vugs/voids (Fig. 7.11a) also reflected in the geophysical data (Fig. 7.10). Some pebbles were found in a sediment depth of about 50 cm. Shell fragments are found in three depth levels

(Fig. 7.11b). The average density is quite constant ( $1.5-1.6 \text{ g/cm}^3$ , few peaks) except for 5 main drops due to void occurrence. The susceptibility is low (around  $4 \cdot 10^{-8} \text{ SI}$ ) with two significant peaks (up to  $14 \cdot 10^{-8} \text{ SI}$ ) that, visually, cannot be referred to any changes in the sediments.

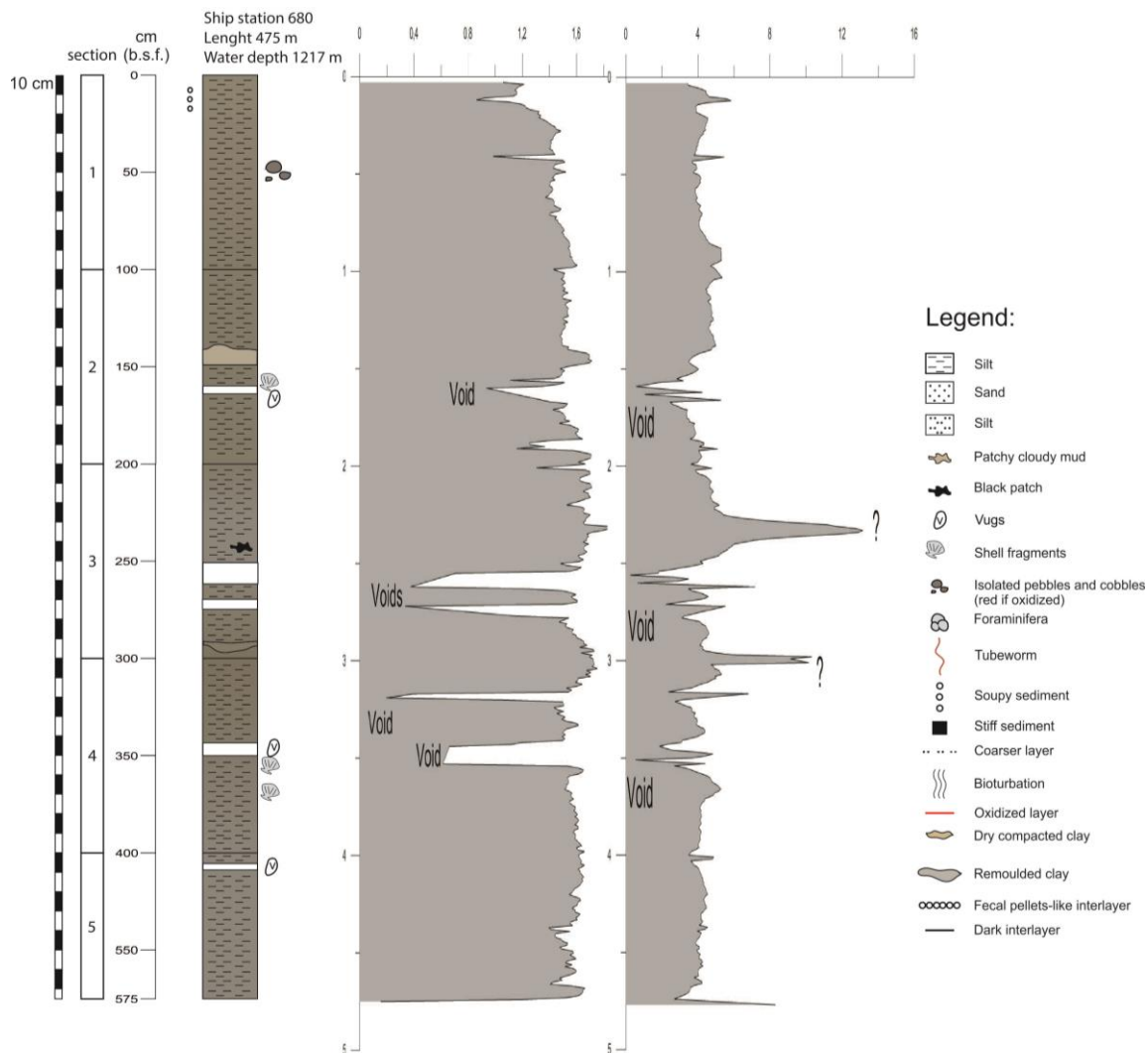


Fig. 7.16 Gravity core GC-16, including sediment description, density plot (middle, in  $\text{g/cm}^3$ ) and magnetic susceptibility plot (right, in  $10^{-8} \text{ SI}$ ).

#### CAGE 14-1-GC-17

The clayey core shows a uniform sediment color (2.5Y 5/1. Charts, M. S. C. 1975) and changes at a depth of around 390 cm into black. Several big voids are found (up to 50 cm thick). Remoulded clay was documented in the top of the core (40-80 cm). Fecal pellets-like interlayers are found at 0-20 cm and 80-120 cm in core depth and black interlayers at depths of 20-40, 130-140 and 340-350 cm. The measured density is quite constant ( $1.6 \text{ g/cm}^3$ ) and the MS-values rather low ( $3-12 \cdot 10^{-8} \text{ SI}$ ), with one unexplained peak up to  $16 \cdot 10^{-8} \text{ SI}$ .

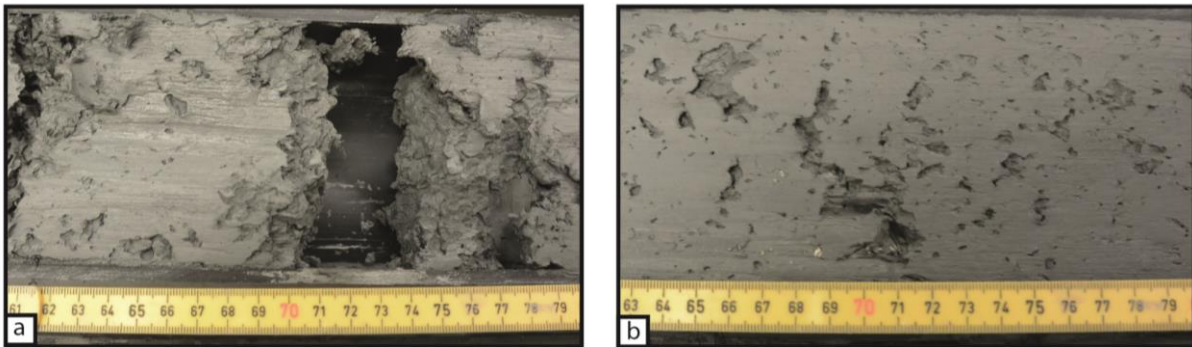


Figure 17: Sediments of gravity core 16. a) Voids at 360 cm core depth, b) Shell fragments at 270 cm core depth.

### 7.3. Synthesis

As clay is identified as the overall dominating grain size, the sediment must have transported by ocean currents for some distance. The significant changes of clay color reflect changes in the lithology of the source area. The clay source may have changed over time, with different current pulses in different time periods. The coarser thin silty layers could reflect higher-energy pulses of these currents.

The sediment units defined by color changes do usually not correlate with trends in density and magnetic susceptibility. MS values can potentially give information about the source, with low MS-values correlating with low terrigenous input. The signal absence or drop during multi-sensor core logging could be directly associated with the presence of gas in the sediments.

Oxic/Anoxic conditions may have changed in space and time. The identified black layers are probably results of pyratization in sediment pores, and consist now of iron sulfide (mainly pyrite). These units have probably had anoxic conditions. The brownish sediment unit at the top was identified in several cores (GC-06, 07, 08, 09, 10, 11). It usually includes bioturbation and is interpreted to be the oxidized top of the core. In the cores with methane hydrates (GC-12, 16, 17), this layer could not be identified.

The silty interlayers could be reflected by higher MS-values ( $24 \cdot 10^{-8}$  SI, GC06). Visually detected isolated pebbles often correlate with peaks in density (up to  $2.0 \text{ g/cm}^3$ , GC06) and MS (up to  $24 \cdot 10^{-8}$  SI, GC06 and GC09). The small-scale color change identified in core GC-09 and GC-11 can probably be correlated (Figure 7.9a and Figure 7.9b).

## 8. References

- ACIA (2005), Arctic Climate Impact Assessment-Scientific Report *Rep. 0521865093*, Cambridge University Press.
- Ambrose, W. G., P. E. Renaud, F. R. Cottier, J. Berge, M. L. Carroll, B. Levin, and S. Ryan (2012), Growth line deposition and variability in growth of two circumpolar bivalves (*Serripes groenlandicus*, and *Clinocardium ciliatum*), *Polar biology*, 35(3), 345-354.
- Anisimov, O. A., D. G. Vaughan, T. Callaghan, C. Furgal, H. Marchant, T. D. Prowse, H. Vilhjálmsson, and J. E. Walsh (2007), Polar regions (arctic and antarctic), *Climate change*, 15, 653-685.
- Berge, J., G. Johnsen, F. Nilsen, B. Gulliksen, and D. Slagstad (2005), Ocean temperature oscillations enable reappearance of blue mussels *Mytilus edulis* in Svalbard after a 1000 year absence.
- Berge, J., P. E. Renaud, K. Eiane, B. Gulliksen, F. R. Cottier, Ø. Varpe, and T. Brattegard (2009), Changes in the decapod fauna of an Arctic fjord during the last 100 years (1908–2007), *Polar biology*, 32(7), 953-961.
- Berndt, C., S. Bünz, T. Clayton, J. Mienert, and M. Saunders (2004), Seismic character of bottom simulating reflectors: examples from the mid-Norwegian margin, *Marine and Petroleum Geology*, 21(6), 723-733.
- Berndt, C., T. Feseker, T. Treude, S. Krastel, V. Liebetrau, H. Niemann, V. J. Bertics, I. Dumke, K. Dünnbier, and B. Ferré (2014), Temporal Constraints on Hydrate-Controlled Methane Seepage off Svalbard, *Science*, 343(6168), 284-287.
- Biddle, K. T., and C. C. Wielchowsky (1994), Hydrocarbon traps, *MEMOIRS-AMERICAN ASSOCIATION OF PETROLEUM GEOLOGISTS*, 219-219.
- Black, M., K. Halanych, P. Maas, W. Hoeh, J. Hashimoto, D. Desbruyeres, R. Lutz, and R. Vrijenhoek (1997), Molecular systematics of vestimentiferan tubeworms from hydrothermal vents and cold-water seeps, *Marine Biology*, 130(2), 141-149.
- Boetius, A., and E. Suess (2004), Hydrate Ridge: a natural laboratory for the study of microbial life fueled by methane from near-surface gas hydrates, *Chemical Geology*, 205(3), 291-310.
- Borowski, W. S., C. K. Paull, and W. Ussler (1996), Marine pore-water sulfate profiles indicate in situ methane flux from underlying gas hydrate, *Geology*, 24(7), 655-658, doi:10.1130/0091-7613(1996)024<0655:mpwspi>2.3.co;2.
- Brown, A. R. (2004), *Interpretation of Three-Dimensional Seismic Data*, 6 ed., AAPG and the Society of Exploration Geophysicists, Tulsa, Oklahoma, USA.
- Buenz, S., Petersen, C.J., Hustoft, S., Mienert, J., 2008. Environmentally-sensitive gas hydrates on the W-Svalbard margin at the gateway to the Arctic Ocean. Proceedings of the 6th International Conference on Gas Hydrates, Vancouver, British Columbia, Canada.
- Buenz, S., Polyanov, S., Vadakkepuliambatta, S., Consolaro, C., and Mienert, J., 2012. Active gas venting through hydrate-bearing sediments on the Vestnesa Ridge, offshore W-Svalbard. *Marine Geology*, 332-334, p.189-197.
- Carroll, M. L., B. J. Johnson, G. A. Henkes, K. W. McMahon, A. Voronkov, W. G. Ambrose Jr, and S. G. Denisenko (2009), Bivalves as indicators of environmental variation and potential anthropogenic impacts in the southern Barents Sea, *Marine pollution bulletin*, 59(4), 193-206.
- Cathles, L.M., Su, Z., Chen, D., 2010. The physics of gas chimneys and pockmark formation, with implications for assessment of seafloor hazards and gas sequestration. *Marine and Petroleum Geology* 27, p. 82-91.
- Chand, S., Rise, L., Ottesen, D., Dolan, M.F.J., Bellec, V., Bøe, R., 2009. Pockmark like depressions near the Goliat hydrocarbon field, Barents Sea: morphology and genesis. *Marine Petroleum Geology* 26, p. 1035–1042.
- Chand, S., Thorsnes, T., Rise, L., Brunstad, H., Stoddart, D., Bøe, R., Lågstad, P., Svolsbru T., 2012. Multiple episodes of fluid flow in the SW Barents Sea (Loppa High) evidenced by gas flares,

- pockmarks and gas hydrate accumulation. *Earth and Planetary Science Letters*, 331– 332(0), p. 305-314. doi: 10.1016/j.epsl.2012.03.021.
- Charts, M. S. C. 1975: Charts, M. S. C. (1975). *Munsell soil color charts*. Kollmorgen, Baltimore.
- Christiansen, J. S., C. W. Mecklenburg, and O. V. Karamushko (2014), Arctic marine fishes and their fisheries in light of global change, *Global change biology*, 20(2), 352-359.
- Clark, M. R., and A. A. Rowden (2009), Effect of deepwater trawling on the macro-invertebrate assemblages of seamounts on the Chatham Rise, New Zealand, *Deep Sea Research Part I: Oceanographic Research Papers*, 56(9), 1540-1554.
- Clarke, A., and C. M. Harris (2003), Polar marine ecosystems: major threats and future change, *Environmental Conservation*, 30(01), 1-25.
- Cochrane, S., T. Pearson, M. Greenacre, J. Costelloe, I. Ellingsen, S. Dahle, and B. Gulliksen (2012), Benthic fauna and functional traits along a Polar Front transect in the Barents Sea—advancing tools for ecosystem-scale assessments, *Journal of Marine Systems*, 94, 204-217.
- Cottier, F., V. Tverberg, M. Inall, H. Svendsen, F. Nilsen, and C. Griffiths (2005), Water mass modification in an Arctic fjord through cross-shelf exchange: The seasonal hydrography of Kongsfjorden, Svalbard, *Journal of Geophysical Research: Oceans* (1978–2012), 110(C12).
- Dando, P., A. Southward, E. Southward, P. Lamont, and R. Harvey (2008), Interactions between sediment chemistry and frenulate pogonophores (Annelida) in the north-east Atlantic, *Deep Sea Research Part I: Oceanographic Research Papers*, 55(8), 966-996.
- Eiken, O., Hinz, K., 1993. Contourites in the Fram Strait. *Sedimentary Geology* 82, p. 15-32.
- Engen, Ø. Faleide, J.I., Karlberg Dyreng, T., 2008. Opening of the Fram Strait gateway: A review of plate tectonic constraints, *Tectonophysics*, Volume 450/1–4, 51-69.
- Froelich, P. N., G. P. Klinkhammer, M. L. Bender, N. A. Luedtke, G. R. Heath, D. Cullen, P. Dauphin, D. Hammond, B. Hartman, and V. Maynard (1979), Early oxidation of organic matter in pelagic sediments of the eastern equatorial Atlantic: suboxic diagenesis, *Geochimica et Cosmochimica Acta*, 43(7), 1075-1090, doi:[http://dx.doi.org/10.1016/0016-7037\(79\)90095-4](http://dx.doi.org/10.1016/0016-7037(79)90095-4).
- Gage, J. D. (1996), Why are there so many species in deep-sea sediments?, *Journal of Experimental Marine Biology and Ecology*, 200(1), 257-286.
- Gentz, T., E. Damm, J. Schneider von Deimling, S. Mau, D. F. McGinnis, and M. Schlüter (2014), A water column study of methane around gas flares located at the West Spitsbergen continental margin, *Continental Shelf Research*, 72, 107-118.
- Granin, N. G., S. I. Muyakshin, M. M. Makarov, K. M. Kucher, A. A. Il'ya, L. Z. Granina, and I. B. Mizandroutsev (2012), Estimation of methane fluxes from bottom sediments of Lake Baikal, *Geo-Marine Letters*, 32(5-6), 427-436.
- Gulliksen, B., B. Holte, and K. Jakola (1985), The soft bottom fauna in Van Mijenfjord and Raudfjord, Svalbard, *Marine biology of polar regions and effects of stress on marine organisms*, 199-215.
- Halanych, K. M. (2005), Molecular phylogeny of siboglinid annelids (aka pogonophorans): a review, *Hydrobiologia*, 535(1), 297-307.
- Hamilton, L.J., Parnum, I., 2011. Acoustic seabed segmentation from direct statistical clustering of entire multibeam sonar backscatter curves. *Continental Shelf Research*, 31:138- 148.
- Hell, B., 2011. Mapping bathymetry - From measurements to applications, Doctoral thesis in marine geosciences, Department of Geological Sciences, Stockholm University.
- Hilario, A., M. Capa, T. G. Dahlgren, K. M. Halanych, C. T. Little, D. J. Thornhill, C. Verna, and A. G. Glover (2011), New perspectives on the ecology and evolution of siboglinid tubeworms, *PLoS one*, 6(2), e16309.
- Hovland, M., Gardner, J.V., Judd, A.G., 2002. The significance of pockmarks to understanding fluid flow processes and geohazards. *Geofluids* 2-2, p. 127-136.
- Howe, J.A., Shimmiel, T.M., Harland, R.E.X., Eyles, N., 2008. Late quaternary contourites and glaciomarine sedimentation in the Fram Strait. *Sedimentology* 55, 179-200.
- Hustoft, S., Bünz, S., Mienert, J., Chand, S., 2009. Gas hydrate reservoir and active methane-venting province in sediments on 20 Ma young oceanic crust in the Fram Strait, offshore NW-Svalbard. *Earth and Planetary Science Letters* 284, 12–24

- Ingvaldsen, R. B., and H. Loeng (2009), Physical Oceanography, in *Ecosystem Barents sea*, edited by E. Sakshaug, G. Johnsen and K. M. Kovacs, Tapir Academic Press, Trondheim.
- Ingólfsson, Ó., Landvik, J.Y., 2013. The Svalbard-Barents Sea ice-sheet – Historical, current and future perspectives. *Quaternary Science Reviews*, 64, p. 33-60.
- Ivanov, A. (1956), On the systematic position of Pogonophora, *Systematic Zoology*, 5(4), 165-173.
- Jones, D. S. (1983), Sclerochronology: Reading the Record of the Molluscan Shell: Annual growth increments in the shells of bivalve molluscs record marine climatic changes and reveal surprising longevity, *American Scientist*, 71(4), 384-391, doi:10.2307/27852138.
- Joye, S. B., M. W. Bowles, V. A. Samarkin, K. S. Hunter, and H. Niemann (2010), Biogeochemical signatures and microbial activity of different cold-seep habitats along the Gulf of Mexico deep slope, *Deep Sea Research Part II: Topical Studies in Oceanography*, 57(21), 1990-2001.
- Judd, A.G., Hovland, M., 2007. Seabed Fluid Flow: The Impact on Geology, Biology and the Marine Environment, first ed. Cambridge University Press, Cambridge.
- Kandilarov, A., Landa, H., Mjelde, R., Pedersen, R.B., Okino, K., Murai, Y., 2010. Crustal structure of the ultra-slow spreading Knipovich Ridge, North Atlantic, along a presumed ridge segment center. *Marine Geophysics Research*, 31, p. 173-195.
- Knies, J., Damm, E., Gutt, J., Mann, U., and Pimnturier, L. 2004. Near-surface hydrocarbon anomalies in shelf sediments off Spitsbergen: Evidence for past seepages, *Geochemistry, Geophysics, Geosystems* 5, doi:10.1029/2003GC000687.
- Kvenvolden, K. A., 1998. A primer on the geological occurrence of gas hydrate. In Henriet, J. P. and Mienert, J. (Eds.), In: *Gas hydrates: Relevance to the World Margin Stability and Climate Change*. Geological Society, London, Special Publications, 137, p. 9-30.
- Landvik, J. Y., O. Ingólfsson, J. Mienert, S. J. Lehman, A. Solheim, A. Elverhøi, and D. Ottesen 2005. Rethinking LateWeichselian ice-sheet dynamics in coastal NW Svalbard, *Boreas*, 34, p. 7– 24.
- Lundin, E.R., Dore, A.G., 2002. Mid-Cenozoic post-breakup deformation in ‘passive’ margins bordering the Norwegian-GreenlandSea. *Mar. Pet. Geol.* 19, p. 79-93.
- Long, D., S. Lammers, and P. Linke (1998), Possible hydrate mounds within large sea-floor craters in the Barents Sea, *Geological Society, London, Special Publications*, 137(1), 223-237.
- Lösekan, T., K. Knittel, T. Nadalig, B. Fuchs, H. Niemann, A. Boetius, and R. Amann (2007), Diversity and abundance of aerobic and anaerobic methane oxidizers at the Haakon Mosby Mud Volcano, Barents Sea, *Applied and environmental microbiology*, 73(10), 3348-3362.
- Masetti, G., Calder, B., 2012. Remote identification of a shipwreck site from MBES backscatter. *Journal of Environmental Management*, 111:44-52
- Maslin, M., M. Owen, R. A. Betts, S. Day, T. D. Jones, and A. Ridgwell (2012), Assessing the Past and Future Stability of Global Gas Hydrate Reservoirs, *Climate Forcing of Geological Hazards*, 250-277.
- McMillen et al., 1977: McMillen, K. J., Warme, J. E., & Hemmen, E. H. (1977). *An electro-osmotic knife for slicing large box cores*. *Journal of Sedimentary Research*, 47(2)
- Niemann, H., T. Lösekan, D. De Beer, M. Elvert, T. Nadalig, K. Knittel, R. Amann, E. J. Sauter, M. Schlüter, and M. Klages (2006), Novel microbial communities of the Haakon Mosby mud volcano and their role as a methane sink, *Nature*, 443(7113), 854-858.
- Nikolovska, A., H. Sahling, and G. Bohrmann (2008), Hydroacoustic methodology for detection, localization, and quantification of gas bubbles rising from the seafloor at gas seeps from the eastern Black Sea, *Geochemistry, Geophysics, Geosystems*, 9(10).
- Nilsen, F., F. Cottier, R. Skogseth, and S. Mattsson (2008), Fjord–shelf exchanges controlled by ice and brine production: The interannual variation of Atlantic Water in Isfjorden, Svalbard, *Continental Shelf Research*, 28(14), 1838-1853, doi:<http://dx.doi.org/10.1016/j.csr.2008.04.015>.
- Nilsson, H. C., and R. Rosenberg (2000), Succession in marine benthic habitats and fauna in response to oxygen deficiency: analysed by sediment profile-imaging and by grab samples, *Marine ecology progress series*, 197, 139-149.

- Pecher, I. A., N. Kukowski, C. Huebscher, J. Greinert, and J. Bialas (2001), The link between bottom-simulating reflections and methane flux into the gas hydrate stability zone—new evidence from Lima Basin, Peru Margin, *Earth and Planetary Science Letters*, 185(3), 343-354.
- Penrose, J.D., Siwabessy, P.J.W., Gavrillov, A., Parnum, I., Hamilton, L.J., Bickers, A., Brooke, B., Ryan, D.A., Kennedy, P., 2005. Acoustic Techniques for Seabed Classification. Cooperative Research Centre for Coastal Zone Estuary and Waterway Management, Technical report 32.
- Pleijel, F., T. G. Dahlgren, and G. W. Rouse (2009), Progress in systematics: from Siboglinidae to Pogonophora and Vestimentifera and back to Siboglinidae, *Comptes rendus biologiques*, 332(2), 140-148.
- Rasmussen, T.L., et al., 2007. Paleoceanographic evolution of the SW Svalbard margin (76N°) since 200,000 C<sup>14</sup> yr BP. *Quaternary Research* 67, 100-114.
- Rouse, G. W. (2001), A cladistic analysis of Siboglinidae Caullery, 1914 (Polychaeta, Annelida): formerly the phyla Pogonophora and Vestimentifera, *Zoological Journal of the Linnean Society*, 132(1), 55-80.
- Sahling, H., G. Bohrmann, V. Spiess, J. Bialas, M. Breitzke, M. Ivanov, S. Kasten, S. Krastel, and R. Schneider (2008), Pockmarks in the Northern Congo Fan area, SW Africa: Complex seafloor features shaped by fluid flow, *Marine Geology*, 249(3), 206-225.
- Sahling, H., M. Römer, T. Pape, B. Bergès, C. dos Santos Fereirra, J. Boelmann, P. Geprägs, M. Tomczyk, N. Nowald, and W. Dimmler (2014), Gas emissions at the continental margin west off Svalbard: mapping, sampling, and quantification, *Biogeosciences Discussions*, 11(5), 7189-7234.
- Seabird, E. (2013), Seasoft V2: SBE Data Processing.
- Seager, R., D. S. Battisti, J. Yin, N. Gordon, N. Naik, A. C. Clement, and M. A. Cane (2002), Is the Gulf Stream responsible for Europe's mild winters?, *Quarterly Journal of the Royal Meteorological Society*, 128(586), 2563-2586.
- Smith, A.J., Mienert, J., Buenz S., Greinert, J., Rasmussen T.L., 2013. 900-m high gas plumes rising from marine sediments containing structure II hydrates at Vestnesa Ridge, offshore W-Svalbard. EGU General Assembly 2013, held 7-12 April, 2013 Vienna, Austria, id. EGU2013-9302.
- Sommer, S., P. Linke, O. Pfannkuche, T. Schleicher, J. Schneider, A. Reitz, M. Haeckel, S. Flögel, and C. Hensen (2009), Seabed methane emissions and the habitat of frenulate tubeworms on the Captain Arutyunov mud volcano (Gulf of Cadiz), *Marine Ecology Progress Series*, 382, 69-86.
- Stocker, T. F., D. Qin, G.-K. Plattner, M. Tignor, S. K. Allen, J. Boschung, A. Nauels, Y. Xia, V. Bex, and P. M. Midgley (2013), Climate Change 2013. The Physical Science Basis. Working Group I Contribution to the Fifth Assessment Report of the Intergovernmental Panel on Climate Change. *Rep.*, Groupe d'experts intergouvernemental sur l'évolution du climat/Intergovernmental Panel on Climate Change-IPCC, C/O World Meteorological Organization, 7bis Avenue de la Paix, CP 2300 CH-1211 Geneva 2 (Switzerland).
- Svendsen, H., A. Beszczynska-Møller, J. O. Hagen, B. Lefauconnier, V. Tverberg, S. Gerland, J. B. Ørbæk, K. Bischof, C. Papucci, and M. Zajaczkowski (2002), The physical environment of Kongsfjorden–Krossfjorden, an Arctic fjord system in Svalbard, *Polar Research*, 21(1), 133-166.
- Søreide, J. E., M. L. Carroll, H. Hop, W. G. Ambrose Jr, E. N. Hegseth, and S. Falk-Petersen (2013), Sympagic-pelagic-benthic coupling in Arctic and Atlantic waters around Svalbard revealed by stable isotopic and fatty acid tracers, *Marine Biology Research*, 9(9), 831-850.
- Søreide, J. E., H. Hop, M. L. Carroll, S. Falk-Petersen, and E. N. Hegseth (2006), Seasonal food web structures and sympagic–pelagic coupling in the European Arctic revealed by stable isotopes and a two-source food web model, *Progress in Oceanography*, 71(1), 59-87.
- Tameler, T., P. E. Renaud, H. Hop, M. L. Carroll, W. G. Ambrose, and K. A. Hobson (2006), Trophic relationships and pelagic-benthic coupling during summer in the Barents Sea Marginal Ice Zone, revealed by stable carbon and nitrogen isotope measurements, *Marine ecology. Progress series*, 310, 33-46.

- Taylor, J. D., and E. A. Glover (2010), Chemosymbiotic bivalves, in *The Vent and Seep Biota*, edited by K. Steffen, Springer.
- Thiede, J., Myhre, A.M., 1996. The palaeo-oceanographic history of the North Atlantic Arctic gateways: synthesis of the Leg 151 drilling results. In: Thiede, J., Myhre, A.M., Firth, J.V., Johnson, G.L., Ruddiman, W.F., (Eds.). Proc., Sci. Res. ODP Leg 11, College Station, TX, p. 645-658.
- Thurber, A. R., K. Kröger, C. Neira, H. Wiklund, and L. A. Levin (2010), Stable isotope signatures and methane use by New Zealand cold seep benthos, *Marine Geology*, 272(1), 260-269.
- Tynan, C. T., and D.P. DeMaster (1997), Observations and predictions of Arctic climatic change: potential effects on marine mammals, *Arctic*, 308-322.
- Vanneste, M., Guidard, D., Mienert, J., 2005a. Bottom-simulating reflections and geothermal gradients across the western Svalbard margin. *Terra Nova* 17, p. 510-516.
- Vanreusel, A., A. C. Andersen, A. Boetius, D. Connelly, M. R. Cunha, C. Decker, A. Hilario, K. A. Kormas, L. Maignien, and K. Olu (2009), Biodiversity of cold seep ecosystems along the European margins, *Oceanography*, 22(1), 110-127.
- Vogt, P. R., Crane, K., Sundvor, E., Max, M. D., and Pfirman, S. L., 1994, Methane-generated (?) pockmarks on young, thickly sedimented oceanic crust in the Arctic: Vestnesa ridge, Fram strait. *Geology* 22, 255-258.
- Weber, T. C., L. Mayer, K. Jerram, J. Beaudoin, Y. Rzhannov, and D. Lovalvo (2014), Acoustic estimates of methane gas flux from the seabed in a 6000 km<sup>2</sup> region in the Northern Gulf of Mexico, *Geochemistry, Geophysics, Geosystems*.
- Westbrook, G., S. Chand, G. Rossi, C. Long, S. Bünz, A. Camerlenghi, J. Carcione, S. Dean, J.-P. Foucher, and E. Flueh (2008), Estimation of gas hydrate concentration from multi-component seismic data at sites on the continental margins of NW Svalbard and the Storegga region of Norway, *Marine and Petroleum Geology*, 25(8), 744-758.
- Westbrook, G. K., K. E. Thatcher, E. J. Rohling, A. M. Piotrowski, H. Pälike, A. H. Osborne, E. G. Nisbet, T. A. Minshull, M. Lanoisellé, and R. H. James (2009), Escape of methane gas from the seabed along the West Spitsbergen continental margin, *Geophysical Research Letters*, 36(15).
- Whiticar, M. J. (1999), Carbon and hydrogen isotope systematics of bacterial formation and oxidation of methane, *Chemical Geology*, 161(1), 291-314.
- Yielding, G., B. Freeman, and D. T. Needham (1997), Quantitative fault seal prediction, *AAPG bulletin*, 81(6), 897-917.
- Zapata-Hernández, G., J. Sellanes, A. R. Thurber, L. A. Levin, F. Chazalon, and P. Linke (2014), New insights on the trophic ecology of bathyal communities from the methane seep area off Concepción, Chile (~ 36° S), *Marine Ecology*, 35(1), 1-21.

#### *Internet sources*

- Jakobsson, M., 2012a. Multibeam and side scan mapping. In Marine Geoscientific Research Methods HT12, Department of Geological Sciences, Stockholm.  
[http://www.geo.su.se/images/file\\_archive/marine\\_geosci\\_res\\_meth/HT12/marinegeophysical-multibeam-2012.pdf](http://www.geo.su.se/images/file_archive/marine_geosci_res_meth/HT12/marinegeophysical-multibeam-2012.pdf)
- Jakobsson, M., 2012b. Sonar application and signal processing. In Marine Geoscientific Research Methods HT12, Department of Geological Sciences, Stockholm.  
[http://www.geo.su.se/images/file\\_archive/marine\\_geosci\\_res\\_meth/HT12/marinegeophysical-methods-processing-2012.pdf](http://www.geo.su.se/images/file_archive/marine_geosci_res_meth/HT12/marinegeophysical-methods-processing-2012.pdf)

## 9. Appendix

### 9.1. Appendix 1

2D line n°	Date: start - end	Time (UTC): start - end	Shot point number: first - last	Comments: (Sailing direction, ship speed, depth sensor, wind speed, air temperature downtime, etc.)
<p><b>General survey parameters:</b>            100 m, 32 channel solid state streamer (65 m behind vessel and 15 m across offset from the gun float)            Ship's speed: 4.5 - 5 kn            Gun system: 2 x mini-GI (15/15 in3) &amp; (40/40 in3)                              at 1.75 m water depth                              33 m behind ship            Shooting pressure: ~160-170 bar</p>				
01	22.06 – 22.06	11:00 - 17:15	0 - 4411	<p>Starting line 1 off PKF flare area heading SW into Knipovich Ridge valley, perpendicular to the slope.</p> <p>Shooting interval: 5 sec            Sampling rate: 0.25 ms            Initial recording length: 2 sec            Initial recording delay: 0 sec (needs to be adjusted as water depth increases)</p> <p>Very good weather conditions, wind 5 m/s from SE, waves at 0.5-1 m</p> <p>Deactivated bad channels 29 and 32 from shot number 50            Adjusted to 1s delay at shot 1352            Adjusted to 2s delay at shot 2340            Shooting interval adjusted to 6s at shot 3337            Shooting interval adjusted to 5s at shot 3385            Sampling rate adjusted to 0.5ms and delay changed to 3s at shot 3392            Record length changed to 1.5s at shot 3403            Beyond shot 4057 there is almost no data in the trace as water depth was too great for our system.</p> <p>Shot interval changed to 6s at shot 4168            Delay changed to 3.5s recording length is 1s at 4174            Rec length 1.5s at 4177</p>

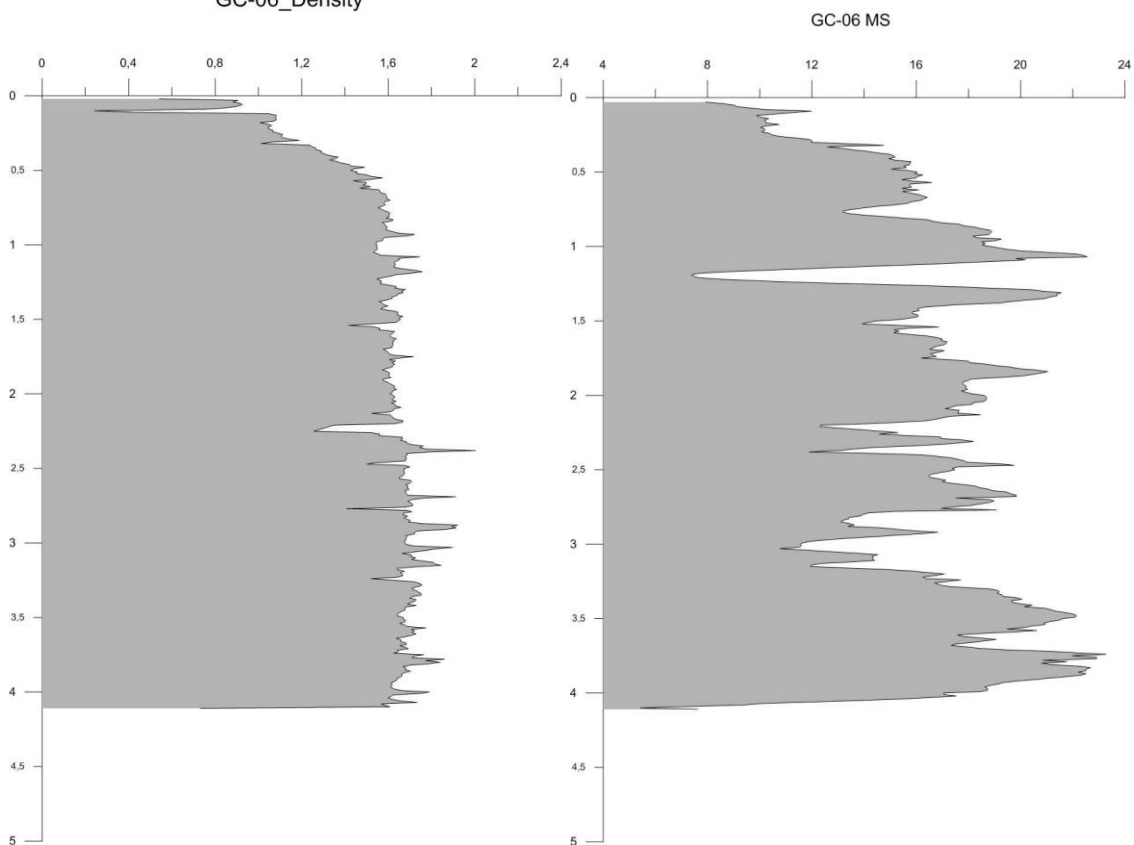
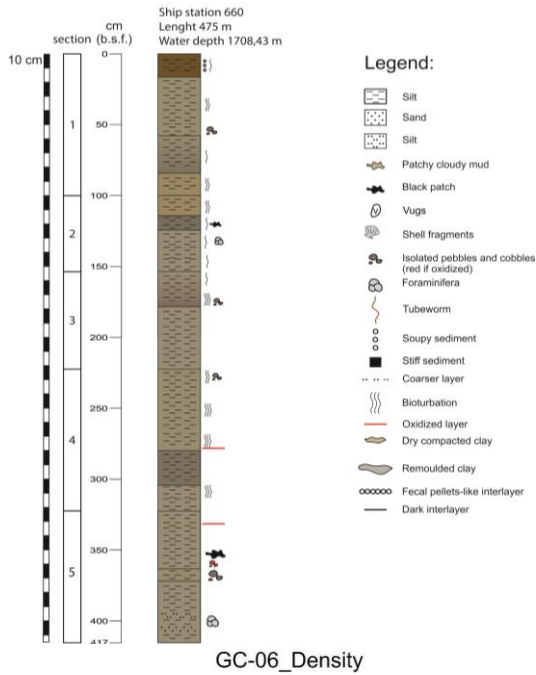
02	22.06 – 22.06	17:16- 20:14	4412-6356	<p>Line 02 leaving Knipovich Ridge valley to the NW, perpendicular to slope, connecting to previous line 008 of Vestnesa 2D 2013 survey.</p> <p>Shooting interval: 6sec Sampling rate: 0.5ms Initial recording length: 1.5s Initial recording delay: 3s (needs adjustment as water depth decreases)</p> <p>Good weather, as line 01 Changed recording delay to 2 sec and recording length to 2.5 at shot 5043. Changed sampling rate to 0.25 sec, recording delay to 2 sec and recording length to 2 at shot 5317. Changed shooting rate from 6 to 5 sec from shot 5340.</p>
03	22.06 – 22.06	20:26 – 22:26	6357 – 7784	<p>Line 03 running NNE down the faulted flank of the ridge valley.</p> <p>Shooting interval: 5 sec Sampling rate: 0.25ms Initial recording length: 2 s Initial recording delay: 2 s (needs adjustment as water depth increases)</p> <p>Good weather, calm sea, 5 m/s winds from NE</p> <p>Changed sampling rate to 0.5 ms, recording delay to 3 sec and recording length to 1.8 sec from shot number 7515. Line ended (shot no. 7725) but keep recording a bit into the turn.</p>
04	22.06 – 23.06	22:38 – 02:41	7785 – 10678	<p>Line 04 running NNW across the Molloy Drift.</p> <p>Shooting interval: 5 sec Sampling rate: 0.5ms Initial recording length: 1.8 s Initial recording delay: 3 s (needs adjustment as water depth decreases)</p> <p>Good weather, calm sea, 3 m/s winds from NE</p> <p>Changed sampling rate to 0.25 ms, recording delay to 2 sec and recording length to 2 sec from shot number 8192.</p> <p>Began turn, kept recording at: File 10026 (UTC 1:46), new heading direction: 24°</p>

05	23.06	02:59	10679 – 14480	<p>Line 05 running across “Joel’s Drift”</p> <p>Shooting interval: 5 sec  Sampling rate: 0.25ms  Initial recording length: 2.0 s  Initial recording delay: 2.0 s</p> <p>Good weather, calm sea,</p> <p>New heading direction: 190°/File No:11562</p>
06	24.06 – 24:06	01:05 – 03:35	14541 – 16336	<p>Line 06 W-E perpendicular across “Joel’s Drift”</p> <p>Shooting interval: 5 sec  Sampling rate: 0.25 ms  Initial recording length: 2 sec  Initial recording delay: 2 sec</p> <p>Good weather – small swell about 1m</p> <p>Channels 29 and 32 have been discarded  Channel 25 very noisy!!  Shots 14541-15079 are set up shots. Line 06 starts at shot 15080</p>
07	24.06 – 24.06	03:36 – 03:53	16337 – 16545	<p>Line 07 N-S parallel to Joel’s Drift.</p> <p>Shooting interval: 5 sec  Sampling rate: 0.25 ms  Initial recording length: 2 sec  Initial recording delay: 2 sec</p> <p>Channels 29 and 32 have been discarded  Shots 16337-16389 are the turn, real line starts at shot 16390</p>
08	24.06 – <b>24.06</b>	03:55 – 05:48	16546 – 17897	<p>Line 08 NE-SW perpendicular to Joel’s drift.</p> <p>Shooting interval: 5 sec  Sampling rate: 0.25 ms  Initial recording length: 2 sec  Initial recording delay: 2 sec</p> <p>Channels 29 and 32 have been discarded  Shots 16546-16624 are the turn, real line starts at shot 16625</p>
09	24.06 – 24.06	05:52 – 09.29	17921 – 19051	<p>Line 09 N-S parallel to “Joel’s Drift”</p> <p>Shooting interval: 5sec  Sampling rate: 0.25ms  Initial recording length: 2s  Initial recording delay: 2s</p> <p>Channels 29 and 32 are discarded  Shots 17921-17968 are the turn, real line starts at shot 17969  Incomplete data file #????</p>

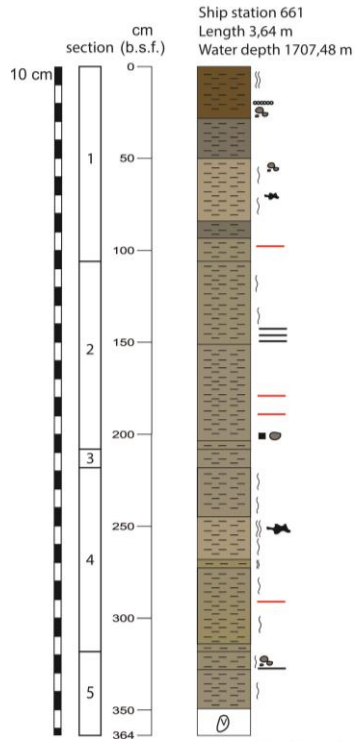
10	24.06 – 24.06	09.29 – 11.24	19052 – 20437	Line 10 SW-NE Shooting interval: 5sec Sampling rate: 0.25ms Initial recording length: 2s Initial recording delay: 2s  Good weather, calm sea, 9 m/s winds from S  Channels 29 and 32 are discarded
----	------------------	------------------	------------------	--

## 9.2. Appendix 2

### CAGE 14-1-GC-06



### CAGE 14-1-GC-07

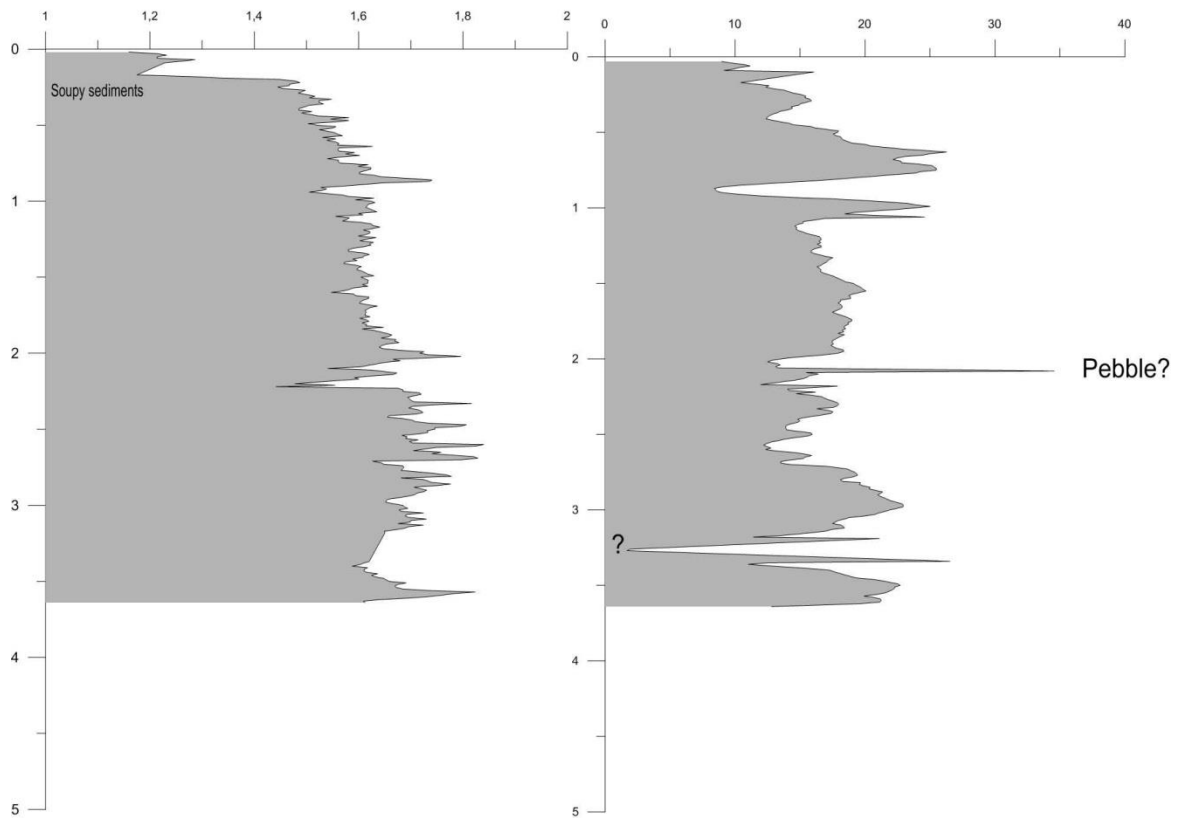


Legend:

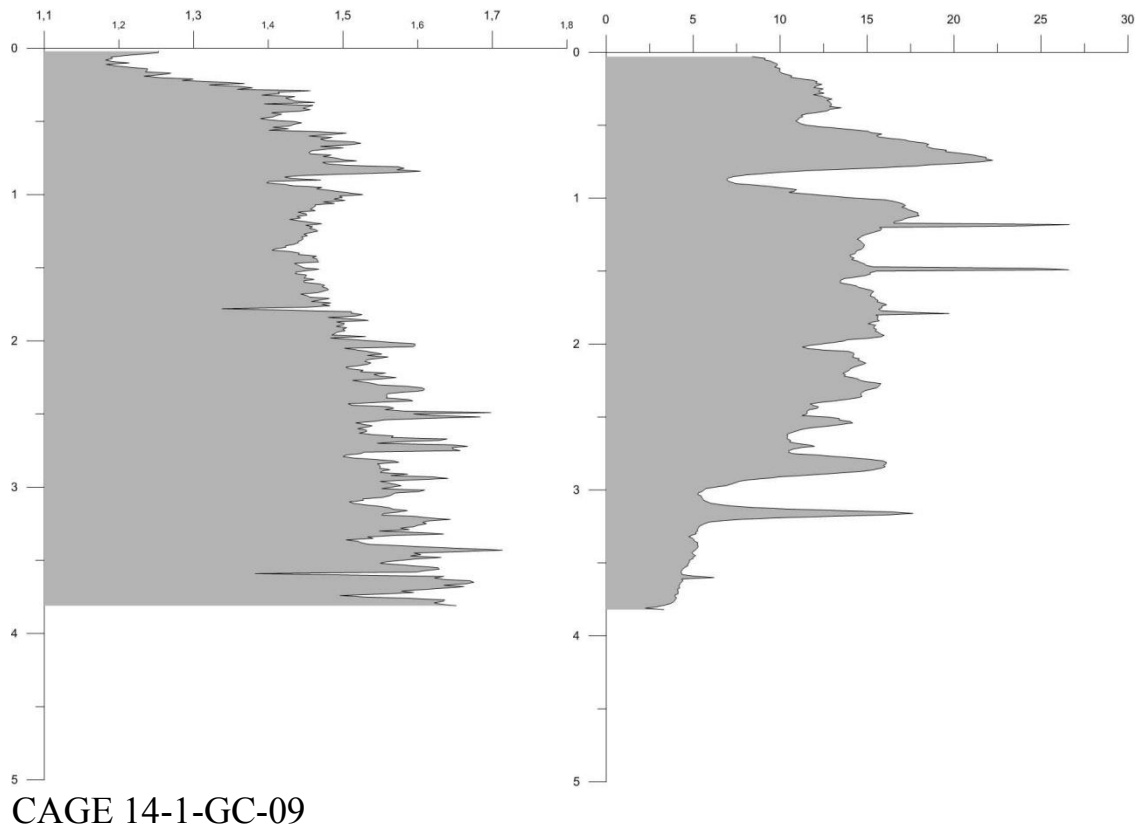
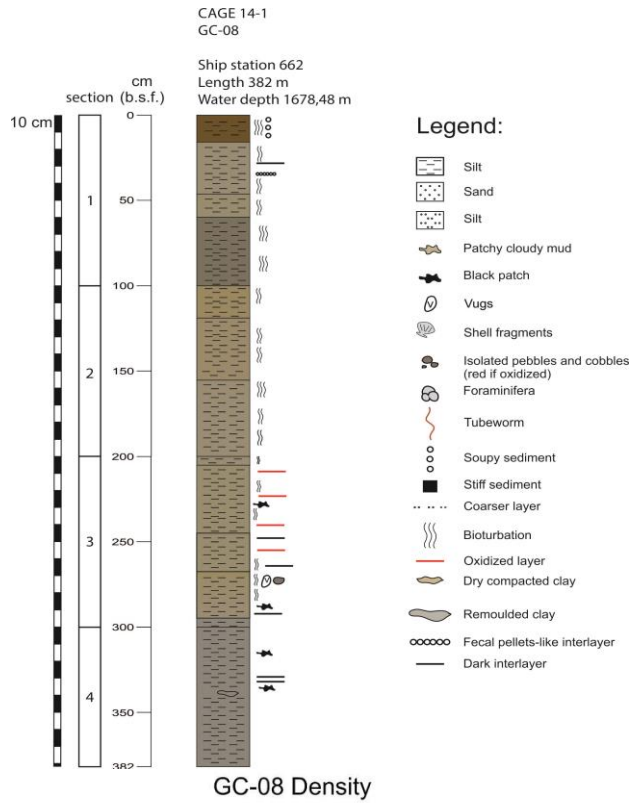
- Silt
- Sand
- Silt
- Patchy cloudy mud
- Black patch
- Vugs
- Shell fragments
- Isolated pebbles and cobbles (red if oxidized)
- Foraminifera
- Tubeworm
- Soupy sediment
- Stiff sediment
- Coarser layer
- Bioturbation
- Oxidized layer
- Dry compacted clay
- Remoulded clay
- Fecal pellets-like interlayer
- Dark interlayer

GC-07 Density

GC-07 MS

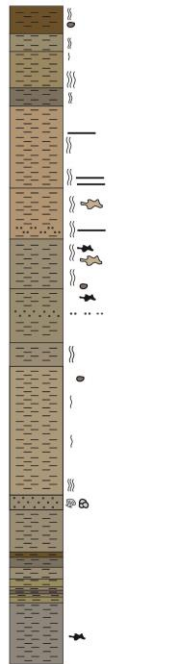
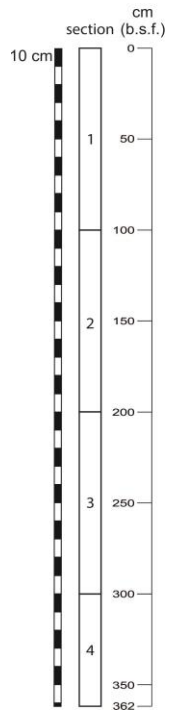


CAGE 14-1-GC-08



CAGE 14-1  
GC-09

Ship station 663  
Length 3,62 m  
Water depth 1574,73 m

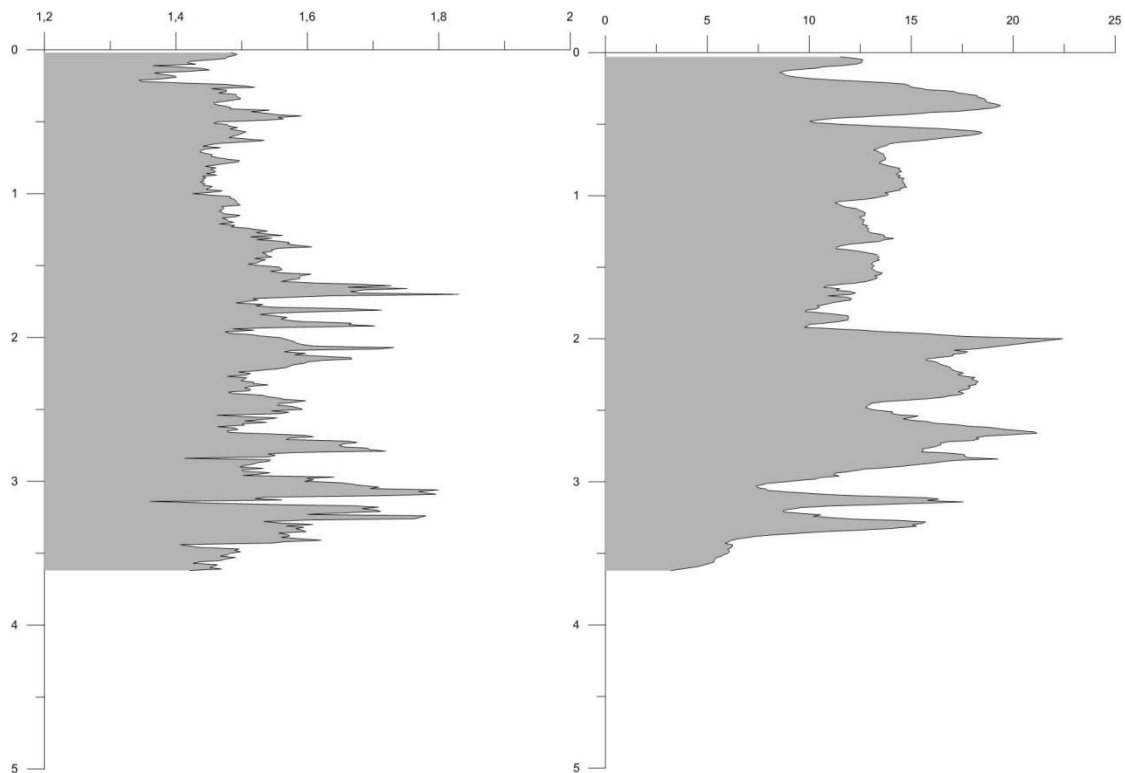


Legend:

- Silt
- Sand
- Silt
- Patchy cloudy mud
- Black patch
- Vugs
- Shell fragments
- Isolated pebbles and cobbles (red if oxidized)
- Foraminifera
- Tubeworm
- Soupy sediment
- Stiff sediment
- Coarser layer
- Bioturbation
- Oxidized layer
- Dry compacted clay
- Remoulded clay
- Fecal pellets-like interlayer
- Dark interlayer

GC-09 Density

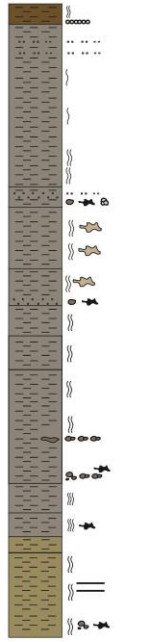
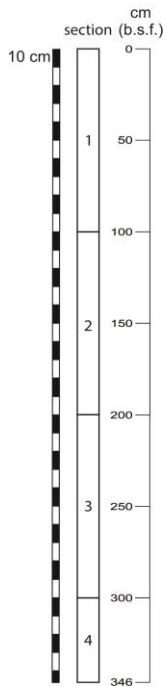
GC-09 MS



# CAGE 14-1-GC-10

CAGE 14-1  
GC-10

Ship station 664  
Length 346m  
Water depth 1611,18 m

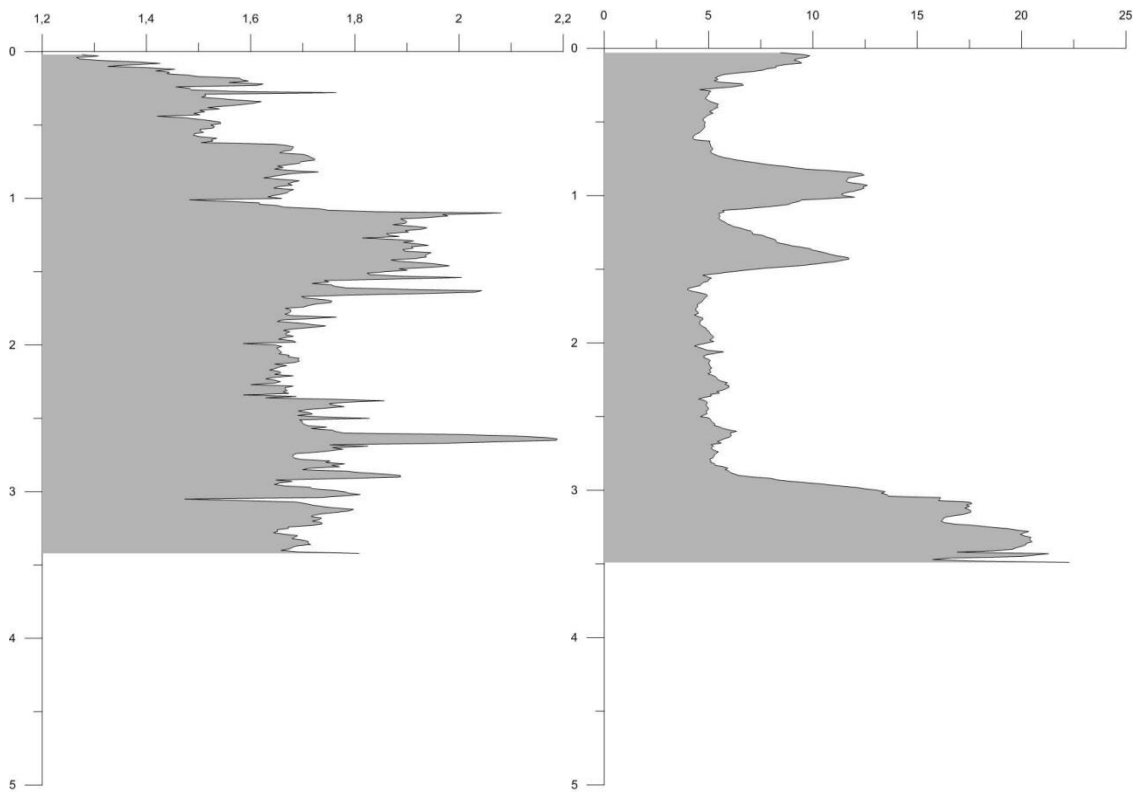


### Legend:

- Silt
- Sand
- Silt
- Patchy cloudy mud
- Black patch
- Vugs
- Shell fragments
- Isolated pebbles and cobbles (red if oxidized)
- Foraminifera
- Tubeworm
- Soupy sediment
- Stiff sediment
- Coarser layer
- Bioturbation
- Oxidized layer
- Dry compacted clay
- Remoulded clay
- Fecal pellets-like interlayer
- Dark interlayer

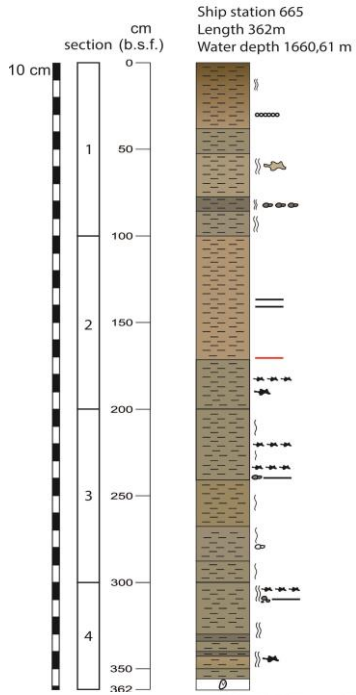
GC-10 Density

GC-10 MS



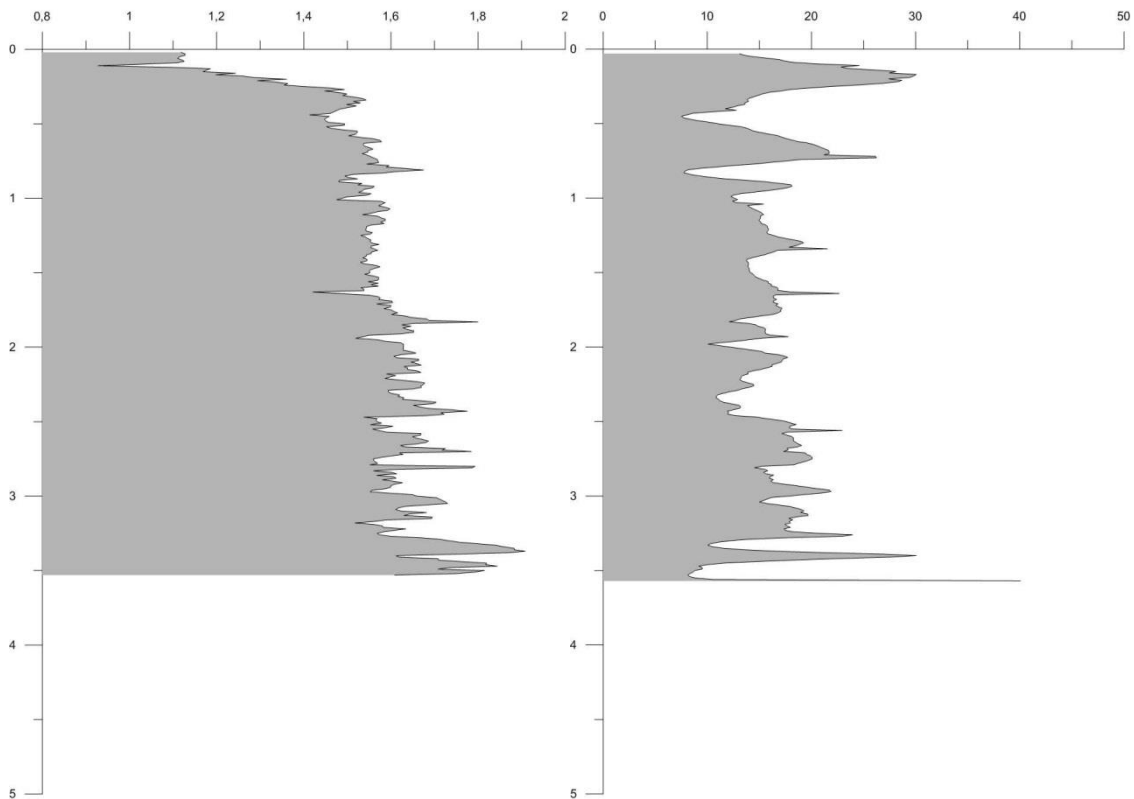
# CAGE 14-1-GC-11

CAGE 14-1  
GC-11

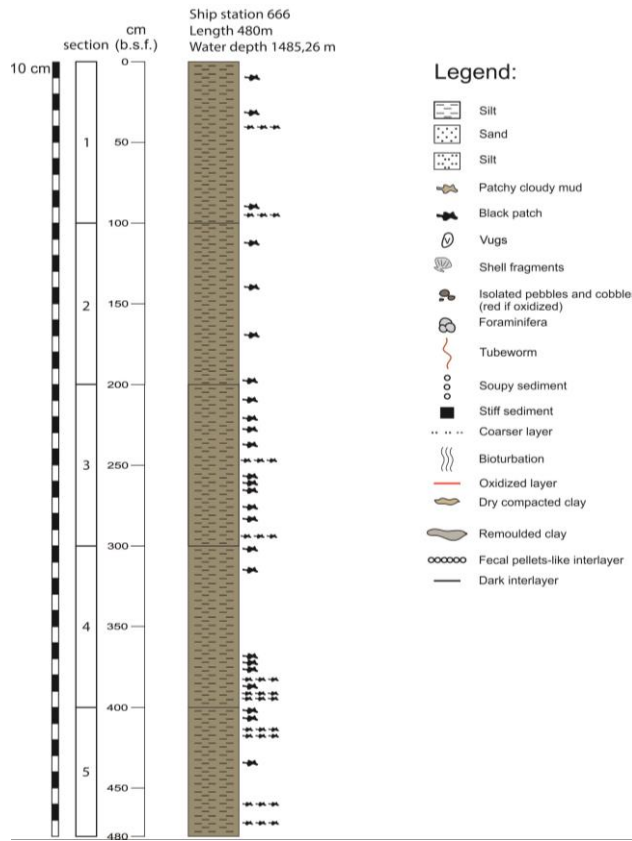


GC-11 Density

GC-11 MS

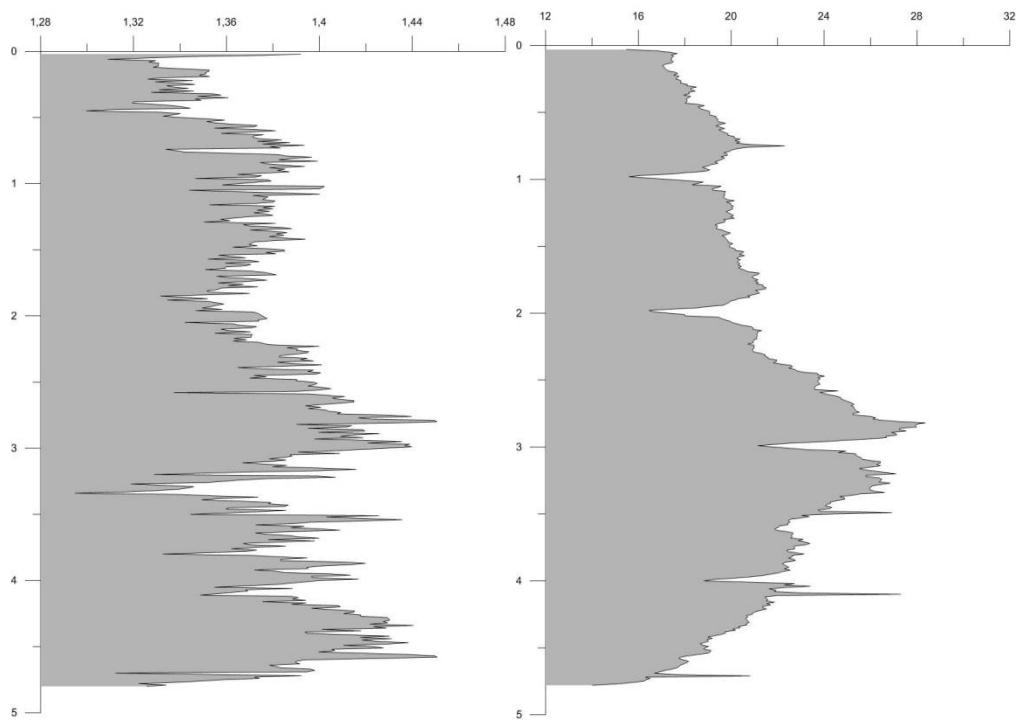


# CAGE 14-1-GC-12

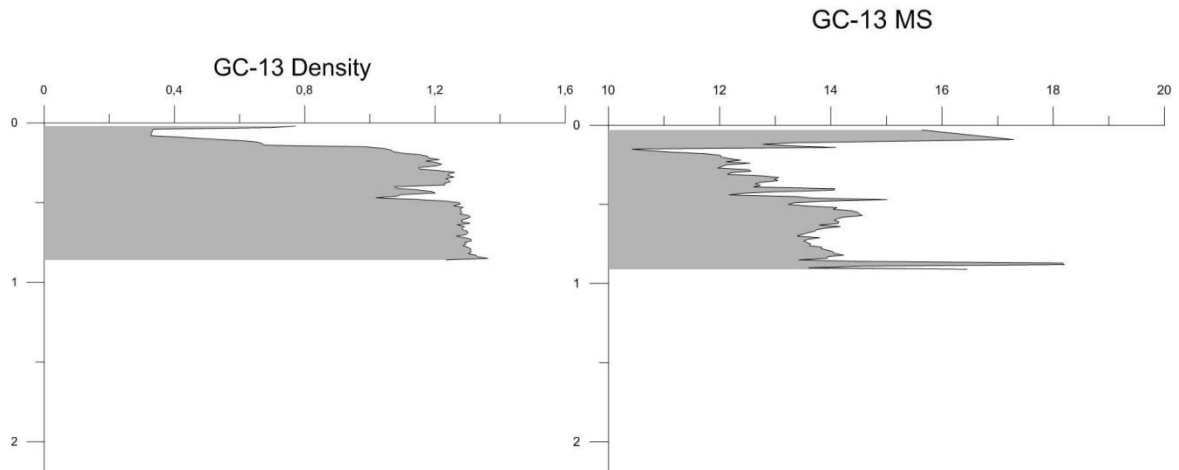


GC-12 Density

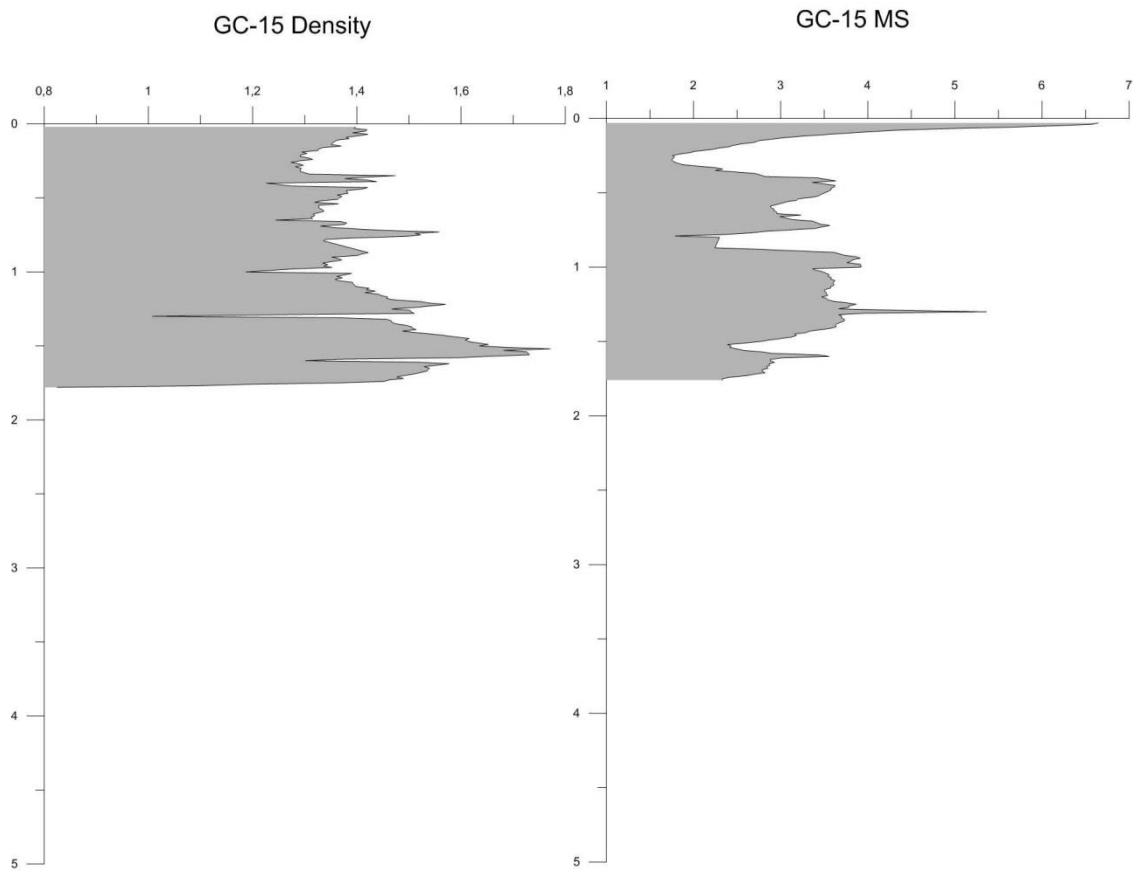
GC-12 MS



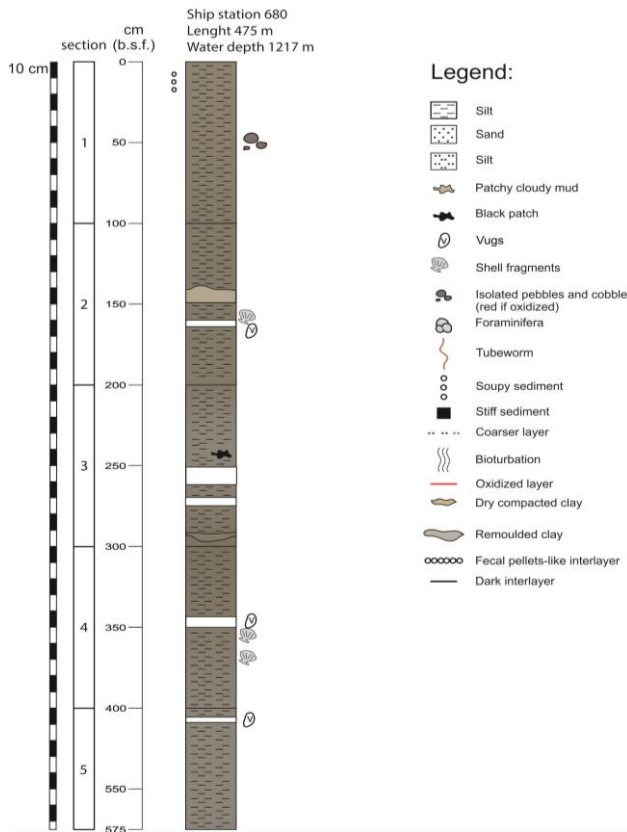
### CAGE 14-1-GC-13



### CAGE 14-1-GC-15

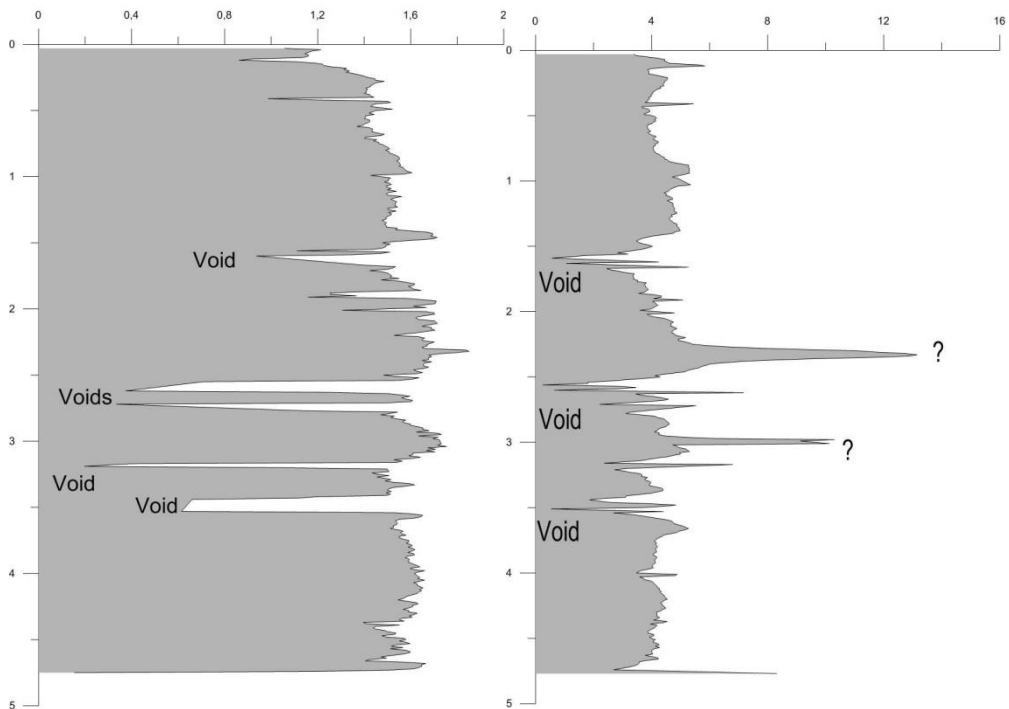


# CAGE 14-1-GC-16



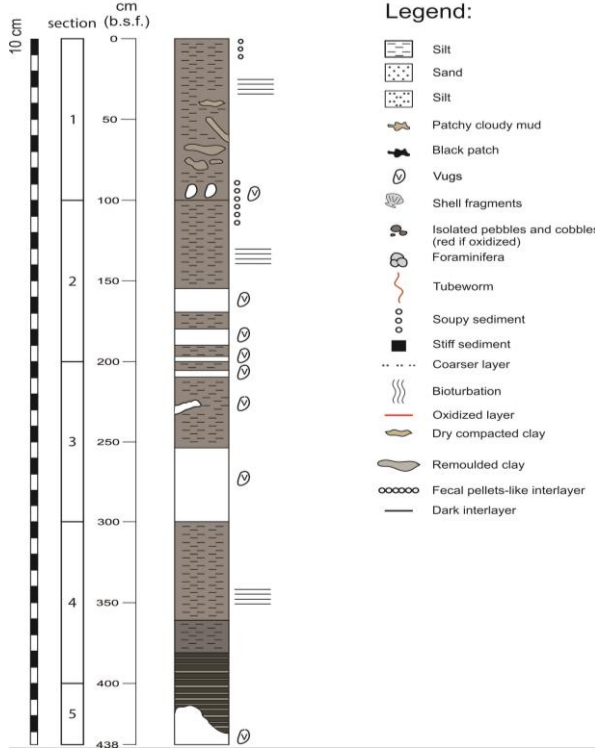
GC-16 Density

GC-16 MS

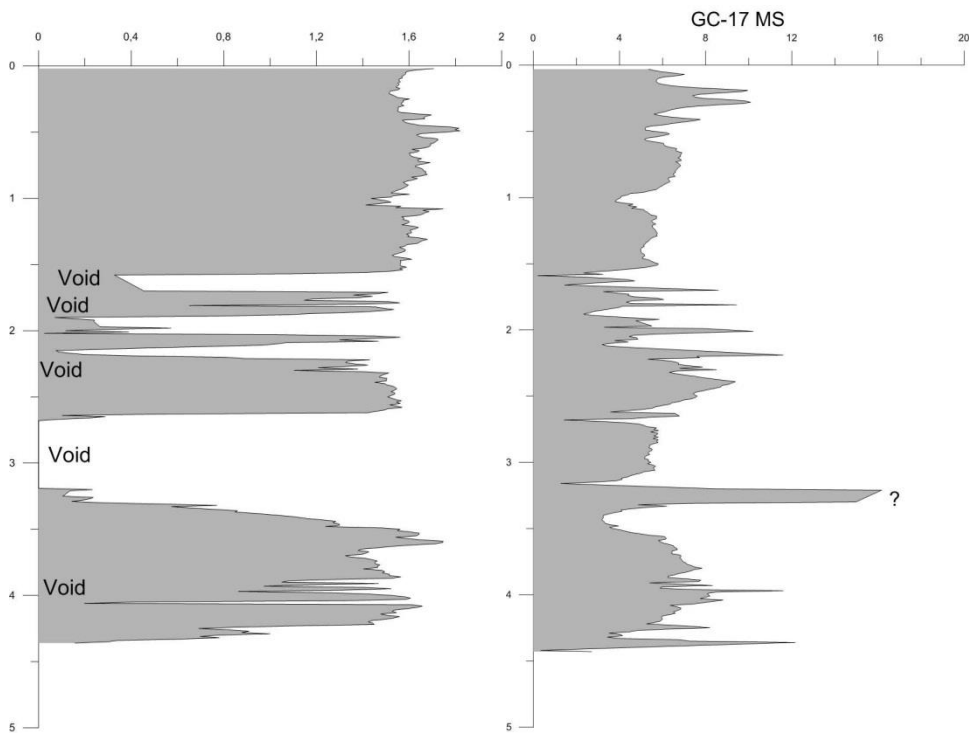


# CAGE 14-1-GC-17

Ship station 681  
 Length 438 m  
 Water depth 1207 m



GC-17 Density



## NARRATIVE OF THE CRUISE

Times in this report are given in local time (local time -2 hrs = UTC), seismic data are logged in UTC time and ship logs are given in UTC time. Weather conditions throughout the cruise were calm with sea state and wave heights not significantly above 1 m, but with mostly grey skies. Air temperatures were between 2 °C and 8 °C. We started to prepare the cruise in Longyearbyen on June 30 with and assembling some of the equipment.

### Thursday, 19.06.

The scientific crew arrived during the afternoon hours. We started to prepare lab areas and to assemble the equipment. RV Helmer Hanssen left Longyearbyen at 20:00 heading towards the first working area in the Kongsfjorden Trough.

### Friday, 20.06

05:00 On our way to Kongsfjorden we cross the shallowest of the gas flare areas at 80 m water depth and make three quick line crossings in order to assess how the Picarro sensors respond to methane concentrations in the surface water.

11:00 Our first station is a reference site on the northern border of the Kongsfjord Trough. Here, we run in order a CTD, 6 bottom grabs, a gravity, a multi and a box core.

16:45 We steam west to the continental slope offshore Prins Karls Foreland.

19:30 We start a CTD transect with 23 stations from the continental slope to the shallow shelf offshore Prins Karls Foreland.

### Saturday, 21.06.

17:00 The CTD transect is finished and we head to the flare site just off the shelf edge in 240 m water depth for sediment and benthic sampling.

### Sunday, 22.06.

02:00 6 grab samples successfully recovered material from the seafloor. On four attempts with the gravity corer we cannot recover any material, most likely due to the fact that the corer does not penetrate the hard ground in this area. However, a box corer then does recover about 30 cm of material consisting of mud and a high amount of dropstones.

09:00 We continue to the flare site in 350-400 m water depth which lies at the upper outcrop of the gas hydrate stability zone and perform one CTD cast and one box core.

12:00 The high-res 2D seismic cable and mini-GI airgun system are deployed and we start on a seismic line heading SW across the Knipovich Ridge valley and towards the sediment drift on the western flank of the Knipovich Ridge, an area called Svyatogor Rise.

19:15 seismic line 2 starts in the Ridge Valley heading west onto the drift and connecting with a seismic line acquired in October 2013.

22:30 Seismic lines 3 and 4 criss-cross the drift and its main sediment ridge at its northern end.

### Monday, 23.06.

05:00 Start of line 5 following the crest of the sedimented drift from its northern end to its southern end and identifying several pockmarks on the seafloor and vertical focussed fluid flow structures in the subseabed.

12:00 Seismic work is completed and several coring stations have been identified along the crest of the sediment drift.

12:40 Prior to start of the coring, we conduct another CTD cast in 1570 m water depth.

14:00 The coring program starts with three box core and three multi core stations.

22:10 three more gravity core stations complete the coring work for the day and we decide to acquire a few more seismic lines over the night.

**Tuesday, 24.06.**

03:00 Three seismic lines connected by transects cross the crest of the sediment drift in its southern half.

**Wednesday, 25.06.**

Picarro, CTD and water-sampling transect over the 80 m seep site

**Thursday, 26.06.**

Picarro, CTD and water-sampling transect over the 80 m seep site

**Friday, 27.06.**

Picarro, CTD and water-sampling transect over the 80 m seep site

**Saturday, 28.06.**

Transfer to Vestnesa Ridge

Sediment coring of the pockmarks on the Vestnesa Ridge

**Sunday, 29.06.**

17:00: Arrival in Longyearbyen. End of cruise.

## ACKNOWLEDGEMENT

We thank the captain and his crew of R/V Helmer Hanssen of the University of Tromsø for their excellent support during the 3D and multicomponent seismic survey. This part of the cruise was conducted under the framework of the Centre of Excellence on Gas Hydrates, Environment and Climate (CAGE) (Norwegian Research Council (NFR) project number 223259/F5 at the University of Tromsø.

